Search for decays of the Higgs boson into a pair of pseudoscalar particles decaying into $b\bar{b}\tau^{+}\tau^{-}$ using pp collisions at $\sqrt{s} = 13$ TeV with the ATLAS detector

G. Aad *et al.*[*]

(ATLAS Collaboration)

This paper presents a search for exotic decays of the Higgs boson into a pair of new pseudoscalar particles, $H \to aa$, where one pseudoscalar decays into a b-quark pair and the other decays into a τ-lepton pair, in the mass range $12 \leq m_a \leq 60$ GeV. The analysis uses pp collision data at $\sqrt{s} = 13$ TeV collected with the ATLAS detector at the LHC, corresponding to an integrated luminosity of 140 fb^{-1}. No significant excess above the Standard Model (SM) prediction is observed. Assuming the SM Higgs boson production cross section, the search sets upper limits at 95% confidence level on the branching ratio of Higgs bosons decaying into $b\bar{b}\tau^{+}\tau^{-}$, $\mathcal{B}(H \to aa \to b\bar{b}\tau^{+}\tau^{-})$, between 2.2% and 3.9% depending on the pseudoscalar mass.

DOI: 10.1103/PhysRevD.110.052013

I. INTRODUCTION

Following the observation of the Higgs boson H with mass m_H near 125 GeV by the ATLAS and CMS collaborations [1,2], studies of its properties have been important programs of research. Global analyses of measurements of Higgs boson properties constrain the branching ratio of the Higgs boson into undetected beyond the Standard Model (BSM) particles to approximately $\mathcal{B}_u \lesssim 12\%$ [3,4]. Higgs boson decays are particularly sensitive to new physics due to the small total width ($\Gamma_H \approx 4$ MeV). Even very small couplings to new particles can give sizable branching ratios and can be compatible with available measurements [5].

Extensions of the Standard Model (SM) that include new light pseudoscalars, called a-bosons, can give rise to exotic Higgs boson decays $H \to aa$. Such new light particles appear in theories with an extended Higgs sector [6–10], dark matter models [11–15], models with a first-order electroweak phase transition [16,17], and theories of neutral naturalness [18,19]. Signatures of $H \to aa$ can also arise in models with hidden-sector particles that are singlets under the SM gauge transformations [5,20–23]. In scenarios where the a-boson mixes with the SM Higgs boson and inherits its Yukawa couplings to fermions, decays of the a-boson into heavy fermions such as b-quarks and τ-leptons

are favored, and the process $H \to aa \to b\bar{b}\tau^{+}\tau^{-}$, shown in Fig. 1, is expected to have a sizeable branching ratio in the mass range $2m_b < m_a < m_H/2$ [5,24].

This paper presents a search for the exotic Higgs boson decay $H \to aa \to b\bar{b}\tau^{+}\tau^{-}$ and uses the full Run-2 dataset of pp collisions at $\sqrt{s} = 13$ TeV recorded with the ATLAS detector corresponding to an integrated luminosity 140 fb^{-1}. The analysis is performed over the mass range $12 < m_a < 60$ GeV and targets the following production modes of the Higgs boson: gluon-gluon fusion (ggF), vector boson fusion (VBF), and associated production with a vector boson (VH). The associated production of a top-antitop-quark pair ($t\bar{t}$) with a Higgs boson provides a negligible signal contribution due to (i) the low cross section and (ii) the additional b-quarks from the top-quark decays resulting in a reduced signal acceptance. Therefore, this production mode is not considered. Different analysis categories are defined depending on the τ-lepton decay modes, which can be into electrons (e), muons (μ), or hadrons (τ_{had}, also "hadronic taus"). Due to the relatively low mass of the Higgs boson and the four-body final state,

---

[*]Full author list given at the end of the article.
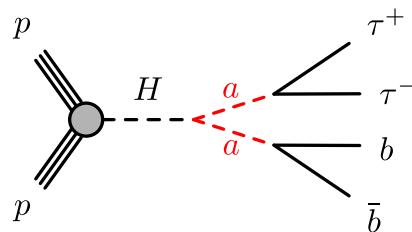
FIG. 1. Feynman diagram for the leading contribution to the $pp \to H \to aa \to b\bar{b}\tau^{+}\tau^{-}$ process.

FIG. 2. The analysis categories used in the search corresponding to different decay modes of the τ-leptons and strategies for identifying heavy-flavor jets, including merged b-jet pairs (B) and single b-jets (b). Note that the categories are exclusive.

the τ-leptons and b-quarks tend to have low transverse momentum (p_T), typically below $p_T \lesssim 50$ GeV. Therefore, the analysis relies on electron or muon triggers, which have lower p_T thresholds compared to triggers using hadronic activity, to select the events of interest and requires an electron or muon in the final state. The analysis defines different event categories depending on τ-lepton decay modes: $e\mu$, $e\tau_{\mathrm{had}}$, and $\mu\tau_{\mathrm{had}}$. The major backgrounds to the signal process are Drell–Yan production of τ-leptons produced in association with heavy-flavor jets, $t\bar{t}$, and nonprompt leptons plus τ_{had}.

For low m_a, the a-boson has a large Lorentz boost and its decay products can be collimated. Consequently, the $a \rightarrow b\bar{b}$ final state is reconstructed as a single jet that contains the hadronization products of the two b-quarks. While several techniques exist to resolve merged jets [25], most of them are only efficient in the case of high-mass and high-p_T jets. Due to the relatively low mass of the Higgs boson, the merged $a \rightarrow b\bar{b}$ jet will have low p_T. This analysis uses a novel, dedicated algorithm to identify low-mass, merged, "double b-quark" jets (B-jets) [26]. For high m_a, the b-quarks decays tend to be well separated and the reconstructed jets capture the hadronization of a single b-quark (b-jet). The analysis considers events with one B-jet, or one or two b-jets, resulting in nine analysis categories, as shown in Fig. 2.

Similar searches in the $b\bar{b}\tau^+\tau^-$ decay channel were performed by the CMS Collaboration [27,28]. The latest search has placed 95% CL upper limits on $\mathcal{B}(H \rightarrow aa \rightarrow b\bar{b}\tau^+\tau^-)$ in the range 1.7–7.7% for $12 \leq m_a \leq 60$ GeV using 138 fb^{-1} of Run 2 data at $\sqrt{s} = 13$ TeV. This analysis improves the sensitivity of previous results [28] in the low mass regime ($m_a < 20$ GeV) by targeting more final states and using a neural network discriminant to increase the separation of signal from background. This search is also complementary to other searches for $H \rightarrow aa$ decays performed by the ATLAS and CMS collaborations

using both $\sqrt{s} = 8$ TeV and $\sqrt{s} = 13$ TeV data in several final states including $\mu^+\mu^-\mu^+\mu^-$ [29–31], $\mu^+\mu^-\tau^+\tau^-$ [32–35], $\tau^+\tau^-\tau^+\tau^-$ [34,36], $b\bar{b}\mu^+\mu^-$ [37–40], $b\bar{b}b\bar{b}$ [41–43], $\gamma\gamma\gamma\gamma$ [44–46], and $\gamma\gamma gg$ [47].

II. ATLAS DETECTOR

The ATLAS detector [48] at the LHC covers nearly the entire solid angle around the collision point.[1] It consists of an inner tracking detector surrounded by a thin superconducting solenoid, electromagnetic and hadronic calorimeters, and a muon spectrometer incorporating three large superconducting air-core toroidal magnets.

The inner-detector system (ID) is immersed in a 2 T axial magnetic field and provides charged-particle tracking in the range $|\eta| < 2.5$. The high-granularity silicon pixel detector covers the vertex region and typically provides four measurements per track, the first hit generally being in the insertable B-layer (IBL) installed before Run 2 [49,50]. It is followed by the SemiConductor Tracker (SCT), which usually provides eight measurements per track. These silicon detectors are complemented by the transition radiation tracker (TRT), which enables radially extended track reconstruction up to $|\eta| = 2.0$. The TRT also provides electron identification information based on the fraction of hits (typically 30 in total) above a higher energy-deposit threshold corresponding to transition radiation.

The calorimeter system covers the pseudorapidity range $|\eta| < 4.9$. Within the region $|\eta| < 3.2$, electromagnetic calorimetry is provided by barrel and end cap high-granularity lead/liquid-argon (LAr) calorimeters, with an additional thin LAr presampler covering $|\eta| < 1.8$ to correct for energy loss in material upstream of the calorimeters. Hadronic calorimetry is provided by the steel/scintillator-tile calorimeter, segmented into three barrel structures within $|\eta| < 1.7$, and two copper/LAr hadronic end cap calorimeters. The solid angle coverage is completed with forward copper/LAr and tungsten/LAr calorimeter modules optimized for electromagnetic and hadronic energy measurements respectively.

The muon spectrometer (MS) comprises separate trigger and high-precision tracking chambers measuring the deflection of muons in a magnetic field generated by the superconducting air-core toroidal magnets. The field integral of the toroids ranges between 2.0 and 6.0 T m across most of the detector. Three layers of precision chambers,

---

[1]ATLAS uses a right-handed coordinate system with its origin at the nominal interaction point (IP) in the centre of the detector and the z-axis along the beam pipe. The x-axis points from the IP to the centre of the LHC ring, and the y-axis points upward. Polar coordinates (r, ϕ) are used in the transverse plane, ϕ being the azimuthal angle around the z-axis. The pseudorapidity is defined in terms of the polar angle θ as $\eta = -\ln \tan(\theta/2)$ and is equal to the rapidity $y = \frac{1}{2}\ln(\frac{E+p_z c}{E-p_z c})$ in the relativistic limit. Angular distance is measured in units of $\Delta R \equiv \sqrt{(\Delta y)^2 + (\Delta \phi)^2}$.

each consisting of layers of monitored drift tubes, cover the region $|\eta| < 2.7$, complemented by cathode-strip chambers in the forward region, where the background is highest. The muon trigger system covers the range $|\eta| < 2.4$ with resistive-plate chambers in the barrel, and thin-gap chambers in the end cap regions.

The luminosity is measured mainly by the LUCID–2 [51] detector that records Cherenkov light produced in the quartz windows of photomultipliers located close to the beampipe. Events are selected by the first-level trigger system implemented in custom hardware, followed by selections made by algorithms implemented in software in the high-level trigger [52]. The first-level trigger accepts events from the 40 MHz bunch crossings at a rate below 100 kHz, which the high-level trigger further reduces in order to record complete events to disk at about 1 kHz. A software suite [53] is used in data simulation, in the reconstruction and analysis of real and simulated data, in detector operations, and in the trigger and data acquisition systems of the experiment.

III. DATA AND SIMULATED EVENT SAMPLES

This search uses pp collision data at $\sqrt{s} = 13$ TeV recorded by the ATLAS experiment from 2015 to 2018. Only events that satisfy data quality requirements that ensure the stable operation of the ATLAS detector [54] are considered. The resulting dataset corresponds to an integrated luminosity of 140.1 ± 1.2 fb^{-1} [55]. Data are selected using a combination of single-electron, and single-muon, and opposite-flavor dilepton ($e\mu$) triggers [56,57].

Several Monte Carlo (MC) event generators are used to simulate the signal and background processes. The MC samples are used to optimize the event selection, evaluate efficiencies and acceptances, and to estimate yields. The main SM backgrounds are Drell–Yan production with decays into τ-leptons $Z/\gamma^* \to \tau^+\tau^-$ produced in association with jets ($Z + $ jets), top-quark production ($t\bar{t}$ or single top quarks) where at least one of the W bosons decay leptonically, and backgrounds where jets are misidentified as leptons. Other backgrounds from Higgs bosons decaying into τ-leptons $H \to \tau^+\tau^-$, $Z/\gamma^* \to \ell^+\ell^-(\ell = e, \mu)$, diboson production, and vector bosons produced in association with $t\bar{t}$ are also included.

Samples of $Z + $ jets and $W + $ jets events were produced using the SHERPA2.2.11 [58] generator with next-to-leading-order (NLO) precision matrix elements for up to two partons, and leading-order (LO) precision for up to five partons in the five-flavor scheme calculated with the COMIX [59] and OPENLOOPS [60–62] libraries. The events were matched with the SHERPA parton shower [63] using the MEPS@NLO prescription [64–67] with a dedicated set of tuned parameters. The NNPDF3.0NNLO set of parton distribution functions (PDF) [68] was used in the sample generation and the samples were normalized to a next-to-next-to-leading-order (NNLO) prediction [69].

Samples of diboson (VV) events were produced with the SHERPA2.2.1 generator for semileptonic final states or SHERPA2.2.2 [58] generator for fully leptonic final states. Fully leptonic final states and semileptonic final states, where one boson decays leptonically and the other hadronically, were generated using matrix elements at NLO accuracy in QCD for up to one additional parton and at LO accuracy for up to three additional parton emissions. Samples for the loop-induced processes $gg \to VV$ were generated using LO-accurate matrix elements for up to one additional parton emission for both the cases of fully leptonic and semileptonic final states. The matrix element calculations were matched and merged with the SHERPA parton shower based on Catani–Seymour dipole factorization [59,63] using the MEPS@NLO prescription. The virtual QCD corrections were provided by the OPENLOOPS library [60–62]. The NNPD3.0NNLO PDF set was used [68], along with a dedicated set of tuned parton-shower parameters.

The production of $t\bar{t}$ events was modeled using the POWHEG BOX v2 [70–73] generator at NLO precision in QCD with the NNPDF3.0NLO PDF set and the h_{damp}[2] parameter was set to 1.5 m_t [74], with the top-quark mass m_t set to 172.5 GeV. The parton shower, hadronization, and underlying event were modeled using PYTHIA8.230 [75] with the A14 set of tuned parameters [76] and using the NNPDF2.3LO PDF set [77]. The decays of bottom and charm hadrons were performed by EVTGEN1.6.0 [78].

Single-top-quark production events were modeled with dedicated samples covering s-channel, t-channel, or W-associated (tW) production. All three production modes were modeled using POWHEG BOX v2 [71–73,79–81] at NLO in QCD with the NNPDF3.0NLO PDF set. For the s-channel and tW production, the calculation is performed in the five-flavor scheme, while the t-channel production uses the four-flavor scheme. Parton shower and hadronization of these events were modeled with PYTHIA8.230 using the A14 tune and the NNPDF2.3LO PDF set.

The signal event samples include Higgs boson production via ggF, VBF, and VH. For the SM production of the $H \to \tau^+\tau^-$ background process, only the ggF and VBF production modes are considered. Top-quark-associated production modes of the SM $H \to \tau^+\tau^-$ background process are negligible.

The sample of Higgs boson production via ggF is generated at NLO accuracy in QCD using POWHEG BOX v2 [71,72,79,82,83]. The simulation achieves NNLO accuracy for $gg \to h$ observables by reweighting the Higgs boson rapidity spectrum in HJ-MINLO [84–86] to that of HNNLO [87]. The Higgs boson production via VBF and VH were simulated with NLO precision using POWHEG BOX v2

---

[2]The h_{damp} parameter regulates singularities in the emission of hard radiation in POWHEG. The value is chosen to provide good description of the $t\bar{t}$ system p_{T}.

[71,72,79,88]. The PDF4LHC15NNLO PDF set [89] was used for all three production modes, while the parton shower and hadronization were performed using PYTHIA 8.244 with the A14 set of tuned parameters.

Each of the simulated Higgs production samples are normalized using dedicated higher-order cross section calculations. The ggF samples are normalized to the next-to-next-to-next-to-leading-order (N^3LO) cross section in QCD plus electroweak corrections at next-to-leading logarithm (NLL) [90–100]. The VBF samples are normalized to an approximate-NNLO QCD cross section with NLO electroweak corrections [101–103]. Similarly, the VH samples are normalized to cross sections calculated at NNLO in QCD with NLO electroweak corrections. The cross section estimate includes the $gg \to ZH$ contribution, even though it is not simulated explicitly. For the signal samples, the decay $H \to aa \to b\bar{b}\tau^+\tau^-$ is performed using PYTHIA 8.244 and eight distinct mass points were simulated for the ggF, VBF, and the VH production modes in the range $m_a = 12$–60 GeV (12, 16, 20, 25, 30, 40, 50 and 60 GeV).

All simulated event samples were processed through a detailed simulation of the ATLAS detector based on GEANT4 [104] or a faster simulation where the full GEANT4 simulation of the calorimeter response is replaced by a detailed parametrization of the shower shapes [105]. The effects of multiple pp interactions in the same and neighboring bunch crossings (pileup) were modeled by overlaying the simulated hard-scattering event with inelastic pp (minimum-bias) events to reproduce the pileup distributions seen in the data. These inelastic events were generated with the soft QCD processes of PYTHIA 8.186 [106] using the NNPDF2.3LO PDF set and the A3 set of tuned parameters [107].

IV. OBJECT AND EVENT RECONSTRUCTION

Events are required to contain at least one reconstructed pp collision vertex candidate with at least two associated ID tracks with $p_T > 0.5$ GeV [108]. The primary vertex (PV) is selected as the vertex with the highest sum of the squared transverse momentum of the associated tracks.

Electrons are reconstructed from a seed cluster in the EM calorimeter matched to a track in the ID [109] and are required to have $p_T > 7$ GeV and $|\eta| < 2.47$. Electrons in the calorimeter barrel–end cap transition region ($1.37 < |\eta| < 1.52$) are excluded from the analysis. Electrons from τ-lepton decays can be displaced from the PV due to the long τ-lepton lifetime, so no requirement on the transverse impact parameter (d_0) is applied. A requirement on the longitudinal impact parameter $|z_0 \sin\theta| < 0.5$ mm is applied to match the electron track to the PV of the event. Electrons must satisfy the *Medium* working point of the likelihood identification criteria [109]. Electrons satisfying these requirements are referred to as baseline electrons.

Signal electrons are defined by additionally applying a tight isolation requirement using both tracking and calorimetry information with p_T-dependent ΔR cone radius [109]. This isolation variable rejects electrons that likely originated from light- or heavy-flavor hadrons. The isolation criterion is corrected for the presence of a nearby muon by subtracting the p_T of the muon track within the isolation cone of the electron from the isolation sum. This is particularly important for low mass signal samples ($m_a \lesssim 20$ GeV), where the electrons and muons from two τ-lepton decays in $a \to \tau^+\tau^-$ are often found to be within the isolation cone of each other.

Several methods are used to reconstruct muons, depending on the availability of tracks in the ID and the MS [110]. In order to benefit from the extended MS coverage up to $|\eta| = 2.7$, an ID track is not required in the region $2.5 < |\eta| < 2.7$. Muons are selected with $p_T > 7$ GeV and $|\eta| < 2.7$. As in the case of electrons, the only impact parameter requirement applied is $|z_0 \sin\theta| < 0.5$ mm. Muons must satisfy the *Medium* identification criterion [110], comprising the baseline muon selection. Signal muons are defined with an additional loose requirement on the isolation in both the inner tracking detector and calorimeters also with a p_T-dependent cone radius [110]. As above, an electron within the isolation cone of a muon is excluded from the calculation.

Jets are reconstructed using the anti-k_t algorithm [111] implemented in the FASTJET package [112,113] with a radius parameter $R = 0.4$. A particle-flow approach [114] is used for the jet reconstruction. The jet energy scale is calibrated to the particle level using simulation and further corrected with in-situ methods [115]. The jet selection requires $p_T > 15$ GeV and $|\eta| < 2.5$. A multivariate jet vertex tagger (JVT) based on tracking information is used to identify a jet as originating from the PV and suppress jets from pileup interactions for jets with $p_T < 60$ GeV and $|\eta| < 2.4$ [116].

The strategy to identify jets containing b-hadrons depends on the kinematics of the signal. For low signal masses ($m_a \lesssim 20$ GeV), pairs of b-hadrons from $a \to b\bar{b}$ decays tend to be merged in the detector and are identified as a single reconstructed jet. DEXTER [26] is an end-to-end algorithm that classifies jets into three categories: merged b-jets, single b-jets, and other jet flavors. Track-jets associated to jets are reconstructed by reclustering jets with $p_T > 20$ GeV and $|\eta| < 2.0$, together with all ID tracks using an anti-k_t algorithm with radius parameter $R = 0.8$. When the track-jet contains a single $R = 0.4$ jet, the jet is called isolated. An exclusive-k_t clustering of the track-jet tracks into precisely two sub-jets (ex-$k_t^{(2)}$) [117] is used to reconstruct the flight axes of the two b-jets within a track-jet. Both ex-$k_t^{(2)}$ track-subjets are required to have $p_T > 5$ GeV, where the transverse momentum of the subjet is estimated by summing the four-momentum of the associated tracks. The DEXTER algorithm uses the tracks

from the $R = 0.8$ track-jets to reconstruct secondary vertices, which provide a distinctive signature of merged b-jets when more than one is reconstructed inside the same jet or when they merge in a single secondary vertex with very high mass. Displaced tracks, secondary vertices, and the properties of the two ex-$k_t^{(2)}$ jets are used in a deep set neural network (NN) to classify the flavor of the jet. The NN exploits the presence of highly displaced tracks along the two flight axes as well as the reconstruction of multiple secondary vertices with large mass to resolve the two b-jets.

In the case of jets which are not merged, the jet flavor is identified with the DLlr algorithm [118] combining track impact parameter values with information from secondary vertices reconstructed within the jet. A working point corresponding to 60% efficiency for identifying B-jets is used for DEXTER, and a working point corresponding to 85% efficiency for identifying b-jets is used for DLlr.

The b-jet identification efficiency of the DLlr algorithm is measured in collider data by using $t\bar{t}$, Z + jets, W + jets, and multijet events [119–121]. A dedicated measurement of the DLlr algorithm identification efficiency for jets with $15 < p_T < 20$ GeV was performed for this search. The B-jet identification efficiency of the DEXTER algorithm is also measured in collider data by using $t\bar{t}$ and $Z + g(\to b\bar{b})$ events [26]. These measurements are used to correct the identification efficiency of heavy-flavored jets in simulation. The calibration procedure corrects the identification efficiency in simulation as a function of the jet p_T and η to match the one observed in data. Discrepancies between the identification efficiency in simulation and in data stem from both mismodeling of the detector response and of the underlying physics processes.

The reconstruction of τ_had candidates is seeded using jets reconstructed using the anti-k_t algorithm with distance parameter $R = 0.4$ whose inputs are topoclusters, three-dimensional clusters of calorimeter cells [122]. Reconstructed τ_had candidates have $p_T > 20$ GeV and $|\eta| < 2.5$, excluding the region $1.37 < |\eta| < 1.52$. The identification of τ_had uses a recurrent neural network (RNN) algorithm, which uses as inputs tracks and calorimeter clusters associated to τ_had candidates, as well as high-level discriminating variables [123]. Baseline τ_had candidates are required to pass the *very loose* working point, while signal τ_had candidates are further required to satisfy the *medium* working point [123]. A dedicated multivariate electron veto is applied to τ_had candidates to reject electrons misidentified as τ_had. The *medium* working point is used for the boosted-decision-tree-based electron veto [124].

A dedicated τ-jet-vertex algorithm (TJVA) is used to associate τ_had candidates to a PV [125]. The algorithm does not apply impact parameter requirements and finds the vertex with the largest fraction of the p_T from the tracks associated with the τ_had within a distance of $R = 0.2$ around the candidate. While TJVA does not apply impact parameter requirements, tracks must be sufficiently close to the

τ_had vertex, so two selections are applied on the impact parameters of tracks: $|d_0^\mathrm{TJVA}| < 1.0$ mm and $|z_0^\mathrm{TJVA} \sin\theta| < 1.5$ mm [126].

An overlap removal procedure is applied to prevent double counting of objects. This procedure is applied to the objects described previously that satisfy the baseline criteria, with the exception of muons where candidates satisfying the *very loose* identification criterion are used for the overlap removal and the *medium* identification criteria is used after overlap removal for the baseline selection criteria. This reduces backgrounds from $Z/\gamma^* \to \mu^+\mu^-$ events where a *very loose* muon can be misidentified as a τ_had candidate.

The overlap removal procedure is executed as follows. The closest jet within a radius of $\Delta R = 0.2$ of a selected electron is removed. If the nearest jet is within $\Delta R = 0.4$ of an electron, the electron is excluded from the analysis. Muons are excluded from the analysis if they are separated from the nearest jet by $\Delta R < 0.4$, since this reduces the background from heavy-flavor decays inside jets. However, if the jet has fewer than three associated tracks, the muon is selected and the jet is excluded from the analysis instead. This avoids an inefficiency for high-energy muons undergoing significant energy loss in the calorimeter. Electrons are excluded from the analysis if they share their track with a muon.

From the remaining jets, isolated jets that satisfy the 60% DEXTER working point are classified as B-jets. Isolated jets that do not satisfy the 60% DEXTER working point and satisfy the 85% DLlr working point are classified as selected b-jets. Isolated jets that do not satisfy the 60% DEXTER working point and do not satisfy the 85% DLlr working point are not used in the analysis. Non-isolated jets that satisfy the 85% DLlr working point are also classified as b-jets, while those that fail are excluded from the analysis. Muons in the annular region $0.4 < \Delta R < 0.8$ region around a B-jet which have a relative calorimeter-based isolation larger than 0.1 are excluded. Electrons satisfying the same criteria are also removed from the analysis. Finally, any B-jet with either an electron or a muon in the annular $0.4 < \Delta R < 0.8$ region and relative calorimeter-based isolation less than 0.1 are excluded from the analysis.

Muons that are excluded in the overlap removal procedure, but that are within $\Delta R < 0.3$ of a b-jet or within $\Delta R < 0.3$ of either of the ex-$k_t^{(2)}$ track-subjets of a B-jet are classified as soft muons. The leading soft muon associated to a b-jet or to a ex-$k_t^{(2)}$ track-subjet is added to the jet four momentum to account for semileptonic decays of b-hadrons in the jet energy.

The missing transverse momentum $\vec{p}_T^\mathrm{miss}$, with magnitude E_T^miss, is calculated using the magnitude of the vector sum of the p_T of all reconstructed objects and any additional tracks not associated to any reconstructed objects in the event [127]. The missing transverse energy (E_T^miss)

measures the imbalance of the transverse momentum in the detector. In this search E_T^{miss} is expected to arise from the neutrinos from τ-lepton decays.

V. EVENT SELECTION

Events are placed in exclusive categories defined by the final state objects from the $\tau^+\tau^-$ and $b\bar{b}$ systems, as shown in Fig. 2. The trigger strategy used to select events depends on the leptons in the final state. For the $e\mu$ categories, three orthogonal trigger regions are defined. If the event has at least one electron with $p_T > 27$ GeV, the single electron trigger is used and is required to match the selected electron. If the event has no such electron, but has a muon with $p_T > 27$ GeV, the single muon trigger is equivalently used and is required to match the selected muon. If there are no electrons nor muons satisfying the previous criteria, then opposite-flavor $e\mu$ triggers are used, also requiring trigger matching for both leptons. For the $e\tau_{\text{had}}$ and $\mu\tau_{\text{had}}$ categories, the single electron or muon trigger of the corresponding flavor with $p_T > 27$ GeV is used and matched to the electron or muon respectively.

Events in the $e\mu$ categories are required to have exactly one electron and one muon with opposite-sign (OS) charge that satisfy the signal selection criteria. In addition, events should have at most one baseline and no signal τ_{had} candidate. In the $e\tau_{\text{had}}$ and $\mu\tau_{\text{had}}$ categories, events are required to have exactly one electron and one muon, respectively, and exactly one signal τ_{had} with OS charge. For the $e\mu$ categories, the electron and muon are required to be separated by $\Delta R(e, \mu) > 0.1$ and for the $e\tau_{\text{had}}$ and $\mu\tau_{\text{had}}$ categories, this requirement is $\Delta R(e/\mu, \tau_{\text{had}}) > 0.2$, to reduce backgrounds from low-mass hadronic decays.

The analysis categories are also defined by requiring one *B*-jet, or one or two *b*-jets.

Two additional criteria are applied in each category to define regions enhanced in backgrounds. These criteria are based on the kinematics of the visible τ-lepton decay products, i.e., excluding the neutrinos. The visible mass of the τ-lepton decay products $m^{\text{vis}}(\tau\tau)$ is lower for signal than for the $Z \to \tau^+\tau^-$ background, due to the lower mass of the *a*-boson. A requirement is thus applied on the visible mass for all categories: $m^{\text{vis}}(\tau\tau) = m^{\text{vis}}(e\mu) < 45$ GeV for the $e\mu$ categories and $m^{\text{vis}}(\tau\tau) = m^{\text{vis}}(e\tau_{\text{had}})$ or $m^{\text{vis}}(\mu\tau_{\text{had}}) < 60$ GeV for the $e\tau_{\text{had}}$ and $\mu\tau_{\text{had}}$ categories. The difference in the requirements is due to the smaller number of neutrinos in the categories with a hadronic τ-lepton compared to the $e\mu$ case. A low mass requirement on the visible mass of $m^{\text{vis}}(\tau\tau) > 4$ GeV is also applied to reduce backgrounds from hadronic decays. The sample obtained by inverting the higher requirement on the visible mass is used to correct the modeling of the $Z +$ jets background (see Sec. VI), and is called the "Z region." Figure 3(a) demonstrates the ability of the background prediction to model the data in the most sensitive $\mu\tau_{\text{had}}$ category. The background model performs similarly well in the $e\tau_{\text{had}}$ and $e\mu$ categories.

When compared to the background, leptons from signal processes also have lower transverse mass calculated with the τ-lepton visible transverse momentum $p_T^{\text{vis}}(\tau)$ and E_T^{miss}. In the case of leptonic decays of the τ-lepton, the visible p_T is defined as the transverse momentum of the electron or muon. The transverse mass is defined as: $m_T(\tau) = \sqrt{2p_T^{\text{vis}}(\tau)E_T^{\text{miss}}(1 - \cos(\Delta\phi))}$, where $\Delta\phi$ is the difference in the azimuthal angle between $p_T^{\text{vis}}(\tau)$ and E_T^{miss}.
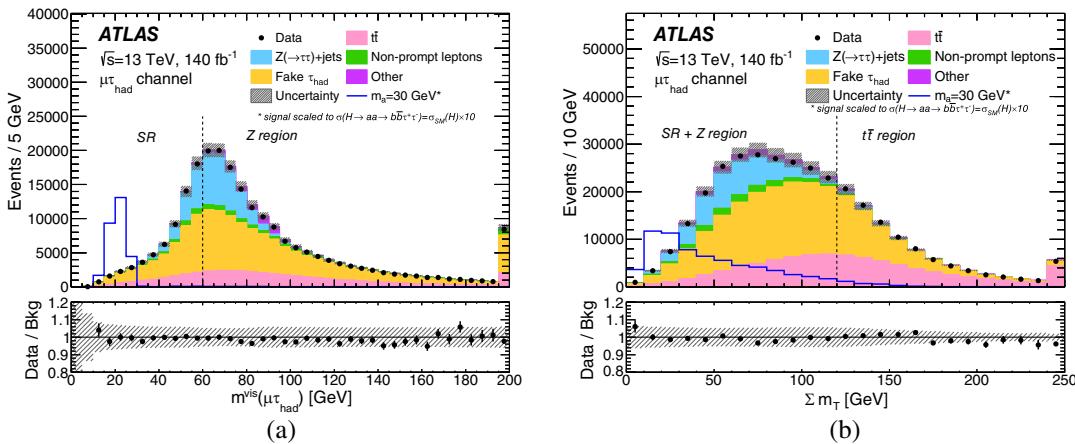
FIG. 3. (a) Visible mass $m^{\text{vis}}(\mu\tau_{\text{had}})$ and (b) sum of the transverse mass Σm_T distributions for signal and the expected background. Events with high $m^{\text{vis}}(\mu\tau_{\text{had}})$ and high Σm_T are included in the $t\bar{t}$ region. In order to compare the shapes, the expected signal distribution is shown assuming ten times the production cross section of the Higgs boson and a 100% branching ratio to $b\bar{b}\tau^+\tau^-$. The yields for the backgrounds correspond to the values obtained after applying the corrections to the background modeling described in Sec. VI. The cuts separating the signal region (SR) from the Z and $t\bar{t}$ regions are indicated by the vertical dashed line. The hashed area represents the total uncertainty of the background. Overflow events are included in the last bins.

TABLE I. Event selection for the analysis categories and the background regions. The background regions only list the requirements that are different from the signal region. The definition of signal leptons can be found in Sec. IV.

Region	$e\mu$	$e\tau_{\mathrm{had}}$ or $\mu\tau_{\mathrm{had}}$
Signal region	1 OS signal $e\mu$ pair 0 signal τ_{had} $\Delta R(e, \mu) > 0.1$ $4 < m^{\mathrm{vis}}(\tau\tau) < 45$ GeV	1 OS signal $e\tau_{\mathrm{had}}$ or $\mu\tau_{\mathrm{had}}$ pair 1 signal τ_{had} $\Delta R(\ell, \tau) > 0.2$ $4 < m^{\mathrm{vis}}(\tau\tau) < 60$ GeV
	$\Sigma m_T < 120$ GeV	
	1 B-jet or 1 or 2 b-jets	
Z region	$m^{\mathrm{vis}}(\tau\tau) > 45$ GeV	$m^{\mathrm{vis}}(\tau\tau) > 60$ GeV
$t\bar{t}$ region	$\Sigma m_T > 120$ GeV, no $m^{\mathrm{vis}}(\tau\tau)$ requirement	
SS region	1 SS signal $e\mu$ pair	1 SS signal $e\tau_{\mathrm{had}}$ or $\mu\tau_{\mathrm{had}}$ pair

A requirement is applied on the sum of the transverse mass calculated for the two τ-leptons $\Sigma m_{\mathrm{T}} < 120$ GeV, where $\Sigma m_{\mathrm{T}} = m_{\mathrm{T}}(\tau^{\mathrm{lead}}) + m_{\mathrm{T}}(\tau^{\mathrm{sublead}})$. Figure 3(b) shows the distribution of Σm_{T} in the $\mu\tau_{\mathrm{had}}$ categories. The sample obtained by inverting the requirement on Σm_{T} and is used to correct the modeling of the $t\bar{t}$ background (see Section VI), and is called the "$t\bar{t}$ region." There is small signal contamination into the Z and $t\bar{t}$ regions, only ≈ 1 signal event is expected assuming $\mathcal{B}(H \to aa \to b\bar{b}\tau^+\tau^-) = 10\%$.

Finally, a same-sign (SS) region, enhanced in backgrounds containing jets that are misidentified as electrons, muons or hadronic taus, is defined by applying the same selection criteria as the signal region but requiring the e, μ. and τ_{had} to have same-sign charge. This region is used to estimate backgrounds with nonprompt leptons (see Sec. VI). Table I summarizes the event selection used in the analysis.

VI. BACKGROUND ESTIMATION

Several SM processes can produce final states that satisfy the object and event selections described previously. The contributions from these processes are estimated with simulation or data-driven methods. Background processes with all leptons originating from the decay of vector bosons are defined as prompt and described by simulation. The dominant sources of prompt backgrounds are top-quark production, from $t\bar{t}$ and single-top events, and Z + jets where the Z boson decays into pairs of τ-leptons. Other backgrounds estimated from simulation include $h \to \tau^+\tau^-$, diboson production, $t\bar{t}$ in association with a vector boson, and $Z/\gamma^* \to \ell^+\ell^-$ where one lepton is misidentified as a τ_{had} in the $e\tau_{\mathrm{had}}$ and $\mu\tau_{\mathrm{had}}$ categories.

The modeling of two of the main prompt backgrounds, Z + jets and $t\bar{t}$, in simulation is corrected to match the data in regions enhanced in these backgrounds (see Sec. V). For the $t\bar{t}$ background, the simulation is reweighted to match the number of b-jets and the number of jets in the $t\bar{t}$ region.

The $t\bar{t}$ region is devoid of Z + jets events and performing the $t\bar{t}$ correction first minimizes the need for further iterations. In the $e\mu$ categories, an additional correction is applied as a function of the variable H_T, defined as the scalar sum of the p_{T} of all jets and leptons in the event. The reweighting procedure improves the description of the p_{T} of the $t\bar{t}$ system and the description of the number of additional jets produced in association with the $t\bar{t}$ system. The same strategy was applied in other ATLAS searches with large $t\bar{t}$ background [128,129]. After the $t\bar{t}$ reweighting, the Z + jets background is corrected with two normalization factors. The $Z \to \tau^+\tau^-$ and $Z \to e^+e^-$ backgrounds are scaled so that the predicted yields from simulation in two $m_{\ell\ell}$ bins match the observed number of events in the Z region.

Background processes with at least one lepton originating from the nonprompt decay of a hadron, from photon conversions, or from the misidentification of other particles are defined as nonprompt backgrounds. A tight-to-loose data-driven method [130] is used to estimate this background contribution. As described in Sec. IV, each lepton has two criteria baseline and signal. Leptons that satisfy the baseline selection but not the signal one are called loose (L), while those satisfying the signal selection are called tight (T). The estimates of the nonprompt backgrounds are obtained by assigning a weight $w_L = f\varepsilon/(\varepsilon - f)$ to each loose lepton and a weight $w_T = \varepsilon(1 - f)/(\varepsilon - f)$ to each tight lepton [130]. Here, f and ε are, respectively, the rate with which nonprompt and prompt leptons that satisfy the baseline selection also satisfy the signal criteria. The sign of the overall event weight is adjusted depending on the number of loose leptons to avoid double-counting of background events.

The nonprompt rates for electrons and muons are measured with events in the SS region that satisfy $\Delta R(e, \mu) > 1.4$. Events with one baseline muon (electron) and one signal electron (muon) are used to estimate the muon (electron) nonprompt rate f_μ (f_e). The electron and

muon nonprompt rates are parametrized as a function of the lepton p_T, η, whether or not the lepton is matched to a trigger object, and the number of b-jets in the event. The prompt rates for electrons (muons) ϵ_e (ϵ_μ) are estimated as a function of the same variables from simulations of $Z \to \tau^+ \tau^-$ events.

The condition $\Delta R(e, \mu) > 1.4$ ensures that the leptons do not interfere in their identification efficiency. When the weights are applied in the $e\mu$ signal region, a geometrical correction is necessary to account for the overlap of isolation cones with $\Delta R(e, \mu) < 0.6$. The correction is applied to events with two loose leptons and is parametrized as

$$(-w_L^e w_L^\mu)^{\text{corr}} = (1 - f(\Delta R))(-w_L^e w_L^\mu) + f(\Delta R)$$
$$\times \frac{1}{2}(w_L^e w_T^\mu + w_T^e w_L^\mu),$$

$$f(\Delta R) = c \times \left(\frac{2}{\pi}\arccos\left(\frac{\Delta R}{2r}\right) - \frac{\Delta R}{\pi r^2}\sqrt{r^2 - \frac{(\Delta R)^2}{4}} \right),$$

where $f(\Delta R)$ is the fraction of the isolation cone that overlaps, c is an arbitrary constant fit from the data in the SS region, and $r = 0.3$ is the radius of the isolation cone.

For hadronic taus, the prompt rate is taken as $\epsilon_\tau = 1$ in the weights w_L and w_T, and MC simulation is used to remove the contribution from prompt loose taus. The nonprompt rate is measured separately with three different processes: $Z(\to \mu^+\mu^-) + \tau_{\text{had}}$, jet $+ \tau_{\text{had}}$ where the τ_{had} candidate has high JVT score, and jet $+ \tau_{\text{had}}$ with low JVT score. In each region, the nonprompt rate is parameterized as a function of the τ_{had} p_T, η, decay mode, and the number of b-jets in the event. The τ_{had} nonprompt rate used to estimate the nonprompt background is written as a linear combination of the three estimates

$$f_\tau = [f_{Z \to \mu^+\mu^-}(1 - r_{\text{QCD}}) + f_{\text{high JVT}} r_{\text{QCD}}](1 - r_{\text{LJVT}})$$
$$+ f_{\text{low JVT}} r_{\text{LJVT}},$$

where the coefficient r_{QCD} is the fraction of nonprompt background events with two nonprompt leptons in each $e\tau_{\text{had}}$ and $\mu\tau_{\text{had}}$ categories and the coefficient r_{LJVT} is determined by a maximum-likelihood fit to the baseline τ_{had} seed jet width distribution. The coefficients r_{QCD} and r_{LJVT} are determined separately for each category and region of the analysis, as well as for each τ-lepton decay mode.

VII. ANALYSIS STRATEGY

In each analysis category, a NN is trained using the kinematic variables of the reconstructed heavy-flavor jets and τ-leptons. The NN is parametrized as a function of the a-boson mass in order to obtain an optimal discriminant for each different simulated mass [131]. During training, the background is assigned a random value as the value of m_a,

while for signal the simulated mass is used. The signal events have different correlations between physical observables and the generated mass than the background, which the network exploits. Once the network is trained, the NN output score is calculated with the true mass replaced by the mass hypothesis under consideration for all events, be they signal, background, or data.

Due to the neutrinos in the decays of the τ-leptons, the four-momentum of the two τ-leptons cannot be directly reconstructed. An algorithm called missing-mass calculator (MMC) [132] uses a Markov-chain MC to perform a maximum likelihood estimate of the neutrinos four-momenta, which is then used to reconstruct the input variables of the parameterized NN (pNN).

Beyond the true a-boson mass $m^{\text{true}}(\tau\tau)$, the pNNs for all categories use the visible mass $m^{\text{vis}}(\tau\tau)$, the MMC-based mass of the neutrino pair $m^{\text{MMC}}(\nu\nu)$ in each $\tau \to e\nu_\tau\bar{\nu}_e$ or $\tau \to \mu\nu_\tau\bar{\nu}_\mu$ decay, the missing transverse energy E_T^{miss}, the two transverse masses calculated with the visible p_T of the final-state τ-leptons $m_T(\tau)$, the leading heavy-flavor jet $p_T(b^{\text{lead}})$, and the visible transverse momentum $p_T^{\text{vis}}(\tau\tau b^{\text{lead}})$. The variable D_ζ [133], defined as

$$D_\zeta = [\vec{p}_T^{\text{miss}} - 0.85\vec{p}_T^{\text{vis}}(\tau\tau)] \cdot \vec{\zeta},$$

where $\vec{\zeta}$ is a unit vector in the direction of the bisector between the two τ-leptons, is also used as input to the network in all categories. D_ζ provides an estimate of the misalignment between the missing transverse momentum and the visible $\tau\tau$ subsystem.

In categories with two b-jets or one B-jet, additional input variables are used: the subleading heavy-flavor jet $p_T(b^{\text{sublead}})$, the transverse momentum $p_T(bb)$ and mass $m(bb)$ of the bb subsystem, as well as the visible $m^{\text{vis}}(bb\tau\tau)$ and MMC-based $m^{\text{MMC}}(bb\tau\tau)$ mass estimates of the Higgs boson. In categories with a B-jet, the four-momentum of the two ex-$k_t^{(2)}$ track-subjets are used as proxies for individual heavy-flavor jets. Table II summarizes the variables used as input for the NN. Distributions of the pNN input variables for the ($\mu\tau_{\text{had}}$, 2b) category are shown in Fig. 4. Distributions of the pNN(m_a) output variable for a value of $m_a = 30$ GeV in the ($\mu\tau_{\text{had}}$, 2b) category and for $m_a = 12$ GeV in the ($e\mu$, 1B) category are shown in Fig. 5.

Each pNN is a fully connected network with three hidden layers with 15 neurons each. The activation function is a leaky ReLU activation function with slope of 0.01 when the input is negative. The Objax [134] framework is used with the Adam optimization algorithm [135] and a binary cross entropy loss function. The signal sample used in the NN training contains all $H \to aa \to b\bar{b}\tau^+\tau^-$ simulated samples, which are normalized so that each of them has the expected number of observed events. The background sample used in the NN training is composed of composed of top-quark, $Z(\to \tau\tau) +$ jets and nonprompt events.

TABLE II.   Neural-network input variables with a summary of the final-state property it describes.

Feature	Description
$m^{\text{true}}(\tau\tau)$	During training: generated a-boson mass for signal MC. Background events are assigned a random value of the eight signal masses.
	During testing: the mass hypothesis under consideration.
$m^{\text{vis}}(\tau\tau)$	Visible mass of the $\tau\tau$ system.
$p_{\text{T}}(\tau\tau)$	p_{T} of the $\tau\tau$ system.
$m^{\text{MMC}}(\nu\nu)$	MMC-based mass of the two neutrinos in $\tau \to e\nu_\tau\bar{\nu}_e$ or $\tau \to e\nu_\tau\bar{\nu}_\mu$ decays.
$E_{\text{T}}^{\text{miss}}$	Missing transverse energy.
$m_{\text{T}}(\tau)$	Transverse mass calculated with the visible p_{T} of the final-state τ-leptons.
$p_{\text{T}}(b^{\text{lead}})$	Transverse momentum of the leading final-state b-jet.
$p_{\text{T}}^{\text{vis}}(\tau\tau b^{\text{lead}})$	Visible p_{T} of the $\tau\tau b^{\text{lead}}$ system.
D_ζ	Misalignment between the $\vec{E}_T^{\text{miss}}$ vector and the $\tau\tau$ system.
	Categories with a B-jet or 2b-jets
$p_{\text{T}}(b^{\text{sublead}})$	Transverse momentum of the subleading final-state b-jet.
$p_{\text{T}}(bb)$	Transverse momentum of the bb system.
$m(bb)$	Mass of the bb system.
$m^{\text{vis}}(bb\tau\tau)$	Visible mass of the Higgs boson system.
$m^{\text{MMC}}(bb\tau\tau)$	MMC-based mass of the Higgs boson system.
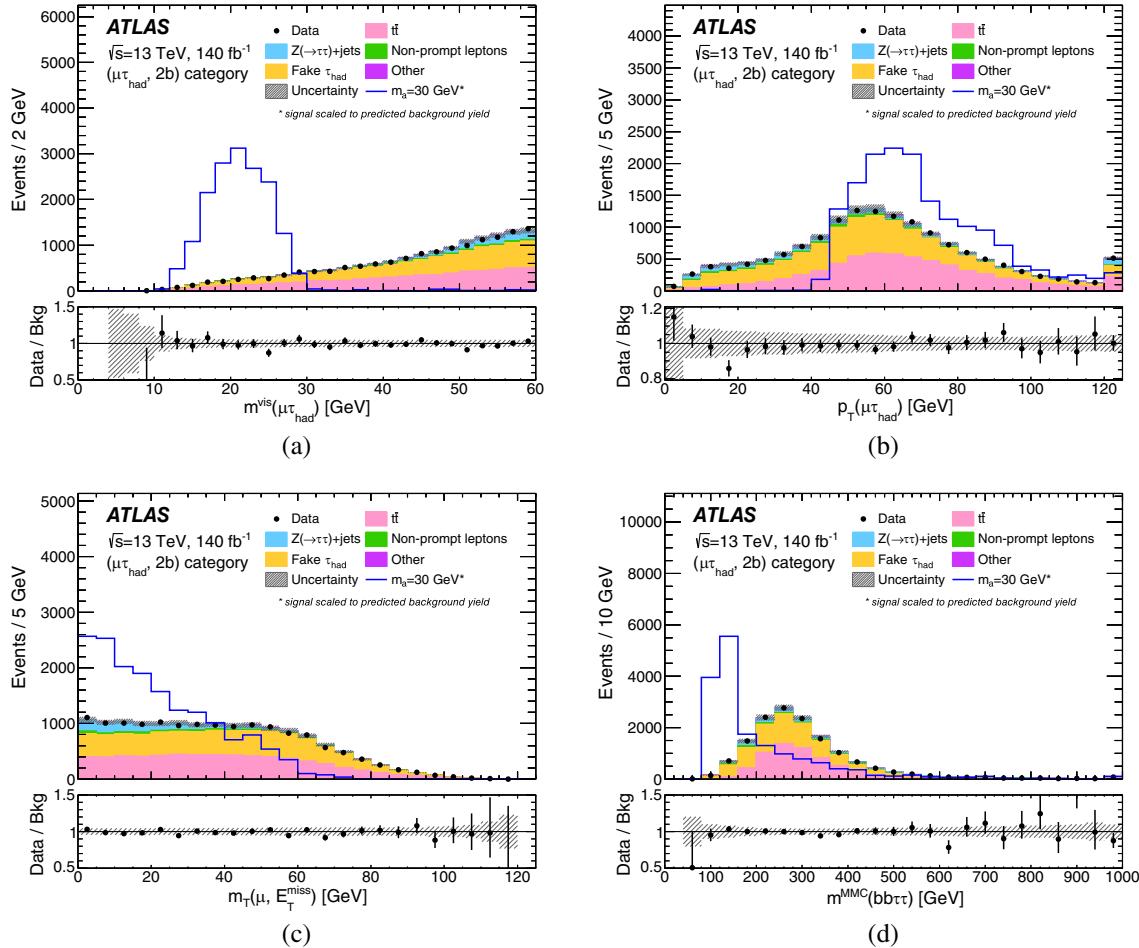
FIG. 4.   The pNN input variables (a) visible mass $m^{\text{vis}}(\mu\tau_{\text{had}})$, (b) visible transverse momentum $p_{\text{T}}^{\text{vis}}(\mu\tau_{\text{had}})$, (c) transverse mass $m_{\text{T}}(\mu, E_{\text{T}}^{\text{miss}})$, and (d) MMC mass $m^{\text{MMC}}(bb\tau\tau)$ are shown in the SR with no cut on the pNN discriminant. The signal shape is normalized to the same integral as the total background prediction. The hashed area represents the total uncertainty of the background. Overflow events are included in the last bins.
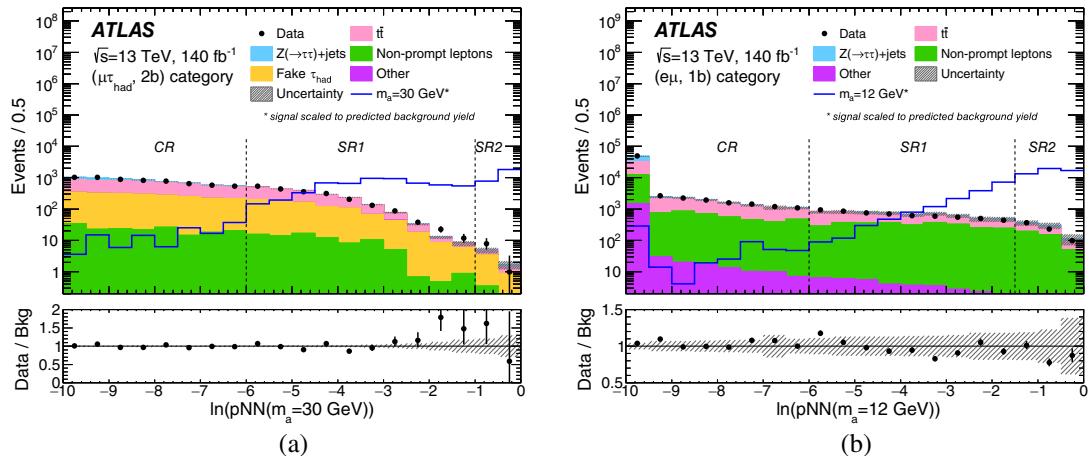
FIG. 5.   Distribution of ln(pNN) output score in the (a) $(\mu\tau_{\text{had}}, 2b)$ category with $m_a = 30$ GeV and (b) $(e\mu, 1b)$ category with $m_a = 12$ GeV. The signal shape is normalized to the integral of the total background model. The hashed area represents the total uncertainty of the background. Underflow and overflow events are included in the first and last bins, respectively.

For each a-boson hypothesis m_a, a statistical analysis is performed simultaneously in all nine categories of the analysis. To reduce the correlation among different m_a hypotheses, only events which satisfy $0.95m_a - 6$ GeV $\leq m^{\text{MMC}}(\tau\tau) \leq 1.15m_a + 1$ GeV in the $e\tau_{\text{had}}$ and $\mu\tau_{\text{had}}$ categories, or $0.75m_a - 6$ GeV $\leq m^{\text{MMC}}(\tau\tau) \leq 1.25m_a + 1$ GeV in the $e\mu$ categories are used. The pNN score calculated with this subset of events and $m^{\text{true}}(\tau\tau) = m_a$ is split into three bins with different signal-to-background ratios (S/B). These bins are called CR, SR1, and SR2, in order of increasing S/B. Figure 6 shows the ranges for each mass hypothesis tested in this paper while Fig. 7 shows the three regions used to search for a signal with $m_a = 30$ GeV.

A test statistic is built from a profile likelihood ratio calculated using the pyhf software [136]. The likelihood is given by the product of Poisson probability distributions for the three bins in each of the nine categories and the Gaussian distributions, which implement constraint terms for each source of systematic uncertainty as a function of nuisance parameters (NP).

$$L(\mu, \vec{\alpha}) = \prod_c^{N_{\text{cat}}} \prod_{j=1}^3 \frac{(\mu s_{c,j}(\vec{\alpha}) + b_{c,j}(\vec{\alpha}))^{n_{c,j}}}{n_{c,j}!} e^{-(\mu s_{c,j}(\vec{\alpha}) + b_{c,j}(\vec{\alpha}))}$$
$$\times \prod_{k=1}^{N_{\text{syst}}} \frac{1}{\sqrt{2\pi}} e^{-\frac{\alpha_k^2}{2}},$$
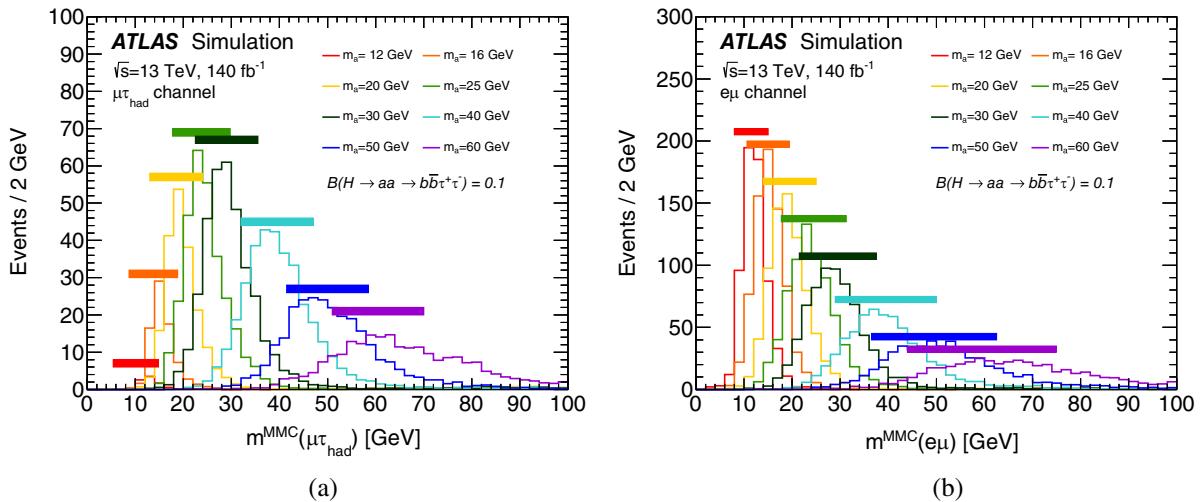
FIG. 6.   Mass distribution of the $\tau\tau$ system for each of the generated MC signal mass points for the (a) $\mu\tau_h$ and (b) $e\mu$ categories. The rectangle above each histogram shows the domain used to test each mass hypothesis. Note that nearby mass hypotheses have overlapping regions. All distributions are normalized assuming $\mathcal{B}(H \rightarrow aa \rightarrow b\bar{b}\tau^+\tau^-) = 10\%$.
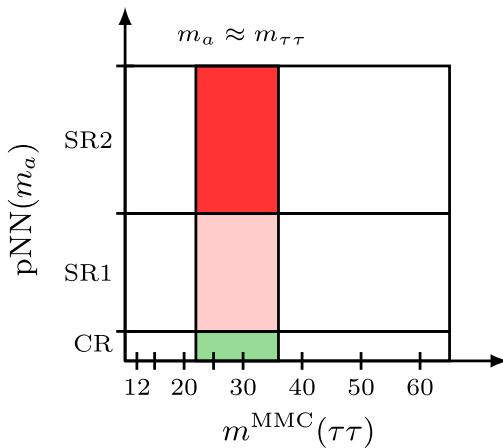
FIG. 7. As an illustration, the binning used in the two-dimensional plane of pNN score and mass for the $\mu\tau_{\text{had}}$ categories and the $m_a = 30$ GeV mass hypothesis is shown.

where μ is the signal strength, $\vec{\alpha}$ is the vector of nuisance parameters, $s_{c,j}$ and $b_{c,j}$ are the expected number of signal and background events in the jth bin of the category c, and $n_{c,j}$ is the observed number of events. Since the signal templates are normalized to the SM Higgs inclusive cross section, the signal strength is equal to $(\sigma(H)/\sigma_{\text{SM}}(H))\mathcal{B}(H \to aa \to b\bar{b}\tau^+\tau^-)$. Note that the values $s_{c,j}$ and $b_{c,j}$ are themselves functions of the set of NPs. Each systematic uncertainty is fully correlated across all bins and categories.

Categories with very low signal acceptance are suppressed from the likelihood product. For the $m_a = 12$ GeV hypothesis, only the $e\mu$ categories are used. At this mass hypothesis, the cut $\Delta R > 0.2$ between the τ-leptons and lepton removes nearly all signal acceptance. For $m_a > 30$ GeV, the categories with B-jets are similarly not used. Removing these categories does not impact the observed limit due to the lack of signal acceptance. The one-sided alternative likelihood ratio test statistic for upper limits $\tilde{q}_\mu$ [137] was used.

VIII. SYSTEMATIC UNCERTAINTIES

Systematic uncertainties include experimental uncertainties in the reconstructed objects, uncertainties in the data-driven model for the nonprompt-lepton background, and modeling uncertainties in the simulated background and signal samples.

Experimental uncertainties include momentum scale and resolution uncertainties for all reconstructed objects: muons, electrons, hadronic τ-leptons, jets, and missing transverse energy. These uncertainties are estimated by using calibrations performed for each individual object and by comparing them among different simulation models. These uncertainties are considered in the $E_{\text{T}}^{\text{miss}}$ reconstruction, and additional uncertainties for soft tracks are estimated from data [127].

Uncertainties in the reconstruction, identification and trigger efficiency of electrons [56,109] and muons [57,110] are determined from tag-and-probe efficiency measurements using $Z \to \ell^+\ell^-$ and $J/\psi \to \ell^+\ell^-$ events. Similarly, uncertainties in the reconstruction and identification efficiency of τ_{had} are determined from tag-and-probe efficiency measurements using $Z \to \tau_\mu\tau_{\text{had}}$ events (where τ_μ denotes a $\tau \to \mu\nu_\mu\nu_\tau$ decay) and by varying the physical models used for the simulation of hadronic interactions in the detector [123,126]. An additional uncertainty is estimated for the electron-veto efficiency based on a tag-and-probe measurement using $Z \to ee$ events [124].

Uncertainties in the jet vertex tagger efficiency are estimated from efficiency measurements using $Z(\to \mu^+\mu^-)$ events with a single jet recoiling against the dimuon pair [116]. A dedicated efficiency measurement for jets with $15 \leq p_{\text{T}} \leq 20$ GeV was performed for this search.

Uncertainties in the DLlr identification efficiency are estimated from a combination of several measurements sensitive to the true jet flavor. The efficiency is measured in several bins of jet p_{T}, η, and separately for true b-, c-, and light-jets [119–121]. A dedicated efficiency measurement for jets with $15 \leq p_{\text{T}} \leq 20$ GeV was performed for this search. The measurement uses $t\bar{t}$ and $Z + $ jets events to measure the efficiency of the DLlr algorithm in different η bins for b- and non-b-jets (i.e., c- and light-jets, which are considered together in this dedicated measurement). The uncertainties in the flavor-tagging efficiency of at low jet p_{T} are considered uncorrelated with the ones for jet $p_{\text{T}} > 20$ GeV, but the correlations between different jet η bins and between the different true jet flavors are accounted for.

Uncertainties in the DEXTER identification efficiency are estimated from the efficiency measurement using $t\bar{t}$ and $Z(\to \ell\ell) + g(\to bb)$ events [26]. The efficiency and associated uncertainties are determined in bins of jet p_{T}, η, and separately for b- and B-jets. The number of light-jets satisfying the DEXTER identification selection is negligible.

Modeling uncertainties for $t\bar{t}$ and $Z + $ jets background processes and for the Higgs boson signal process are estimated by varying the hard-process renormalization and factorization scales, and by using the NNPDF replicas to estimate PDF uncertainties. For the $t\bar{t}$ background process, additional modeling uncertainties are estimated by comparing the prediction from POWHEG and MADGRAPH5_MC@NLO [138], by varying the renormalization scale used to simulate the initial- and final-state radiation, and by comparing the prediction using PYTHIA and HERWIG [139] as parton showers. For the $Z + $ jets background process, additional modeling uncertainties in the fraction of heavy-flavored associated jets are estimated by varying the resummation (QSF) and merging (CKKM) scales in SHERPA [58,63]. For simplicity, the variations are estimated without detector simulation, but in a fiducial region identical to the one used in the search. In addition to

generator-based estimates, uncertainties associated with the reweighting procedure in the $t\bar{t}$ and Z regions are propagated to the final result.

Several uncorrelated sources of systematic uncertainties are considered for background events with nonprompt leptons. Statistical uncertainties coming from the limited number of events in the regions used to measure the prompt and nonprompt lepton efficiencies are generally negligible. Statistical uncertainties coming from the limited number of

data events with at least one loose lepton are propagated to the final result. In addition to uncertainties of a statistical source, the following uncertainties are considered for background events with nonprompt leptons. Each uncertainty is estimated separately for electrons, muons, and hadronic taus.

(i) Prompt-lepton efficiency: the uncertainty is estimated by comparing the efficiency determined from simulated Z + jets events with the one estimated from simulated $t\bar{t}$ events.
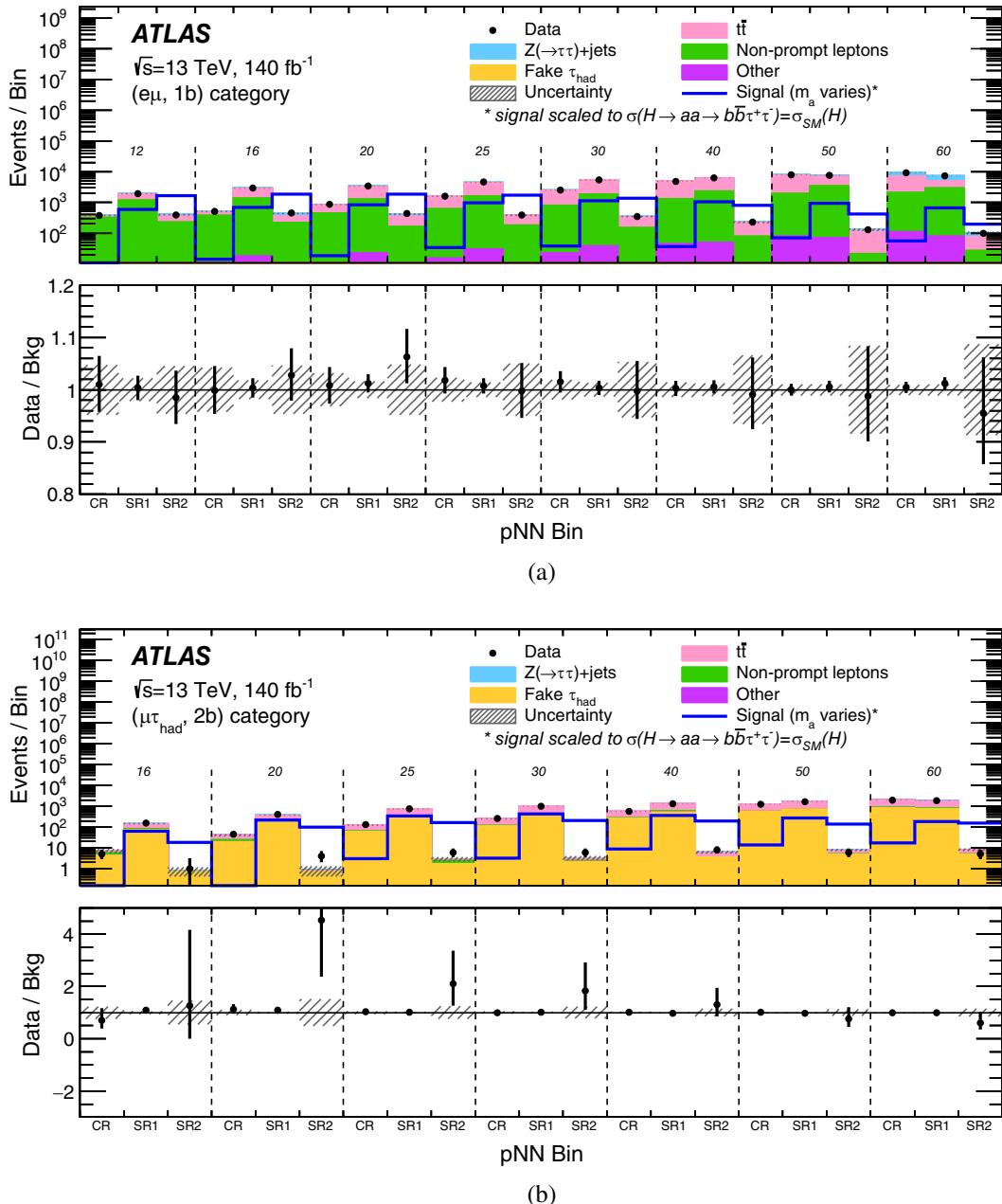
FIG. 8.   The pNN spectrum in the three bins are shown separately for each mass hypothesis in the (a) $(e\mu, 1b)$ and (b) $(\mu\tau_{had}, 2b)$ category. The signal shape (normalized to $\mathcal{B}(H \to aa \to b\bar{b}\tau^+\tau^-) = 1$) for each corresponding mass hypothesis is overlaid on top of the SM prediction. The bins divided by vertical dashed lines are used for testing different m_a hypotheses indicated as a text in the figure. Bins used for different m_a hypotheses are not statistically independent. Note that the 12 GeV mass point is not shown for the $(\mu\tau_{had}, 2b)$ category because the signal acceptance is very low. The hashed area represents the total uncertainty of the background.

(ii) Nonprompt-lepton composition: for electrons and muons, this uncertainty is estimated by comparing the nonprompt-lepton efficiency measured in the different analysis categories with the efficiency measured in a region with zero b- and B-jets. For hadronic taus, this uncertainty is obtained by using the same region without heavy-flavored jets to estimate variations on r_{QCD} and r_{LJVT}.

(iii) Prompt-lepton subtraction: the uncertainty is estimated by varying the cross section of processes with prompt leptons by 30% in the regions used to estimate nonprompt efficiencies.

The uncertainty in the combined 2015-2018 integrated luminosity is 0.83% [55], obtained using the LUCID-2 detector for the main luminosity measurement, and complemented by measurements using the ID and the
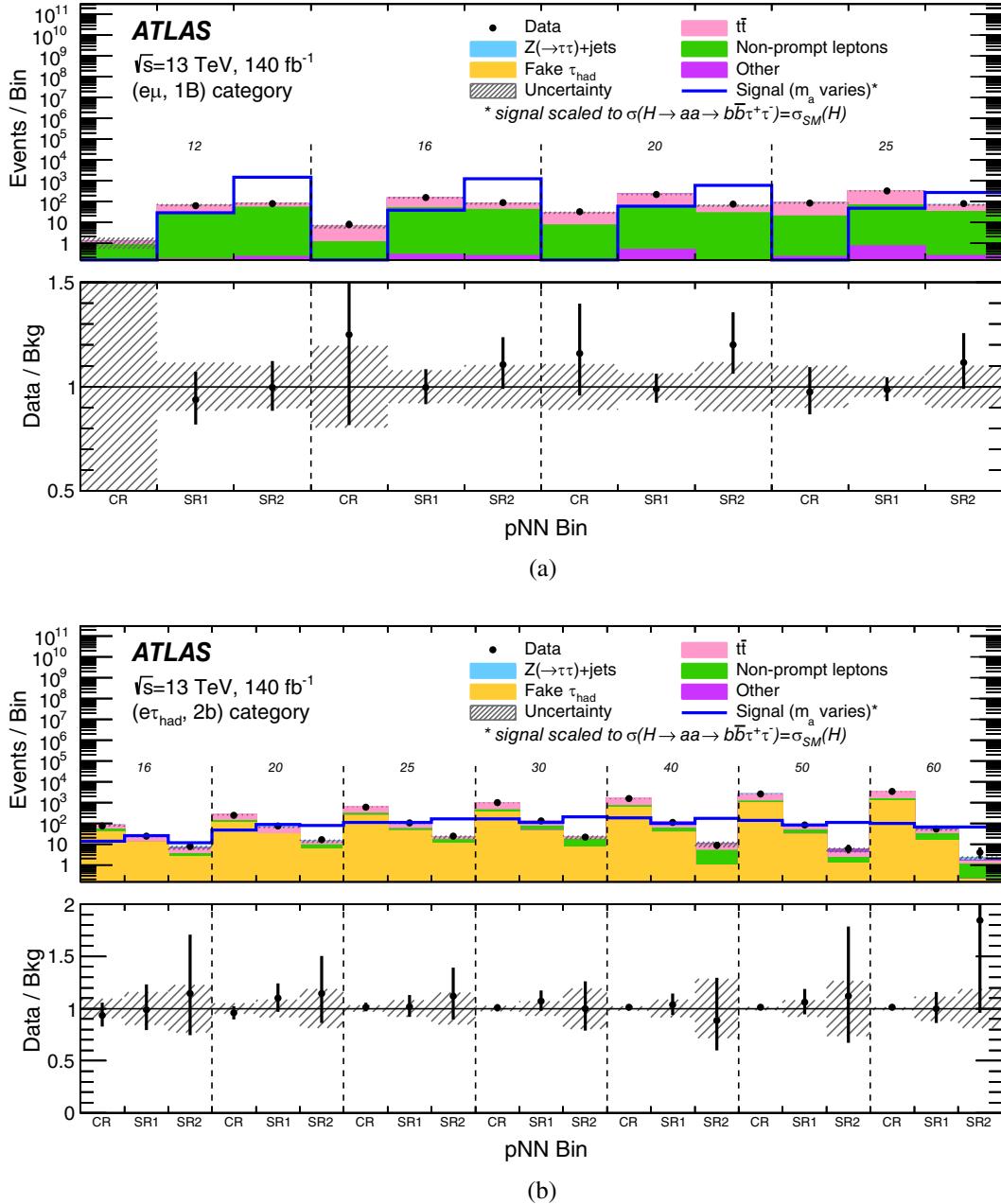
FIG. 9. The pNN spectrum in the three bins are shown separately for each mass hypothesis in the (a) ($e\mu$, 1B) and (b) ($e\tau_{\mathrm{had}}$, 2b) categories. The signal shape (normalized to $\mathcal{B}(H \to aa \to bb\tau\tau) = 1$) for each corresponding mass hypothesis is overlaid on top of the SM prediction. The bins divided by vertical dashed lines are used for testing different m_a hypotheses indicated as a text in the figure. Bins used for different m_a hypotheses are not statistically independent. The hashed area represents the total uncertainty of the background.

calorimeters. The uncertainty in the pileup model is determined by varying the estimate of the inelastic pp cross section between the value estimated by using only the LUCID-2 detector and the value estimated using only the ID.

IX. RESULTS

Different a-boson mass hypotheses are tested $m_a = (12, 16, 20, 25, 30, 40, 50, 60)$ GeV. Figures 8 and 9 show the pNN distribution for each hypothesis in the three pNN bins used this search for the ($e\mu$, 1b) and ($e\tau_{\mathrm{had}}$) categories, respectively. While the $m^{\mathrm{MMC}}(\tau\tau)$ window reduces the correlation between different hypotheses, the events in the histogram for different masses are not completely independent. No significant excess over the background expectation is observed for any m_a hypothesis. The largest deviation is a local p-value of 0.055 at $m_a = 20$ GeV.

Upper limits on $(\sigma(H)/\sigma_{\mathrm{SM}}(H))\mathcal{B}(H \to aa \to b\bar{b}\tau^+\tau^-)$ are determined at 95% confidence level (CL) using the CL$_s$ technique [137] and the $\tilde{q}_\mu$ test statistic described in Sec. VII. The SM Higgs boson production cross section used is $\sigma_{\mathrm{SM}}(H) = 55.7$ pb [140]. Table III shows the

impact of dominant sources of systematic uncertainties in the expected upper limit for different m_a hypotheses. The impact is estimated by the difference between the expected upper limit when only a group of uncertainties are considered and the case where no systematic uncertainty is considered. B-jet identification efficiency uncertainty is an important source of systematic uncertainty at low value of m_a due to the difficulty in measuring the identification efficiency of merged B-jets with low mass and low p_{T}. Figure 10(a) compares the observed upper limits with the expected limits assuming the median value of $\tilde{q}_\mu$ under the background-only hypothesis. Figure 10(b) compares the expected limits for categories with heavy-flavor objects (B- or b-jets). The category using a B-jet is especially sensitive in the low-mass regime, where the $b\bar{b}$ system is collimated into a single object. Regarding the τ-lepton-decay mode, the $\mu\tau_{\mathrm{had}}$ channel dominates the sensitivity, except for the low-mass regime where $e\mu$ dominates due to the isolation criterion, which is corrected for the presence of nearby leptons.

This is the first search in ATLAS for exotic decays of the Higgs boson in the final state $H \to aa \to b\bar{b}\tau^+\tau^-$. The observed limit is up to a factor of two better at low masses when compared to previous results [28] due to the use of a

TABLE III. Impact of different group of systematic uncertainties on the upper limit on $(\sigma(H)/\sigma_{\mathrm{SM}}(H)) \times \mathcal{B}(H \to aa \to b\bar{b}\tau^+\tau^-)$. The different systematic uncertainties group are considered individually in each line of the table. The larger the difference relative to the expected limit without systematic uncertainties (stat-only), the more important the uncertainty group is for the final result. The entries with "–" change by less than 1% relative to the stat-only limit.

	Expected limit on $(\sigma(H)/\sigma_{\mathrm{SM}}(H))\mathcal{B}(H \to aa \to b\bar{b}\tau^+\tau^-)$		
Uncertainty source	$m_a = 12$ GeV	$m_a = 25$ GeV	$m_a = 60$ GeV
Stat-only limit	1.34	1.79	3.00
Observed limit	2.89	2.02	3.37
MC statistics	1.42	1.81	3.04
Experimental	2.72	1.94	3.21
Detector response	2.43	1.84	3.03
Luminosity and pileup	1.37	$\cdots$	$\cdots$
b-tagging	$\cdots$	1.81	$\cdots$
B-tagging	2.35	$\cdots$	$\cdots$
Jet and $E_{\mathrm{T}}^{\mathrm{miss}}$	$\cdots$	1.83	$\cdots$
Electrons	1.36	$\cdots$	$\cdots$
Muons	1.35	$\cdots$	$\cdots$
Taus	$\cdots$	$\cdots$	$\cdots$
Data-driven normalization	1.58	1.94	3.19
Non-prompt leptons	1.58	1.85	3.16
Non-prompt taus	$\cdots$	1.86	3.10
MC reweighting	$\cdots$	$\cdots$	$\cdots$
Theoretical modeling	1.38	1.89	3.04
Signal	$\cdots$	$\cdots$	$\cdots$
Background	1.37	1.87	3.03
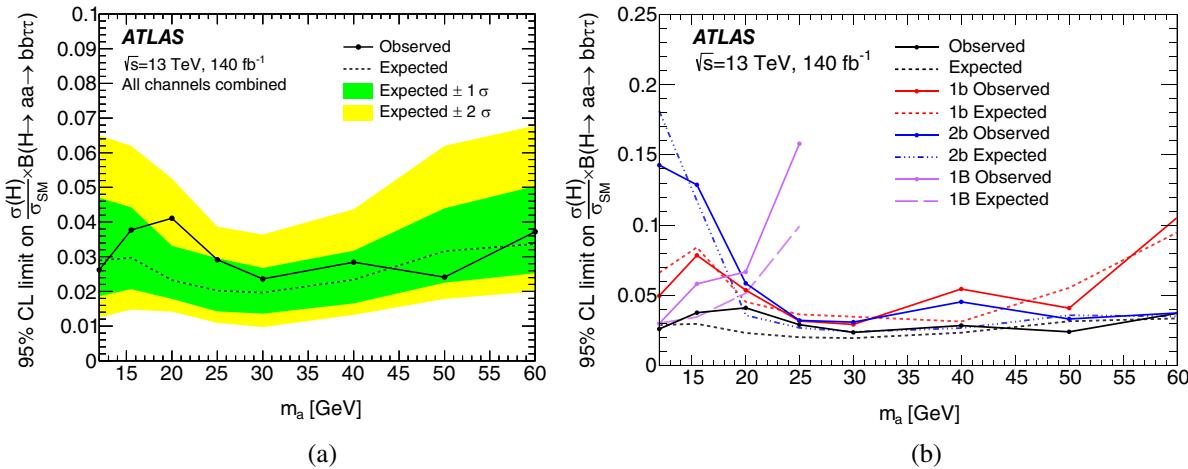
FIG. 10. The observed (solid) 95% C.L. upper limits on $(\sigma(H)/\sigma_{\mathrm{SM}}(H))\mathcal{B}(H \rightarrow aa \rightarrow b\bar{b}\tau^+\tau^-)$ as a function of m_a and the expected (dashed) limits under the background-only hypothesis when (a) combining all categories and (b) considering different categories based on the heavy-flavor objects separately. In the combined plot (a) the inner green and outer yellow shaded bands show the $\pm 1\sigma$ and $\pm 2\sigma$ uncertainties of the expected limits. The mass hypothesis m_a is probed between 12 and 60 GeV for the values shown with markers. A linear interpolation validated with MC simulation between adjacent mass points is used.

novel identification algorithm for low-mass merged B-jets. In several BSM models, final state with b-quarks have large branching ratio and the result provided here can place strict limits on the existence of exotic decays of the Higgs boson.

X. CONCLUSION

This paper presents the first search by the ATLAS experiment for exotic decays of the Higgs boson into a pair of pseudoscalar particles, $H \rightarrow aa$, where the a-boson decays into two b-quarks and two τ-leptons. The analysis is performed using the 140 fb^{-1} of proton–proton collision data at a center-of-mass energy of 13 TeV recorded by the ATLAS detector at the LHC between 2015 and 2018. The search makes use of heavy-flavor-tagging techniques to target collimated $a \rightarrow b\bar{b}$ decays and a mass-parameterized neural network to enhance the sensitivity. The analysis categorizes events depending on the τ-lepton decay modes: $e\mu$, $e\tau_{\mathrm{had}}$, and $\mu\tau_{\mathrm{had}}$, as well as the strategy for identifying heavy-flavor jets: a merged b-jet pair, B-jet, and one or two single b-jets. No significant excess above the SM background expectation is observed, and upper limits at 95% confidence level are set on $\mathcal{B}(H \rightarrow aa \rightarrow b\bar{b}\tau^+\tau^-)$ of 2.2%–3.9% for pseudoscalar mass values in the range 12 GeV $\leq m_a \leq$ 60 GeV, assuming the SM Higgs boson production cross section. These results contribute to the broad program of searches for $H \rightarrow aa$ decays in ATLAS and can be used to set constraints on a variety of BSM scenarios featuring such exotic Higgs decays.

---

[1] ATLAS Collaboration, Observation of a new particle in the search for the Standard Model Higgs boson with the ATLAS detector at the LHC, Phys. Lett. B **716**, 1 (2012).

[2] CMS Collaboration, Observation of a new boson at a mass of 125 GeV with the CMS experiment at the LHC, Phys. Lett. B **716**, 30 (2012).

[3] ATLAS Collaboration, A detailed map of Higgs boson interactions by the ATLAS experiment ten years after the discovery, Nature (London) **607**, 52 (2022); **612**, E24 (2022).

[4] CMS Collaboration, A portrait of the Higgs boson by the CMS experiment ten years after the discovery, Nature (London) **607**, 60 (2022); **623**, E4 (2023).

[5] D. Curtin *et al.*, Exotic decays of the 125 GeV Higgs boson, Phys. Rev. D **90**, 075004 (2014).

[6] B. A. Dobrescu and K. T. Matchev, Light axion within the next-to-minimal supersymmetric standard model, J. High Energy Phys. 09 (2000) 031.

[7] U. Ellwanger, J. F. Gunion, C. Hugonie, and S. Moretti, Towards a no lose theorem for NMSSM Higgs discovery at the LHC, arXiv:hep-ph/0305109.

[8] R. Dermisek and J. F. Gunion, Escaping the large fine tuning and little hierarchy problems in the next to minimal supersymmetric model and $h \to aa$ decays, Phys. Rev. Lett. **95**, 041801 (2005).

[9] S. Chang, R. Dermisek, J. F. Gunion, and N. Weiner, Nonstandard Higgs boson decays, Annu. Rev. Nucl. Part. Sci. **58**, 75 (2008).

[10] D. E. Morrissey and A. Pierce, Modified Higgs boson phenomenology from gauge or gaugino mediation in the NMSSM, Phys. Rev. D **78**, 075029 (2008).

[11] V. Silveira and A. Zee, Scalar phantoms, Phys. Lett. **161B**, 136 (1985).

[12] M. Pospelov, A. Ritz, and M. B. Voloshin, Secluded WIMP dark matter, Phys. Lett. B **662**, 53 (2008).

[13] P. Draper, T. Liu, C. E. M. Wagner, L.-T. Wang, and H. Zhang, Dark light Higgs, Phys. Rev. Lett. **106**, 121805 (2011).

[14] S. Ipek, D. McKeen, and A. E. Nelson, A renormalizable model for the Galactic center gamma ray excess from dark matter annihilation, Phys. Rev. D **90**, 055021 (2014).

[15] A. Martin, J. Shelton, and J. Unwin, Fitting the Galactic center gamma-ray excess with cascade annihilations, Phys. Rev. D **90**, 103513 (2014).

[16] J. Kozaczuk, M. J. Ramsey-Musolf, and J. Shelton, Exotic Higgs boson decays and the electroweak phase transition, Phys. Rev. D **101**, 115035 (2020).

[17] M. Carena, Z. Liu, and Y. Wang, Electroweak phase transition with spontaneous Z_2-breaking, J. High Energy Phys. 08 (2020) 107.

[18] N. Craig, A. Katz, M. Strassler, and R. Sundrum, Naturalness in the dark at the LHC, J. High Energy Phys. 07 (2015) 105.

[19] D. Curtin and C. B. Verhaaren, Discovering uncolored naturalness in exotic Higgs decays, J. High Energy Phys. 12 (2015) 072.

[20] T. Robens and T. Stefaniak, Status of the Higgs singlet extension of the standard model after LHC run 1, Eur. Phys. J. C **75**, 104 (2015).

[21] T. Robens and T. Stefaniak, LHC benchmark scenarios for the real Higgs singlet extension of the standard model, Eur. Phys. J. C **76**, 268 (2016).

[22] T. Robens, T. Stefaniak, and J. Wittbrodt, Two-real-scalar-singlet extension of the SM: LHC phenomenology and benchmark scenarios, Eur. Phys. J. C **80**, 151 (2020).

[23] M. Bauer, M. Neubert, and A. Thamm, Collider probes of axion-like particles, J. High Energy Phys. 12 (2017) 044.

[24] U. Haisch, J. F. Kamenik, A. Malinauskas, and M. Spira, Collider constraints on light pseudoscalars, J. High Energy Phys. 03 (2018) 178.

[25] A. J. Larkoski, I. Moult, and B. Nachman, Jet substructure at the large hadron collider: A review of recent advances in theory and machine learning, Phys. Rep. **841**, 1 (2020).

[26] ATLAS Collaboration, DeXTer: Deep sets based neural networks for low-p_T $X \to b\bar{b}$ identification in ATLAS, Report No. ATL-PHYS-PUB-2022-042, 2022, https://cds.cern.ch/record/2825434.

[27] CMS Collaboration, Search for an exotic decay of the Higgs boson to a pair of light pseudoscalars in the final state with two b quarks and two τ leptons in proton–proton collisions at $\sqrt{s} = 13$ TeV, Phys. Lett. B **785**, 462 (2018).

[28] CMS Collaboration, Search for exotic decays of the Higgs boson to a pair of pseudoscalars in the $\mu\mu$bb and $\tau\tau$bb final states, Eur. Phys. J. C **84**, 493 (2024).

[29] ATLAS Collaboration, Search for new light gauge bosons in Higgs boson decays to four-lepton final states in pp collisions at $\sqrt{s} = 8$ TeV with the ATLAS detector at the LHC, Phys. Rev. D **92**, 092001 (2015).

[30] ATLAS Collaboration, Search for Higgs boson decays to beyond-the-Standard-Model light bosons in four-lepton events with the ATLAS detector at $\sqrt{s} = 13$ TeV, J. High Energy Phys. 06 (2018) 166.

[31] ATLAS Collaboration, Search for Higgs bosons decaying into new spin-0 or spin-1 particles in four-lepton final states with the ATLAS detector with 139 fb^{-1} of pp collision data at $\sqrt{s} = 13$ TeV, J. High Energy Phys. 03 (2022) 041.

[32] ATLAS Collaboration, Search for Higgs bosons decaying to aa in the $\mu\mu\tau\tau$ final state in pp collisions at $\sqrt{s} = 8$ TeV with the ATLAS experiment, Phys. Rev. D **92**, 052002 (2015).

[33] CMS Collaboration, Search for an exotic decay of the Higgs boson to a pair of light pseudoscalars in the final state of two muons and two τ leptons in proton–proton collisions at $\sqrt{s} = 13$ TeV, J. High Energy Phys. 11 (2018) 018.

[34] CMS Collaboration, Search for light pseudoscalar boson pairs produced from decays of the 125 GeV Higgs boson in final states with two muons and two nearby tracks in pp collisions at $\sqrt{s} = 13$ TeV, Phys. Lett. B **800**, 135087 (2020).

[35] CMS Collaboration, Search for a light pseudoscalar Higgs boson in the boosted $\mu\mu\tau\tau$ final state in proton–proton collisions at $\sqrt{s} = 13$ TeV, J. High Energy Phys. 08 (2020) 139.

[36] CMS Collaboration, Search for a very light NMSSM Higgs boson produced in decays of the 125 GeV scalar boson and decaying into τ leptons in pp collisions at $\sqrt{s} = 8$ TeV, J. High Energy Phys. 01 (2016) 079.

[37] ATLAS Collaboration, Search for Higgs boson decays into a pair of light bosons in the $bb\mu\mu$ final state in pp collision at $\sqrt{s} = 13$ TeV with the ATLAS detector, Phys. Lett. B **790**, 1 (2019).

[38] ATLAS Collaboration, Search for Higgs boson decays into a pair of pseudoscalar particles in the $bb\mu\mu$ final state with the ATLAS detector in pp collisions at $\sqrt{s} = 13$ TeV, Phys. Rev. D **105**, 012006 (2022).

[39] CMS Collaboration, Search for light bosons in decays of the 125 GeV Higgs boson in proton–proton collisions at $\sqrt{s} = 8$ TeV, J. High Energy Phys. 10 (2017) 076.

[40] CMS Collaboration, Search for an exotic decay of the Higgs boson to a pair of light pseudoscalars in the final state with two muons and two b quarks in pp collisions at 13 TeV, Phys. Lett. B **795**, 398 (2019).

[41] ATLAS Collaboration, Search for the Higgs boson produced in association with a W boson and decaying to four b-quarks via two spin-zero particles in pp collisions at 13 TeV with the ATLAS detector, Eur. Phys. J. C **76**, 605 (2016).

[42] ATLAS Collaboration, Search for the Higgs boson produced in association with a vector boson and decaying into two spin-zero particles in the $H \to aa \to 4b$ channel in pp collisions at $\sqrt{s} = 13$ TeV with the ATLAS detector, J. High Energy Phys. 10 (2018) 031.

[43] ATLAS Collaboration, Search for Higgs boson decays into two new low-mass spin-0 particles in the $4b$ channel with the ATLAS detector using pp collisions at $\sqrt{s} = 13$ TeV, Phys. Rev. D **102**, 112006 (2020).

[44] ATLAS Collaboration, Search for new phenomena in events with at least three photons collected in pp collisions

at $\sqrt{s} = 8$ TeV with the ATLAS detector, Eur. Phys. J. C **76,** 210 (2016).

[45] CMS Collaboration, Search for the exotic decay of the Higgs boson into two light pseudoscalars with four photons in the final state in proton–proton collisions at $\sqrt{s} = 13$ TeV, J. High Energy Phys. 07 (2023) 148.

[46] CMS Collaboration, Search for exotic Higgs boson decays $H \to \mathcal{A}\mathcal{A} \to 4\gamma$ with events containing two merged diphotons in proton–proton collisions at $\sqrt{s} = 13$ TeV, Phys. Rev. Lett. **131,** 101801 (2023).

[47] ATLAS Collaboration, Search for Higgs boson decays into pairs of light (pseudo)scalar particles in the $\gamma\gamma jj$ final state in pp collisions at $\sqrt{s} = 13$ TeV with the ATLAS detector, Phys. Lett. B **782,** 750 (2018).

[48] ATLAS Collaboration, The ATLAS experiment at the CERN Large Hadron Collider, J. Instrum. **3,** S08003 (2008).

[49] ATLAS Collaboration, ATLAS insertable B-layer: Technical design report, Reports No. ATLAS-TDR-19, No. CERN-LHCC-2010-013, 2010, https://cds.cern.ch/record/1291633; Addendum: Reports No. ATLAS-TDR-19-ADD-1, No. CERN-LHCC-2012-009, 2012, https://cds.cern.ch/record/1451888.

[50] B. Abbott *et al.*, Production and integration of the ATLAS insertable B-layer, J. Instrum. **13,** T05008 (2018).

[51] G. Avoni *et al.*, The new LUCID-2 detector for luminosity measurement and monitoring in ATLAS, J. Instrum. **13,** P07017 (2018).

[52] ATLAS Collaboration, Performance of the ATLAS trigger system in 2015, Eur. Phys. J. C **77,** 317 (2017).

[53] ATLAS Collaboration, Software and computing for Run 3 of the ATLAS experiment at the LHC, arXiv:2404.06335.

[54] ATLAS Collaboration, ATLAS data quality operations and performance for 2015–2018 data-taking, J. Instrum. **15,** P04003 (2020),

[55] ATLAS Collaboration, Luminosity determination in pp collisions at $\sqrt{s} = 13$ TeV using the ATLAS detector at the LHC, Eur. Phys. J. C **83,** 982 (2023).

[56] ATLAS Collaboration, Performance of electron and photon triggers in ATLAS during LHC Run 2, Eur. Phys. J. C **80,** 47 (2020).

[57] ATLAS Collaboration, Performance of the ATLAS muon triggers in Run 2, J. Instrum. **15,** P09015 (2020).

[58] E. Bothmann *et al.*, Event generation with Sherpa 2.2, SciPost Phys. **7,** 034 (2019).

[59] T. Gleisberg and S. Höche, Comix, a new matrix element generator, J. High Energy Phys. 12 (2008) 039.

[60] F. Buccioni, J.-N. Lang, J. M. Lindert, P. Maierhöfer, S. Pozzorini, H. Zhang, and M. F. Zoller, OpenLoops 2, Eur. Phys. J. C **79,** 866 (2019).

[61] F. Cascioli, P. Maierhöfer, and S. Pozzorini, Scattering amplitudes with open loops, Phys. Rev. Lett. **108,** 111601 (2012).

[62] A. Denner, S. Dittmaier, and L. Hofer, Collier: A fortran-based complex one-loop library in extended regularizations, Comput. Phys. Commun. **212,** 220 (2017).

[63] S. Schumann and F. Krauss, A parton shower algorithm based on Catani–Seymour dipole factorisation, J. High Energy Phys. 03 (2008) 038.

[64] S. Höche, F. Krauss, M. Schönherr, and F. Siegert, A critical appraisal of NLO + PS matching methods, J. High Energy Phys. 09 (2012) 049.

[65] S. Höche, F. Krauss, M. Schönherr, and F. Siegert, QCD matrix elements + parton showers. The NLO case, J. High Energy Phys. 04 (2013) 027.

[66] S. Catani, F. Krauss, B. R. Webber, and R. Kuhn, QCD matrix elements + parton showers, J. High Energy Phys. 11 (2001) 063.

[67] S. Höche, F. Krauss, S. Schumann, and F. Siegert, QCD matrix elements and truncated showers, J. High Energy Phys. 05 (2009) 053.

[68] R. D. Ball *et al.* (NNPDF Collaboration), Parton distributions for the LHC run II, J. High Energy Phys. 04 (2015) 040.

[69] C. Anastasiou, L. Dixon, K. Melnikov, and F. Petriello, High-precision QCD at hadron colliders: Electroweak gauge boson rapidity distributions at next-to-next-to leading order, Phys. Rev. D **69,** 094008 (2004).

[70] S. Frixione, G. Ridolfi, and P. Nason, A positive-weight next-to-leading-order Monte Carlo for heavy flavour hadroproduction, J. High Energy Phys. 09 (2007) 126.

[71] P. Nason, A new method for combining NLO QCD with shower Monte Carlo algorithms, J. High Energy Phys. 11 (2004) 040.

[72] S. Frixione, P. Nason, and C. Oleari, Matching NLO QCD computations with parton shower simulations: The POWHEG method, J. High Energy Phys. 11 (2007) 070.

[73] S. Alioli, P. Nason, C. Oleari, and E. Re, NLO single-top production matched with shower in POWHEG: s- and t-channel contributions, J. High Energy Phys. 09 (2009) 111.

[74] ATLAS Collaboration, Studies on top-quark Monte Carlo modelling for Top2016, Report No. ATL-PHYS-PUB-2016-020, 2016, https://cds.cern.ch/record/2216168.

[75] T. Sjöstrand, S. Ask, J. R. Christiansen, R. Corke, N. Desai, P. Ilten, S. Mrenna, S. Prestel, C. O. Rasmussen, and P. Z. Skands, An introduction to PYTHIA 8.2, Comput. Phys. Commun. **191,** 159 (2015).

[76] ATLAS Collaboration, ATLAS Pythia 8 tunes to 7 TeV data, Report No. ATL-PHYS-PUB-2014-021, 2014, https://cds.cern.ch/record/1966419.

[77] R. D. Ball *et al.* (NNPDF Collaboration), Parton distributions with LHC data, Nucl. Phys. **B867,** 244 (2013).

[78] D. J. Lange, The EvtGen particle decay simulation package, Nucl. Instrum. Methods Phys. Res., Sect. A **462,** 152 (2001).

[79] S. Alioli, P. Nason, C. Oleari, and E. Re, A general framework for implementing NLO calculations in shower Monte Carlo programs: The POWHEG BOX, J. High Energy Phys. 06 (2010) 043.

[80] R. Frederix, E. Re, and P. Torrielli, Single-top t-channel hadroproduction in the four-flavour scheme with POWHEG and aMC@NLO, J. High Energy Phys. 09 (2012) 130.

[81] E. Re, Single-top Wt-channel production matched with parton showers using the POWHEG method, Eur. Phys. J. C **71,** 1547 (2011).

[82] K. Hamilton, P. Nason, E. Re, and G. Zanderighi, NNLOPS simulation of Higgs boson production, J. High Energy Phys. 10 (2013) 222.

[83] K. Hamilton, P. Nason, and G. Zanderighi, Finite quark-mass effects in the NNLOPS POWHEG + MiNLO Higgs generator, J. High Energy Phys. 05 (2015) 140.

[84] K. Hamilton, P. Nason, and G. Zanderighi, MINLO: Multi-scale improved NLO, J. High Energy Phys. 10 (2012) 155.

[85] J. M. Campbell, R. Keith Ellis, R. Frederix, P. Nason, C. Oleari, and C. Williams, NLO Higgs boson production plus one and two jets using the POWHEG BOX, Mad-Graph4 and MCFM, J. High Energy Phys. 07 (2012) 092.

[86] K. Hamilton, P. Nason, C. Oleari, and G. Zanderighi, Merging H/W/Z + 0 and 1 jet at NLO with no merging scale: A path to parton shower + NNLO matching, J. High Energy Phys. 05 (2013) 082.

[87] S. Catani and M. Grazzini, Next-to-next-to-leading-order subtraction formalism in hadron collisions and its application to Higgs-boson production at the large hadron collider, Phys. Rev. Lett. **98,** 222002 (2007).

[88] P. Nason and C. Oleari, NLO Higgs boson production via vector-boson fusion matched with shower in POWHEG, J. High Energy Phys. 02 (2010) 037.

[89] J. Butterworth et al., PDF4LHC recommendations for LHC Run II, J. Phys. G **43,** 023001 (2016).

[90] D. de Florian et al., Handbook of LHC Higgs cross sections: 4. Deciphering the nature of the Higgs sector, arXiv:1610.07922.

[91] C. Anastasiou, C. Duhr, F. Dulat, E. Furlan, T. Gehrmann, F. Herzog, A. Lazopoulos, and B. Mistlberger, High precision determination of the gluon fusion Higgs boson cross-section at the LHC, J. High Energy Phys. 05 (2016) 058.

[92] C. Anastasiou, C. Duhr, F. Dulat, F. Herzog, and B. Mistlberger, Higgs boson gluon-fusion production in QCD at three loops, Phys. Rev. Lett. **114,** 212001 (2015).

[93] F. Dulat, A. Lazopoulos, and B. Mistlberger, iHixs 2—Inclusive Higgs cross sections, Comput. Phys. Commun. **233,** 243 (2018).

[94] R. V. Harlander and K. J. Ozeren, Finite top mass effects for hadronic Higgs production at next-to-next-to-leading order, J. High Energy Phys. 11 (2009) 088.

[95] R. V. Harlander and K. J. Ozeren, Top mass effects in Higgs production at next-to-next-to-leading order QCD: Virtual corrections, Phys. Lett. B **679,** 467 (2009).

[96] R. V. Harlander, H. Mantler, S. Marzani, and K. J. Ozeren, Higgs production in gluon fusion at next-to-next-to-leading order QCD for finite top mass, Eur. Phys. J. C **66,** 359 (2010).

[97] A. Pak, M. Rogal, and M. Steinhauser, Finite top quark mass effects in NNLO Higgs boson production at LHC, J. High Energy Phys. 02 (2010) 025.

[98] S. Actis, G. Passarino, C. Sturm, and S. Uccirati, NLO electroweak corrections to Higgs boson production at hadron colliders, Phys. Lett. B **670,** 12 (2008).

[99] S. Actis, G. Passarino, C. Sturm, and S. Uccirati, NNLO computational techniques: The cases $H \to \gamma\gamma$ and $H \to gg$, Nucl. Phys. **B811,** 182 (2009).

[100] M. Bonetti, K. Melnikov, and L. Tancredi, Higher order corrections to mixed QCD-EW contributions to Higgs boson production in gluon fusion, Phys. Rev. D **97,** 056017 (2018); **97,** 099906(E) (2018).

[101] M. Ciccolini, A. Denner, and S. Dittmaier, Strong and electroweak corrections to the production of a Higgs boson +2 jets via weak interactions at the large hadron collider, Phys. Rev. Lett. **99,** 161803 (2007).

[102] M. Ciccolini, A. Denner, and S. Dittmaier, Electroweak and QCD corrections to Higgs production via vector-boson fusion at the CERN LHC, Phys. Rev. D **77,** 013002 (2008).

[103] P. Bolzoni, F. Maltoni, S.-O. Moch, and M. Zaro, Higgs boson production via vector-boson fusion at next-to-next-to-leading order in QCD, Phys. Rev. Lett. **105,** 011801 (2010).

[104] GEANT4 Collaboration, GEANT4–a simulation toolkit, Nucl. Instrum. Methods Phys. Res., Sect. A **506,** 250 (2003).

[105] ATLAS Collaboration, The ATLAS simulation infrastructure, Eur. Phys. J. C **70,** 823 (2010).

[106] T. Sjöstrand, S. Mrenna, and P. Skands, A brief introduction to PYTHIA 8.1, Comput. Phys. Commun. **178,** 852 (2008).

[107] ATLAS Collaboration, The Pythia 8 A3 tune description of ATLAS minimum bias and inelastic measurements incorporating the Donnachie–Landshoff diffractive model, Report No. ATL-PHYS-PUB-2016-017, 2016, https://cds.cern.ch/record/2206965.

[108] ATLAS Collaboration, Vertex reconstruction performance of the ATLAS detector at $\sqrt{s} = 13$ TeV, Report No. ATL-PHYS-PUB-2015-026, 2015, https://cds.cern.ch/record/2037717.

[109] ATLAS Collaboration, Electron and photon performance measurements with the ATLAS detector using the 2015–2017 LHC proton–proton collision data, J. Instrum. **14,** P12006 (2019).

[110] ATLAS Collaboration, Muon reconstruction and identification efficiency in ATLAS using the full Run $2pp$ collision data set at $\sqrt{s} = 13$ TeV, Eur. Phys. J. C **81,** 578 (2021).

[111] M. Cacciari, G. P. Salam, and G. Soyez, The anti-k_t jet clustering algorithm, J. High Energy Phys. 04 (2008) 063.

[112] M. Cacciari, G. P. Salam, and G. Soyez, FastJet user manual, Eur. Phys. J. C **72,** 1896 (2012).

[113] M. Cacciari and G. P. Salam, Dispelling the N^3 myth for the k_t jet-finder, Phys. Lett. B **641,** 57 (2006).

[114] ATLAS Collaboration, Jet reconstruction and performance using particle flow with the ATLAS detector, Eur. Phys. J. C **77,** 466 (2017).

[115] ATLAS Collaboration, Jet energy scale and resolution measured in proton–proton collisions at $\sqrt{s} = 13$ TeV with the ATLAS detector, Eur. Phys. J. C **81,** 689 (2021).

[116] ATLAS Collaboration, Performance of pile-up mitigation techniques for jets in pp collisions at $\sqrt{s} = 8$ TeV using the ATLAS detector, Eur. Phys. J. C **76,** 581 (2016).

[117] S. D. Ellis and D. E. Soper, Successive combination jet algorithm for hadron collisions, Phys. Rev. D **48,** 3160 (1993).

[118] ATLAS Collaboration, ATLAS flavour-tagging algorithms for the LHC Run $2pp$ collision dataset, Eur. Phys. J. C **83,** 681 (2023).

[119] ATLAS Collaboration, ATLAS *b*-jet identification performance and efficiency measurement with $t\bar{t}$ events in pp collisions at $\sqrt{s}$ = 13 TeV, Eur. Phys. J. C **79**, 970 (2019).

[120] ATLAS Collaboration, Measurement of the *c*-jet mistagging efficiency in $t\bar{t}$ events using pp collision data at $\sqrt{s}$ = 13 TeV collected with the ATLAS detector, Eur. Phys. J. C **82**, 95 (2022).

[121] ATLAS Collaboration, Calibration of the light-flavour jet mistagging efficiency of the *b*-tagging algorithms with Z + jets events using 139 fb^{-1} of ATLAS proton–proton collision data at $\sqrt{s}$ = 13 TeV, Eur. Phys. J. C **83**, 728 (2023).

[122] ATLAS Collaboration, Topological cell clustering in the ATLAS calorimeters and its performance in LHC Run 1, Eur. Phys. J. C **77**, 490 (2017).

[123] ATLAS Collaboration, Identification of hadronic tau lepton decays using neural networks in the ATLAS experiment, Report No. ATL-PHYS-PUB-2019-033, 2019, https://cds.cern.ch/record/2688062.

[124] ATLAS Collaboration, Reconstruction, energy calibration, and identification of hadronically decaying tau leptons in the ATLAS experiment for Run-2 of the LHC, Report No. ATL-PHYS-PUB-2015-045, 2015, https://cds.cern.ch/record/2064383.

[125] ATLAS Collaboration, Identification and energy calibration of hadronically decaying tau leptons with the ATLAS experiment in pp collisions at $\sqrt{s}$ = 8 TeV, Eur. Phys. J. C **75**, 303 (2015).

[126] ATLAS Collaboration, Measurement of the tau lepton reconstruction and identification performance in the ATLAS experiment using pp collisions at $\sqrt{s}$ = 13 TeV, Report No. ATLAS-CONF-2017-029, 2017, https://cds.cern.ch/record/2261772.

[127] ATLAS Collaboration, The performance of missing transverse momentum reconstruction and its significance with the ATLAS detector using 140 fb^{-1} of $\sqrt{s}$ = 13 TeV pp collisions, arXiv:2402.05858.

[128] ATLAS Collaboration, Search for charged Higgs bosons decaying into a top quark and a bottom quark at $\sqrt{s}$ = 13 TeV with the ATLAS detector, J. High Energy Phys. 06 (2021) 145.

[129] ATLAS Collaboration, Search for a new scalar resonance in flavour-changing neutral-current top-quark decays $t \to qX (q = u, c)$, with $X \to b\bar{b}$, in proton–proton collisions at $\sqrt{s}$ = 13 TeV with the ATLAS detector, J. High Energy Phys. 07 (2023) 199.

[130] ATLAS Collaboration, Tools for estimating fake/non-prompt lepton backgrounds with the ATLAS detector at the LHC, J. Instrum. **18**, T11004 (2023).

[131] P. Baldi, K. Cranmer, T. Faucett, P. Sadowski, and D. Whiteson, Parameterized neural networks for high-energy physics, Eur. Phys. J. C **76**, 235 (2016).

[132] A. Elagin, P. Murat, A. Pranko, and A. Safonov, A new mass reconstruction technique for resonances decaying to di-tau, Nucl. Instrum. Methods Phys. Res., Sect. A **654**, 481 (2011).

[133] CMS Collaboration, Search for neutral MSSM Higgs bosons decaying to a pair of tau leptons in pp collisions, J. High Energy Phys. 10 (2014) 160.

[134] Objax Developers, Objax, version 1.2.0, 2020, https://github.com/google/objax.

[135] D. P. Kingma and J. Ba, Adam: A method for stochastic optimization, arXiv:1412.6980.

[136] L. Heinrich, M. Feickert, G. Stark, and K. Cranmer, pyhf: Pure-Python implementation of HistFactory statistical models, J. Open Source Softwaare **6**, 2823 (2021).

[137] G. Cowan, K. Cranmer, E. Gross, and O. Vitells, Asymptotic formulae for likelihood-based tests of new physics, Eur. Phys. J. C **71**, 1554 (2011); **73**, 2501(E) (2013).

[138] J. Alwall, R. Frederix, S. Frixione, V. Hirschi, F. Maltoni, O. Mattelaer, H.-S. Shao, T. Stelzer, P. Torrielli, and M. Zaro, The automated computation of tree-level and next-to-leading order differential cross sections, and their matching to parton shower simulations, J. High Energy Phys. 07 (2014) 079.

[139] J. Bellm *et al.*, Herwig 7.0/Herwig + + 3.0 release note, Eur. Phys. J. C **76**, 196 (2016).

[140] J. R. Andersen *et al.*, Handbook of LHC Higgs cross sections: 3. Higgs properties, arXiv:1307.1347.

[141] ATLAS Collaboration, ATLAS computing acknowledgements, Report No. ATL-SOFT-PUB-2023-001, 2023, https://cds.cern.ch/record/2869272.

G. Aad[104] E. Aakvaag[17] B. Abbott[123] S. Abdelhameed[119a] K. Abeling[56] N. J. Abicht[50] S. H. Abidi[30] M. Aboelela[45] A. Aboulhorma[36e] H. Abramowicz[154] H. Abreu[153] Y. Abulaiti[120] B. S. Acharya[70a,70b,b] A. Ackermann[64a] C. Adam Bourdarios[4] L. Adamczyk[87a] S. V. Addepalli[27] M. J. Addison[103] J. Adelman[118] A. Adiguzel[22c] T. Adye[137] A. A. Affolder[139] Y. Afik[40] M. N. Agaras[13] J. Agarwala[74a,74b] A. Aggarwal[102] C. Agheorghiesei[28c] F. Ahmadov[39,c] W. S. Ahmed[106] S. Ahuja[97] X. Ai[63c] G. Aielli[77a,77b] A. Aikot[166] M. Ait Tamlihat[36e] B. Aitbenchikh[36a] M. Akbiyik[102] T. P. A. Åkesson[100] A. V. Akimov[38] D. Akiyama[171] N. N. Akolkar[25] S. Aktas[22a] K. Al Khoury[42] G. L. Alberghi[24b] J. Albert[168] P. Albicocco[54] G. L. Albouy[61] S. Alderweireldt[53] Z. L. Alegria[124] M. Aleksa[37] I. N. Aleksandrov[39] C. Alexa[28b] T. Alexopoulos[10] F. Alfonsi[24b] M. Algren[57] M. Alhroob[170] B. Ali[135] H. M. J. Ali[93] S. Ali[32] S. W. Alibocus[94] M. Aliev[34c] G. Alimonti[72a] W. Alkakhi[56] C. Allaire[67] B. M. M. Allbrooke[149] J. F. Allen[53] C. A. Allendes Flores[140f] P. P. Allport[21] A. Aloisio[73a,73b] F. Alonso[92] C. Alpigiani[141] Z. M. K. Alsolami[93] M. Alvarez Estevez[101] A. Alvarez Fernandez[102] M. Alves Cardoso[57] M. G. Alviggi[73a,73b] M. Aly[103] Y. Amaral Coutinho[84b]

A. Ambler[106] C. Amelung,[37] M. Amerl[103] C. G. Ames[111] D. Amidei[108] B. Amini[55] K. J. Amirie,[158]
S. P. Amor Dos Santos[133a] K. R. Amos[166] D. Amperiadou,[155] S. An,[85] V. Ananiev,[128] C. Anastopoulos,[142]
T. Andeen,[11] J. K. Anders,[37] A. C. Anderson,[60] S. Y. Andrean,[48a,48b] A. Andreazza,[72a,72b] S. Angelidakis,[9]
A. Angerami,[42] A. V. Anisenkov,[38] A. Annovi,[75a] C. Antel,[57] E. Antipov,[148] M. Antonelli,[54] F. Anulli,[76a]
M. Aoki,[85] T. Aoki,[156] M. A. Aparo,[149] L. Aperio Bella,[49] C. Appelt,[19] A. Apyan,[27] S. J. Arbiol Val,[88]
C. Arcangeletti,[54] A. T. H. Arce,[52] J-F. Arguin,[110] S. Argyropoulos,[55] J.-H. Arling,[49] O. Arnaez,[4] H. Arnold,[148]
G. Artoni,[76a,76b] H. Asada,[113] K. Asai,[121] S. Asai,[156] N. A. Asbah,[37] R. A. Ashby Pickering,[170] K. Assamagan,[30]
R. Astalos,[29a] K. S. V. Astrand,[100] S. Atashi,[162] R. J. Atkin,[34a] M. Atkinson,[165] H. Atmani,[36f] P. A. Atmasiddha,[131]
K. Augsten,[135] S. Auricchio,[73a,73b] A. D. Auriol,[21] V. A. Austrup,[103] G. Avolio,[37] K. Axiotis,[57] G. Azuelos,[110,d]
D. Babal,[29b] H. Bachacou,[138] K. Bachas,[155,e] A. Bachiu,[35] F. Backman,[48a,48b] A. Badea,[40] T. M. Baer,[108]
P. Bagnaia,[76a,76b] M. Bahmani,[19] D. Bahner,[55] K. Bai,[126] J. T. Baines,[137] L. Baines,[96] O. K. Baker,[175]
E. Bakos,[16] D. Bakshi Gupta,[8] L. E. Balabram Filho,[84b] V. Balakrishnan,[123] R. Balasubramanian,[117]
E. M. Baldin,[38] P. Balek,[87a] E. Ballabene,[24b,24a] F. Balli,[138] L. M. Baltes,[64a] W. K. Balunas,[33] J. Balz,[102]
I. Bamwidhi,[119b] E. Banas,[88] M. Bandieramonte,[132] A. Bandyopadhyay,[25] S. Bansal,[25] L. Barak,[154]
M. Barakat,[49] E. L. Barberio,[107] D. Barberis,[58b,58a] M. Barbero,[104] M. Z. Barel,[117] T. Barillari,[112]
M-S. Barisits,[37] T. Barklow,[146] P. Baron,[125] D. A. Baron Moreno,[103] A. Baroncelli,[63a] A. J. Barr,[129] J. D. Barr,[98]
F. Barreiro,[101] J. Barreiro Guimarães da Costa,[14] U. Barron,[154] M. G. Barros Teixeira,[133a] S. Barsov,[38]
F. Bartels,[64a] R. Bartoldus,[146] A. E. Barton,[93] P. Bartos,[29a] A. Basan,[102] M. Baselga,[50] A. Bassalat,[67,f]
M. J. Basso,[159a] S. Bataju,[45] R. Bate,[167] R. L. Bates,[60] S. Batlamous,[101] B. Batool,[144] M. Battaglia,[139]
D. Battulga,[19] M. Bauce,[76a,76b] M. Bauer,[80] P. Bauer,[25] L. T. Bazzano Hurrell,[31] J. B. Beacham,[52] T. Beau,[130]
J. Y. Beaucamp,[92] P. H. Beauchemin,[161] P. Bechtle,[25] H. P. Beck,[20,g] K. Becker,[170] A. J. Beddall,[83]
V. A. Bednyakov,[39] C. P. Bee,[148] L. J. Beemster,[16] T. A. Beermann,[37] M. Begalli,[84d] M. Begel,[30] A. Behera,[148]
J. K. Behr,[49] J. F. Beirer,[37] F. Beisiegel,[25] M. Belfkir,[119b] G. Bella,[154] L. Bellagamba,[24b] A. Bellerive,[35]
P. Bellos,[21] K. Beloborodov,[38] D. Benchekroun,[36a] F. Bendebba,[36a] Y. Benhammou,[154] K. C. Benkendorfer,[62]
L. Beresford,[49] M. Beretta,[54] E. Bergeaas Kuutmann,[164] N. Berger,[4] B. Bergmann,[135] J. Beringer,[18a]
G. Bernardi,[5] C. Bernius,[146] F. U. Bernlochner,[25] F. Bernon,[37,104] A. Berrocal Guardia,[13] T. Berry,[97] P. Berta,[136]
A. Berthold,[51] S. Bethke,[112] A. Betti,[76a,76b] A. J. Bevan,[96] N. K. Bhalla,[55] S. Bhatta,[148] D. S. Bhattacharya,[169]
P. Bhattarai,[146] K. D. Bhide,[55] V. S. Bhopatkar,[124] R. M. Bianchi,[132] G. Bianco,[24b,24a] O. Biebel,[111]
R. Bielski,[126] M. Biglietti,[78a] C. S. Billingsley,[45] Y. Bimgdi,[36f] M. Bindi,[56] A. Bingul,[22b] C. Bini,[76a,76b]
G. A. Bird,[33] M. Birman,[172] M. Biros,[136] S. Biryukov,[149] T. Bisanz,[50] E. Bisceglie,[44b,44a] J. P. Biswal,[137]
D. Biswas,[144] I. Bloch,[49] A. Blue,[60] U. Blumenschein,[96] J. Blumenthal,[102] V. S. Bobrovnikov,[38] M. Boehler,[55]
B. Boehm,[169] D. Bogavac,[37] A. G. Bogdanchikov,[38] L. S. Boggia,[130] C. Bohm,[48a] V. Boisvert,[97] P. Bokan,[37]
T. Bold,[87a] M. Bomben,[5] M. Bona,[96] M. Boonekamp,[138] C. D. Booth,[97] A. G. Borbély,[60] I. S. Bordulev,[38]
G. Borissov,[93] D. Bortoletto,[129] D. Boscherini,[24b] M. Bosman,[13] J. D. Bossio Sola,[37] K. Bouaouda,[36a]
N. Bouchhar,[166] L. Boudet,[4] J. Boudreau,[132] E. V. Bouhova-Thacker,[93] D. Boumediene,[41] R. Bouquet,[58b,58a]
A. Boveia,[122] J. Boyd,[37] D. Boye,[30] I. R. Boyko,[39] L. Bozianu,[57] J. Bracinik,[21] N. Brahimi,[4] G. Brandt,[174]
O. Brandt,[33] F. Braren,[49] B. Brau,[105] J. E. Brau,[126] R. Brener,[172] L. Brenner,[117] R. Brenner,[164] S. Bressler,[172]
G. Brianti,[79a,79b] D. Britton,[60] D. Britzger,[112] I. Brock,[25] G. Brooijmans,[42] E. M. Brooks,[159b] E. Brost,[30]
L. M. Brown,[168] L. E. Bruce,[62] T. L. Bruckler,[129] P. A. Bruckman de Renstrom,[88] B. Brüers,[49] A. Bruni,[24b]
G. Bruni,[24b] M. Bruschi,[24b] N. Bruscino,[76a,76b] T. Buanes,[17] Q. Buat,[141] D. Buchin,[112] A. G. Buckley,[60]
O. Bulekov,[38] B. A. Bullard,[146] S. Burdin,[94] C. D. Burgard,[50] A. M. Burger,[37] B. Burghgrave,[8]
O. Burlayenko,[55] J. Burleson,[165] J. T. P. Burr,[33] J. C. Burzynski,[145] E. L. Busch,[42] V. Büscher,[102] P. J. Bussey,[60]
J. M. Butler,[26] C. M. Buttar,[60] J. M. Butterworth,[98] W. Buttinger,[137] C. J. Buxo Vazquez,[109] A. R. Buzykaev,[38]
S. Cabrera Urbán,[166] L. Cadamuro,[67] D. Caforio,[59] H. Cai,[132] Y. Cai,[14,114c] Y. Cai,[114a] V. M. M. Cairo,[37]
O. Cakir,[3a] N. Calace,[37] P. Calafiura,[18a] G. Calderini,[130] P. Calfayan,[69] G. Callea,[60] L. P. Caloba,[84b] D. Calvet,[41]
S. Calvet,[41] M. Calvetti,[75a,75b] R. Camacho Toro,[130] S. Camarda,[37] D. Camarero Munoz,[27] P. Camarri,[77a,77b]
M. T. Camerlingo,[73a,73b] D. Cameron,[37] C. Camincher,[168] M. Campanelli,[98] A. Camplani,[43] V. Canale,[73a,73b]
A. C. Canbay,[3a] E. Canonero,[97] J. Cantero,[166] Y. Cao,[165] F. Capocasa,[27] M. Capua,[44b,44a] A. Carbone,[72a,72b]
R. Cardarelli,[77a] J. C. J. Cardenas,[8] G. Carducci,[44b,44a] T. Carli,[37] G. Carlino,[73a] J. I. Carlotto,[13]

B. T. Carlson [132,h] E. M. Carlson [168,159a] J. Carmignani [94] L. Carminati [72a,72b] A. Carnelli [138] M. Carnesale [76a,76b] S. Caron [116] E. Carquin [140f] S. Carrá [72a] G. Carratta [24b,24a] A. M. Carroll [126] T. M. Carter [53] M. P. Casado [13,l] M. Caspar [49] F. L. Castillo [4] L. Castillo Garcia [13] V. Castillo Gimenez [166] N. F. Castro [133a,133e] A. Catinaccio [37] J. R. Catmore [128] T. Cavaliere [4] V. Cavaliere [30] N. Cavalli [24b,24a] L. J. Caviedes Betancourt [23b] Y. C. Cekmecelioglu [49] E. Celebi [83] S. Cella [37] F. Celli [129] M. S. Centonze [71a,71b] V. Cepaitis [57] K. Cerny [125] A. S. Cerqueira [84a] A. Cerri [149] L. Cerrito [77a,77b] F. Cerutti [18a] B. Cervato [144] A. Cervelli [24b] G. Cesarini [54] S. A. Cetin [83] D. Chakraborty [118] J. Chan [18a] W. Y. Chan [156] J. D. Chapman [33] E. Chapon [138] B. Chargeishvili [152b] D. G. Charlton [21] M. Chatterjee [20] C. Chauhan [136] Y. Che [114a] S. Chekanov [6] S. V. Chekulaev [159a] G. A. Chelkov [39,j] A. Chen [108] B. Chen [154] B. Chen [168] H. Chen [114a] H. Chen [30] J. Chen [63c] J. Chen [145] M. Chen [129] S. Chen [156] S. J. Chen [114a] X. Chen [63c] X. Chen [15,k] Y. Chen [63a] C. L. Cheng [173] H. C. Cheng [65a] S. Cheong [146] A. Cheplakov [39] E. Cheremushkina [49] E. Cherepanova [117] R. Cherkaoui El Moursli [36e] E. Cheu [7] K. Cheung [66] L. Chevalier [138] V. Chiarella [54] G. Chiarelli [75a] N. Chiedde [104] G. Chiodini [71a] A. S. Chisholm [21] A. Chitan [28b] M. Chitishvili [166] M. V. Chizhov [39] K. Choi [11] Y. Chou [141] E. Y. S. Chow [116] K. L. Chu [172] M. C. Chu [65a] X. Chu [14,114c] Z. Chubinidze [54] J. Chudoba [134] J. J. Chwastowski [88] D. Cieri [112] K. M. Ciesla [87a] V. Cindro [95] A. Ciocio [18a] F. Cirotto [73a,73b] Z. H. Citron [172] M. Citterio [72a] D. A. Ciubotaru [28b] A. Clark [57] P. J. Clark [53] N. Clarke Hall [98] C. Clarry [158] J. M. Clavijo Columbie [49] S. E. Clawson [49] C. Clement [48a,48b] Y. Coadou [104] M. Cobal [70a,70c] A. Coccaro [58b] R. F. Coelho Barrue [133a] R. Coelho Lopes De Sa [105] S. Coelli [72a] B. Cole [42] J. Collot [61] P. Conde Muiño [133a,133g] M. P. Connell [34c] S. H. Connell [34c] E. I. Conroy [129] F. Conventi [73a,l] H. G. Cooke [21] A. M. Cooper-Sarkar [129] F. A. Corchia [24b,24a] A. Cordeiro Oudot Choi [130] L. D. Corpe [41] M. Corradi [76a,76b] F. Corriveau [106,m] A. Cortes-Gonzalez [19] M. J. Costa [166] F. Costanza [4] D. Costanzo [142] B. M. Cote [122] J. Couthures [4] G. Cowan [97] K. Cranmer [173] D. Cremonini [24b,24a] S. Crépé-Renaudin [61] F. Crescioli [130] M. Cristinziani [144] M. Cristoforetti [79a,79b] V. Croft [117] J. E. Crosby [124] G. Crosetti [44b,44a] A. Cueto [101] H. Cui [98] Z. Cui [7] W. R. Cunningham [60] F. Curcio [166] J. R. Curran [53] P. Czodrowski [37] M. J. Da Cunha Sargedas De Sousa [58b,58a] J. V. Da Fonseca Pinto [84b] C. Da Via [103] W. Dabrowski [87a] T. Dado [37] S. Dahbi [151] T. Dai [108] D. Dal Santo [20] C. Dallapiccola [105] M. Dam [43] G. D'amen [30] V. D'Amico [111] J. Damp [102] J. R. Dandoy [35] D. Dannheim [37] M. Danninger [145] V. Dao [148] G. Darbo [58b] S. J. Das [30,n] F. Dattola [49] S. D'Auria [72a,72b] A. D'avanzo [73a,73b] C. David [34a] T. Davidek [136] I. Dawson [96] H. A. Day-hall [135] K. De [8] R. De Asmundis [73a] N. De Biase [49] S. De Castro [24b,24a] N. De Groot [116] P. de Jong [117] H. De la Torre [118] A. De Maria [114a] A. De Salvo [76a] U. De Sanctis [77a,77b] F. De Santis [71a,71b] A. De Santo [149] J. B. De Vivie De Regie [61] J. Debevc [95] D. V. Dedovich [39] J. Degens [94] A. M. Deiana [45] F. Del Corso [24b,24a] J. Del Peso [101] L. Delagrange [130] F. Deliot [138] C. M. Delitzsch [50] M. Della Pietra [73a,73b] D. Della Volpe [57] A. Dell'Acqua [37] L. Dell'Asta [72a,72b] M. Delmastro [4] P. A. Delsart [61] S. Demers [175] M. Demichev [39] S. P. Denisov [38] L. D'Eramo [41] D. Derendarz [88] F. Derue [130] P. Dervan [94] K. Desch [25] C. Deutsch [25] F. A. Di Bello [58b,58a] A. Di Ciaccio [77a,77b] L. Di Ciaccio [4] A. Di Domenico [76a,76b] C. Di Donato [73a,73b] A. Di Girolamo [37] G. Di Gregorio [37] A. Di Luca [79a,79b] B. Di Micco [78a,78b] R. Di Nardo [78a,78b] K. F. Di Petrillo [40] M. Diamantopoulou [35] F. A. Dias [117] T. Dias Do Vale [145] M. A. Diaz [140a,140b] F. G. Diaz Capriles [25] A. R. Didenko [39] M. Didenko [166] E. B. Diehl [108] S. Díez Cornell [49] C. Diez Pardos [144] C. Dimitriadi [164] A. Dimitrievska [21] J. Dingfelder [25] T. Dingley [129] I-M. Dinu [28b] S. J. Dittmeier [64b] F. Dittus [37] M. Divisek [136] B. Dixit [94] F. Djama [104] T. Djobava [152b] C. Doglioni [103,100] A. Dohnalova [29a] J. Dolejsi [136] Z. Dolezal [136] K. Domijan [87a] K. M. Dona [40] M. Donadelli [84d] B. Dong [109] J. Donini [41] A. D'Onofrio [73a,73b] M. D'Onofrio [94] J. Dopke [137] A. Doria [73a] N. Dos Santos Fernandes [133a] P. Dougan [103] M. T. Dova [92] A. T. Doyle [60] M. A. Draguet [129] E. Dreyer [172] I. Drivas-koulouris [10] M. Drnevich [120] M. Drozdova [57] D. Du [63a] T. A. du Pree [117] F. Dubinin [38] M. Dubovsky [29a] E. Duchovni [172] G. Duckeck [111] O. A. Ducu [28b] D. Duda [53] A. Dudarev [37] E. R. Duden [27] M. D'uffizi [103] L. Duflot [67] M. Dührssen [37] I. Duminica [28g] A. E. Dumitriu [28b] M. Dunford [64a] S. Dungs [50] K. Dunne [48a,48b] A. Duperrin [104] H. Duran Yildiz [3a] M. Düren [59] A. Durglishvili [152b] B. L. Dwyer [118] G. I. Dyckes [18a] M. Dyndal [87a] B. S. Dziedzic [37] Z. O. Earnshaw [149] G. H. Eberwein [129] B. Eckerova [29a] S. Eggebrecht [56] E. Egidio Purcino De Souza [84e] L. F. Ehrke [57] G. Eigen [17] K. Einsweiler [18a] T. Ekelof [164] P. A. Ekman [100] S. El Farkh [36b] Y. El Ghazali [63a] H. El Jarrari [37] A. El Moussaouy [36a] V. Ellajosyula [164] M. Ellert [164]

F. Ellinghaus[174] N. Ellis[37] J. Elmsheuser[30] M. Elsawy[119a] M. Elsing[37] D. Emeliyanov[137] Y. Enari[85] I. Ene[18a] S. Epari[13] P. A. Erland[88] D. Ernani Martins Neto[88] M. Errenst[174] M. Escalier[67] C. Escobar[166] E. Etzion[154] G. Evans[133a] H. Evans[69] L. S. Evans[97] A. Ezhilov[38] S. Ezzarqtouni[36a] F. Fabbri[24b,24a] L. Fabbri[24b,24a] G. Facini[98] V. Fadeyev[139] R. M. Fakhrutdinov[38] D. Fakoudis[102] S. Falciano[76a] L. F. Falda Ulhoa Coelho[37] F. Fallavollita[112] G. Falsetti[44b,44a] J. Faltova[136] C. Fan[165] K. Y. Fan[65b] Y. Fan[14] Y. Fang[14,114c] M. Fanti[72a,72b] M. Faraj[70a,70b] Z. Farazpay[99] A. Farbin[8] A. Farilla[78a] T. Farooque[109] S. M. Farrington[53] F. Fassi[36e] D. Fassouliotis[9] M. Faucci Giannelli[77a,77b] W. J. Fawcett[33] L. Fayard[67] P. Federic[136] P. Federicova[134] O. L. Fedin[38,j] M. Feickert[173] L. Feligioni[104] D. E. Fellers[126] C. Feng[63b] Z. Feng[117] M. J. Fenton[162] L. Ferencz[49] R. A. M. Ferguson[93] S. I. Fernandez Luengo[140f] P. Fernandez Martinez[13] M. J. V. Fernoux[104] J. Ferrando[93] A. Ferrari[164] P. Ferrari[117,116] R. Ferrari[74a] D. Ferrere[57] C. Ferretti[108] D. Fiacco[76a,76b] F. Fiedler[102] P. Fiedler[135] A. Filipčič[95] E. K. Filmer[1] F. Filthaut[116] M. C. N. Fiolhais[133a,133c,o] L. Fiorini[166] W. C. Fisher[109] T. Fitschen[103] P. M. Fitzhugh[138] I. Fleck[144] P. Fleischmann[108] T. Flick[174] M. Flores[34d,p] L. R. Flores Castillo[65a] L. Flores Sanz De Acedo[37] F. M. Follega[79a,79b] N. Fomin[33] J. H. Foo[158] A. Formica[138] A. C. Forti[103] E. Fortin[37] A. W. Fortman[18a] M. G. Foti[18a] L. Fountas[9,q] D. Fournier[67] H. Fox[93] P. Francavilla[75a,75b] S. Francescato[62] S. Franchellucci[57] M. Franchini[24b,24a] S. Franchino[64a] D. Francis[37] L. Franco[116] V. Franco Lima[37] L. Franconi[49] M. Franklin[62] G. Frattari[27] Y. Y. Frid[154] J. Friend[60] N. Fritzsche[37] A. Froch[55] D. Froidevaux[37] J. A. Frost[129] Y. Fu[63a] S. Fuenzalida Garrido[140f] M. Fujimoto[104] K. Y. Fung[65a] E. Furtado De Simas Filho[84e] M. Furukawa[156] J. Fuster[166] A. Gaa[56] A. Gabrielli[24b,24a] A. Gabrielli[158] P. Gadow[37] G. Gagliardi[58b,58a] L. G. Gagnon[18a] S. Gaid[163] S. Galantzan[154] J. Gallagher[1] E. J. Gallas[129] B. J. Gallop[137] K. K. Gan[122] S. Ganguly[156] Y. Gao[53] F. M. Garay Walls[140a,140b] B. Garcia[30] C. García[166] A. Garcia Alonso[117] A. G. Garcia Caffaro[175] J. E. García Navarro[166] M. Garcia-Sciveres[18a] G. L. Gardner[131] R. W. Gardner[40] N. Garelli[161] D. Garg[81] R. B. Garg[146] J. M. Gargan[53] C. A. Garner[158] C. M. Garvey[34a] V. K. Gassmann[161] G. Gaudio[74a] V. Gautam[13] P. Gauzzi[76a,76b] J. Gavranovic[95] I. L. Gavrilenko[38] A. Gavrilyuk[38] C. Gay[167] G. Gaycken[126] E. N. Gazis[10] A. A. Geanta[28b] C. M. Gee[139] A. Gekow[122] C. Gemme[58b] M. H. Genest[61] A. D. Gentry[115] S. George[97] W. F. George[21] T. Geralis[47] P. Gessinger-Befurt[37] M. E. Geyik[174] M. Ghani[170] K. Ghorbanian[96] A. Ghosal[144] A. Ghosh[162] A. Ghosh[7] B. Giacobbe[24b] S. Giagu[76a,76b] T. Giani[117] A. Giannini[63a] S. M. Gibson[97] M. Gignac[139] D. T. Gil[87b] A. K. Gilbert[87a] B. J. Gilbert[42] D. Gillberg[35] G. Gilles[117] L. Ginabat[130] D. M. Gingrich[2,d] M. P. Giordani[70a,70c] P. F. Giraud[138] G. Giugliarelli[70a,70c] D. Giugni[72a] F. Giuli[37] I. Gkialas[9,q] L. K. Gladilin[38] C. Glasman[101] G. R. Gledhill[126] G. Glemža[49] M. Glisic[126] I. Gnesi[44b,r] Y. Go[30] M. Goblirsch-Kolb[37] B. Gocke[50] D. Godin[110] B. Gokturk[22a] S. Goldfarb[107] T. Golling[57] M. G. D. Gololo[34g] D. Golubkov[38] J. P. Gombas[109] A. Gomes[133a,133b] G. Gomes Da Silva[144] A. J. Gomez Delegido[166] R. Gonçalo[133a] L. Gonella[21] A. Gongadze[152c] F. Gonnella[21] J. L. Gonski[146] R. Y. González Andana[53] S. González de la Hoz[166] R. Gonzalez Lopez[94] C. Gonzalez Renteria[18a] M. V. Gonzalez Rodrigues[49] R. Gonzalez Suarez[164] S. Gonzalez-Sevilla[57] L. Goossens[37] B. Gorini[37] E. Gorini[71a,71b] A. Gorišek[95] T. C. Gosart[131] A. T. Goshaw[52] M. I. Gostkin[39] S. Goswami[124] C. A. Gottardo[37] S. A. Gotz[111] M. Gouighri[36b] V. Goumarre[49] A. G. Goussiou[141] N. Govender[34c] R. P. Grabarczyk[129] I. Grabowska-Bold[87a] K. Graham[35] E. Gramstad[128] S. Grancagnolo[71a,71b] C. M. Grant[1,138] P. M. Gravila[28f] F. G. Gravili[71a,71b] H. M. Gray[18a] M. Greco[71a,71b] M. J. Green[1] C. Grefe[25] A. S. Grefsrud[17] I. M. Gregor[49] K. T. Greif[162] P. Grenier[146] S. G. Grewe[112] A. A. Grillo[139] K. Grimm[32] S. Grinstein[13,s] J.-F. Grivaz[67] E. Gross[172] J. Grosse-Knetter[56] L. Guan[108] J. G. R. Guerrero Rojas[166] G. Guerrieri[37] R. Gugel[102] J. A. M. Guhit[108] A. Guida[19] E. Guilloton[170] S. Guindon[37] F. Guo[14,114c] J. Guo[63c] L. Guo[49] Y. Guo[108] R. Gupta[132] S. Gurbuz[25] S. S. Gurdasani[55] G. Gustavino[76a,76b] P. Gutierrez[123] L. F. Gutierrez Zagazeta[131] M. Gutsche[51] C. Gutschow[98] C. Gwenlan[129] C. B. Gwilliam[94] E. S. Haaland[128] A. Haas[120] M. Habedank[49] C. Haber[18a] H. K. Hadavand[8] A. Hadef[51] S. Hadzic[112] A. I. Hagan[93] J. J. Hahn[144] E. H. Haines[98] M. Haleem[169] J. Haley[124] J. J. Hall[142] G. D. Hallewell[104] L. Halser[20] K. Hamano[168] M. Hamer[25] G. N. Hamity[53] E. J. Hampshire[97] J. Han[63b] K. Han[63a] L. Han[114a] L. Han[63a] S. Han[18a] Y. F. Han[158] K. Hanagaki[85] M. Hance[139] D. A. Hangal[42] H. Hanif[145] M. D. Hank[131] J. B. Hansen[43] P. H. Hansen[43] D. Harada[57] T. Harenberg[174] S. Harkusha[38] M. L. Harris[105] Y. T. Harris[25]

J. Harrison,[13] N. M. Harrison,[122] P. F. Harrison,[170] N. M. Hartman,[112] N. M. Hartmann,[111] R. Z. Hasan,[97,137] Y. Hasegawa,[143] F. Haslbeck,[129] S. Hassan,[17] R. Hauser,[109] C. M. Hawkes,[21] R. J. Hawkings,[37] Y. Hayashi,[156] D. Hayden,[109] C. Hayes,[108] R. L. Hayes,[117] C. P. Hays,[129] J. M. Hays,[96] H. S. Hayward,[94] F. He,[63a] M. He,[14,114c] Y. He,[49] Y. He,[98] N. B. Heatley,[96] V. Hedberg,[100] A. L. Heggelund,[128] N. D. Hehir,[96,a] C. Heidegger,[55] K. K. Heidegger,[55] J. Heilman,[35] S. Heim,[49] T. Heim,[18a] J. G. Heinlein,[131] J. J. Heinrich,[126] L. Heinrich,[112,t] J. Hejbal,[134] A. Held,[173] S. Hellesund,[17] C. M. Helling,[167] S. Hellman,[48a,48b] R. C. W. Henderson,[93] L. Henkelmann,[33] A. M. Henriques Correia,[37] H. Herde,[100] Y. Hernández Jiménez,[148] L. M. Herrmann,[25] T. Herrmann,[51] G. Herten,[55] R. Hertenberger,[111] L. Hervas,[37] M. E. Hesping,[102] N. P. Hessey,[159a] M. Hidaoui,[36b] N. Hidic,[136] E. Hill,[158] S. J. Hillier,[21] J. R. Hinds,[109] F. Hinterkeuser,[25] M. Hirose,[127] S. Hirose,[160] D. Hirschbuehl,[174] T. G. Hitchings,[103] B. Hiti,[95] J. Hobbs,[148] R. Hobincu,[28e] N. Hod,[172] M. C. Hodgkinson,[142] B. H. Hodkinson,[129] A. Hoecker,[37] D. D. Hofer,[108] J. Hofer,[49] T. Holm,[25] M. Holzbock,[37] L. B. A. H. Hommels,[33] B. P. Honan,[103] J. J. Hong,[69] J. Hong,[63c] T. M. Hong,[132] B. H. Hooberman,[165] W. H. Hopkins,[6] M. C. Hoppesch,[165] Y. Horii,[113] S. Hou,[151] A. S. Howard,[95] J. Howarth,[60] J. Hoya,[6] M. Hrabovsky,[125] A. Hrynevich,[49] T. Hryn'ova,[4] P. J. Hsu,[66] S.-C. Hsu,[141] T. Hsu,[67] M. Hu,[18a] Q. Hu,[63a] S. Huang,[65b] X. Huang,[14,114c] Y. Huang,[142] Y. Huang,[102] Y. Huang,[14] Z. Huang,[103] Z. Hubacek,[135] M. Huebner,[25] F. Huegging,[25] T. B. Huffman,[129] C. A. Hugli,[49] M. Huhtinen,[37] S. K. Huiberts,[17] R. Hulsken,[106] N. Huseynov,[12,u] J. Huston,[109] J. Huth,[62] R. Hyneman,[146] G. Iacobucci,[57] G. Iakovidis,[30] L. Iconomidou-Fayard,[67] J. P. Iddon,[37] P. Iengo,[73a,73b] R. Iguchi,[156] Y. Iiyama,[156] T. Iizawa,[129] Y. Ikegami,[85] N. Ilic,[158] H. Imam,[84c] G. Inacio Goncalves,[84d] M. Ince Lezki,[57] T. Ingebretsen Carlson,[48a,48b] J. M. Inglis,[96] G. Introzzi,[74a,74b] M. Iodice,[78a] V. Ippolito,[76a,76b] R. K. Irwin,[94] M. Ishino,[156] W. Islam,[173] C. Issever,[19,49] S. Istin,[22a,v] H. Ito,[171] R. Iuppa,[79a,79b] A. Ivina,[172] J. M. Izen,[46] V. Izzo,[73a] P. Jacka,[134] P. Jackson,[1] C. S. Jagfeld,[111] G. Jain,[159a] P. Jain,[49] K. Jakobs,[55] T. Jakoubek,[172] J. Jamieson,[60] W. Jang,[156] M. Javurkova,[105] P. Jawahar,[103] L. Jeanty,[126] J. Jejelava,[152a,w] P. Jenni,[55,x] C. E. Jessiman,[35] C. Jia,[63b] J. Jia,[148] X. Jia,[14,114c] Z. Jia,[114a] C. Jiang,[53] S. Jiggins,[49] J. Jimenez Pena,[13] S. Jin,[114a] A. Jinaru,[28b] O. Jinnouchi,[157] P. Johansson,[142] K. A. Johns,[7] J. W. Johnson,[139] F. A. Jolly,[49] D. M. Jones,[149] E. Jones,[49] K. S. Jones,[8] P. Jones,[33] R. W. L. Jones,[93] T. J. Jones,[94] H. L. Joos,[56,37] R. Joshi,[122] J. Jovicevic,[16] X. Ju,[18a] J. J. Junggeburth,[105] T. Junkermann,[64a] A. Juste Rozas,[13,s] M. K. Juzek,[88] S. Kabana,[140e] A. Kaczmarska,[88] M. Kado,[112] H. Kagan,[122] M. Kagan,[146] A. Kahn,[131] C. Kahra,[102] T. Kaji,[156] E. Kajomovitz,[153] N. Kakati,[172] I. Kalaitzidou,[55] C. W. Kalderon,[30] N. J. Kang,[139] D. Kar,[34g] K. Karava,[129] M. J. Kareem,[159b] E. Karentzos,[55] O. Karkout,[117] S. N. Karpov,[39] Z. M. Karpova,[39] V. Kartvelishvili,[93] A. N. Karyukhin,[38] E. Kasimi,[155] J. Katzy,[49] S. Kaur,[35] K. Kawade,[143] M. P. Kawale,[123] C. Kawamoto,[89] T. Kawamoto,[63a] E. F. Kay,[37] F. I. Kaya,[161] S. Kazakos,[109] V. F. Kazanin,[38] Y. Ke,[148] J. M. Keaveney,[34a] R. Keeler,[168] G. V. Kehris,[62] J. S. Keller,[35] A. S. Kelly,[98] J. J. Kempster,[149] P. D. Kennedy,[102] O. Kepka,[134] B. P. Kerridge,[137] S. Kersten,[174] B. P. Kerševan,[95] L. Keszeghova,[29a] S. Ketabchi Haghighat,[158] R. A. Khan,[132] A. Khanov,[124] A. G. Kharlamov,[38] T. Kharlamova,[38] E. E. Khoda,[141] M. Kholodenko,[133a] T. J. Khoo,[19] G. Khoriauli,[169] J. Khubua,[152b,a] Y. A. R. Khwaira,[130] B. Kibirige,[34g] D. Kim,[6] D. W. Kim,[48a,48b] Y. K. Kim,[40] N. Kimura,[98] M. K. Kingston,[56] A. Kirchhoff,[56] C. Kirfel,[25] F. Kirfel,[25] J. Kirk,[137] A. E. Kiryunin,[112] C. Kitsaki,[10] O. Kivernyk,[25] M. Klassen,[161] C. Klein,[35] L. Klein,[169] M. H. Klein,[45] S. B. Klein,[57] U. Klein,[94] P. Klimek,[37] A. Klimentov,[30] T. Klioutchnikova,[37] P. Kluit,[117] S. Kluth,[112] E. Kneringer,[80] T. M. Knight,[158] A. Knue,[50] D. Kobylianskii,[172] S. F. Koch,[129] M. Kocian,[146] P. Kodyš,[136] D. M. Koeck,[126] P. T. Koenig,[25] T. Koffas,[35] O. Kolay,[51] I. Koletsou,[4] T. Komarek,[88] K. Köneke,[55] A. X. Y. Kong,[1] T. Kono,[121] N. Konstantinidis,[98] P. Kontaxakis,[57] B. Konya,[100] R. Kopeliansky,[42] S. Koperny,[87a] K. Korcyl,[88] K. Kordas,[155,y] A. Korn,[98] S. Korn,[56] I. Korolkov,[13] N. Korotkova,[38] B. Kortman,[117] O. Kortner,[112] S. Kortner,[112] W. H. Kostecka,[118] V. V. Kostyukhin,[144] A. Kotsokechagia,[37] A. Kotwal,[52] A. Koulouris,[37] A. Kourkoumeli-Charalampidi,[74a,74b] C. Kourkoumelis,[9] E. Kourlitis,[112,t] O. Kovanda,[126] R. Kowalewski,[168] W. Kozanecki,[126] A. S. Kozhin,[38] V. A. Kramarenko,[38] G. Kramberger,[95] P. Kramer,[102] M. W. Krasny,[130] A. Krasznahorkay,[37] A. C. Kraus,[118] J. W. Kraus,[174] J. A. Kremer,[49] T. Kresse,[51] L. Kretschmann,[174] J. Kretzschmar,[94] K. Kreul,[19] P. Krieger,[158] M. Krivos,[136] K. Krizka,[21] K. Kroeninger,[50] H. Kroha,[112] J. Kroll,[134] J. Kroll,[131] K. S. Krowpman,[109] U. Kruchonak,[39] H. Krüger,[25] N. Krumnack,[82] M. C. Kruse,[52] O. Kuchinskaia,[38] S. Kuday,[3a] S. Kuehn,[37] R. Kuesters,[55]

T. Kuhl[49], V. Kukhtin[39], Y. Kulchitsky[38,j], S. Kuleshov[140d,140b], M. Kumar[34g], N. Kumari[49], P. Kumari[159b], A. Kupco[134], T. Kupfer[50], A. Kupich[38], O. Kuprash[55], H. Kurashige[86], L. L. Kurchaninov[159a], O. Kurdysh[67], Y. A. Kurochkin[38], A. Kurova[38], M. Kuze[157], A. K. Kvam[105], J. Kvita[125], T. Kwan[106], N. G. Kyriacou[108], L. A. O. Laatu[104], C. Lacasta[166], F. Lacava[76a,76b], H. Lacker[19], D. Lacour[130], N. N. Lad[98], E. Ladygin[39], A. Lafarge[41], B. Laforge[130], T. Lagouri[175], F. Z. Lahbabi[36a], S. Lai[56], J. E. Lambert[168], S. Lammers[69], W. Lampl[7], C. Lampoudis[155,y], G. Lamprinoudis[102], A. N. Lancaster[118], E. Lançon[30], U. Landgraf[55], M. P. J. Landon[96], V. S. Lang[55], O. K. B. Langrekken[128], A. J. Lankford[162], F. Lanni[37], K. Lantzsch[25], A. Lanza[74a], M. Lanzac Berrocal[166], J. F. Laporte[138], T. Lari[72a], F. Lasagni Manghi[24b], M. Lassnig[37], V. Latonova[134], A. Laurier[153], S. D. Lawlor[142], Z. Lawrence[103], R. Lazaridou[170], M. Lazzaroni[72a,72b], B. Le[103], H. D. M. Le[109], E. M. Le Boulicaut[52], L. T. Le Pottier[18a], B. Leban[24b,24a], A. Lebedev[82], M. LeBlanc[103], F. Ledroit-Guillon[61], S. C. Lee[151], S. Lee[48a,48b], T. F. Lee[94], L. L. Leeuw[34c], H. P. Lefebvre[97], M. Lefebvre[168], C. Leggett[18a], G. Lehmann Miotto[37], M. Leigh[57], W. A. Leight[105], W. Leinonen[116], A. Leisos[155,z], M. A. L. Leite[84c], C. E. Leitgeb[19], R. Leitner[136], K. J. C. Leney[45], T. Lenz[25], S. Leone[75a], C. Leonidopoulos[53], A. Leopold[147], R. Les[109], C. G. Lester[33], M. Levchenko[38], J. Levêque[4], L. J. Levinson[172], G. Levrini[24b,24a], M. P. Lewicki[88], C. Lewis[141], D. J. Lewis[4], L. Lewitt[142], A. Li[5], B. Li[63b], C. Li[63a], C-Q. Li[112], H. Li[63a], H. Li[63b], H. Li[114a], H. Li[15], H. Li[63b], J. Li[63c], K. Li[141], L. Li[63c], M. Li[14,114c], S. Li[14,114c], S. Li[63d,63c], T. Li[5], X. Li[106], Z. Li[129], Z. Li[156], Z. Li[14,114c], Z. Li[63a], Z. Li[14,114c], S. Liang[14,114c], Z. Liang[14], M. Liberatore[138], B. Liberti[77a], K. Lie[65c], J. Lieber Marin[84e], H. Lien[69], H. Lin[108], K. Lin[109], R. E. Lindley[7], J. H. Lindon[2], J. Ling[62], E. Lipeles[131], A. Lipniacka[17], A. Lister[167], J. D. Little[69], B. Liu[14], B. X. Liu[114b], D. Liu[63d,63c], E. H. L. Liu[21], J. B. Liu[63a], J. K. K. Liu[33], K. Liu[63d], K. Liu[63d,63c], M. Liu[63a], M. Y. Liu[63a], P. Liu[14], Q. Liu[63d,141,63c], X. Liu[63a], X. Liu[63b], Y. Liu[114b,114c], Y. L. Liu[63b], Y. W. Liu[63a], S. L. Lloyd[96], E. M. Lobodzinska[49], P. Loch[7], T. Lohse[19], K. Lohwasser[142], E. Loiacono[49], M. Lokajicek[134,a], J. D. Lomas[21], J. D. Long[165], I. Longarini[162], R. Longo[165], I. Lopez Paz[68], A. Lopez Solis[49], N. A. Lopez-canelas[7], N. Lorenzo Martinez[4], A. M. Lory[111], M. Losada[119a], G. Löschcke Centeno[149], O. Loseva[38], X. Lou[48a,48b], X. Lou[14,114c], A. Lounis[67], P. A. Love[93], G. Lu[14,114c], M. Lu[67], S. Lu[131], Y. J. Lu[66], H. J. Lubatti[141], C. Luci[76a,76b], F. L. Lucio Alves[114a], F. Luehring[69], I. Luise[148], O. Lukianchuk[67], O. Lundberg[147], B. Lund-Jensen[147,a], N. A. Luongo[6], M. S. Lutz[37], A. B. Lux[26], D. Lynn[30], R. Lysak[134], E. Lytken[100], V. Lyubushkin[39], T. Lyubushkina[39], M. M. Lyukova[148], M. Firdaus M. Soberi[53], H. Ma[30], K. Ma[63a], L. L. Ma[63b], W. Ma[63a], Y. Ma[124], J. C. MacDonald[102], P. C. Machado De Abreu Farias[84e], R. Madar[41], T. Madula[98], J. Maeda[86], T. Maeno[30], H. Maguire[142], V. Maiboroda[138], A. Maio[133a,133b,133d], K. Maj[87a], O. Majersky[49], S. Majewski[126], N. Makovec[67], V. Maksimovic[16], B. Malaescu[130], Pa. Malecki[88], V. P. Maleev[38], F. Malek[61,aa], M. Mali[95], D. Malito[97], U. Mallik[81], S. Maltezos[10], S. Malyukov[39], S. Mamuzic[13], G. Mancini[54], M. N. Mancini[27], G. Manco[74a,74b], J. P. Mandalia[96], S. S. Mandarry[149], I. Mandić[95], L. Manhaes de Andrade Filho[84a], I. M. Maniatis[172], J. Manjarres Ramos[91], D. C. Mankad[172], A. Mann[111], S. Manzoni[37], L. Mao[63c], X. Mapekula[34c], A. Marantis[155,z], G. Marchiori[5], M. Marcisovsky[134], C. Marcon[72a], M. Marinescu[21], S. Marium[49], M. Marjanovic[123], A. Markhoos[55], M. Markovitch[67], E. J. Marshall[93], Z. Marshall[18a], S. Marti-Garcia[166], J. Martin[98], T. A. Martin[137], V. J. Martin[53], B. Martin dit Latour[17], L. Martinelli[76a,76b], M. Martinez[13,s], P. Martinez Agullo[166], V. I. Martinez Outschoorn[105], P. Martinez Suarez[13], S. Martin-Haugh[137], G. Martinovicova[136], V. S. Martoiu[28b], A. C. Martyniuk[98], A. Marzin[37], D. Mascione[79a,79b], L. Masetti[102], J. Masik[103], A. L. Maslennikov[38], P. Massarotti[73a,73b], P. Mastrandrea[75a,75b], A. Mastroberardino[44b,44a], T. Masubuchi[127], T. Mathisen[164], J. Matousek[136], J. Maurer[28b], T. Maurin[60], A. J. Maury[67], B. Maček[95], D. A. Maximov[38], A. E. May[103], R. Mazini[151], I. Maznas[118], M. Mazza[109], S. M. Mazza[139], E. Mazzeo[72a,72b], C. Mc Ginn[30], J. P. Mc Gowan[168], S. P. Mc Kee[108], C. C. McCracken[167], E. F. McDonald[107], A. E. McDougall[117], J. A. Mcfayden[149], R. P. McGovern[131], R. P. Mckenzie[34g], T. C. Mclachlan[49], D. J. Mclaughlin[98], S. J. McMahon[137], C. M. Mcpartland[94], R. A. McPherson[168,m], S. Mehlhase[111], A. Mehta[94], D. Melini[166], B. R. Mellado Garcia[34g], A. H. Melo[56], F. Meloni[49], A. M. Mendes Jacques Da Costa[103], H. Y. Meng[158], L. Meng[93], S. Menke[112], M. Mentink[37], E. Meoni[44b,44a], G. Mercado[118], S. Merianos[155], C. Merlassino[70a,70c], L. Merola[73a,73b], C. Meroni[72a,72b], J. Metcalfe[6], A. S. Mete[6], E. Meuser[102], C. Meyer[69], J-P. Meyer[138], R. P. Middleton[137], L. Mijović[53], G. Mikenberg[172], M. Mikestikova[134], M. Mikuž[95], H. Mildner[102], A. Milic[37]

D. W. Miller[40] E. H. Miller[146] L. S. Miller[35] A. Milov[172] D. A. Milstead,[48a,48b] T. Min,[114a] A. A. Minaenko[38]
I. A. Minashvili[152b] L. Mince[60] A. I. Mincer[120] B. Mindur[87a] M. Mineev[39] Y. Mino[89] L. M. Mir[13]
M. Miralles Lopez[60] M. Mironova[18a] M. C. Missio[116] A. Mitra[170] V. A. Mitsou[166] Y. Mitsumori[113]
O. Miu[158] P. S. Miyagawa[96] T. Mkrtchyan[64a] M. Mlinarevic[98] T. Mlinarevic[98] M. Mlynarikova[37]
S. Mobius[20] P. Mogg[111] M. H. Mohamed Farook[115] A. F. Mohammed[14,114c] S. Mohapatra[42]
G. Mokgatitswane[34g] L. Moleri[172] B. Mondal[144] S. Mondal[135] K. Mönig[49] E. Monnier[104]
L. Monsonis Romero,[166] J. Montejo Berlingen[13] A. Montella,[48a,48b] M. Montella[122] F. Montereali[78a,78b]
F. Monticelli[92] S. Monzani[70a,70c] A. Morancho Tarda[43] N. Morange[67] A. L. Moreira De Carvalho[49]
M. Moreno Llácer[166] C. Moreno Martinez[57] J. M. Moreno Perez[23b] P. Morettini[58b] S. Morgenstern[37] M. Morii[62]
M. Morinaga[156] F. Morodei[76a,76b] L. Morvaj[37] P. Moschovakos[37] B. Moser[129] M. Mosidze[152b]
T. Moskalets[45] P. Moskvitina[116] J. Moss,[32,bb] P. Moszkowicz[87a] A. Moussa[36d] E. J. W. Moyse[105]
O. Mtintsilana[34g] S. Muanza[104] J. Mueller[132] D. Muenstermann[93] R. Müller[37] G. A. Mullier[164] A. J. Mullin,[33]
J. J. Mullin,[131] D. P. Mungo[158] D. Munoz Perez[166] F. J. Munoz Sanchez[103] M. Murin[103] W. J. Murray[170,137]
M. Muškinja[95] C. Mwewa[30] A. G. Myagkov,[38,j] A. J. Myers[8] G. Myers[108] M. Myska[135] B. P. Nachman[18a]
O. Nackenhorst[50] K. Nagai[129] K. Nagano[85] J. L. Nagle,[30,n] E. Nagy[104] A. M. Nairz[37] Y. Nakahama[85]
K. Nakamura[85] K. Nakkalil[5] H. Nanjo[127] E. A. Narayanan[115] I. Naryshkin[38] L. Nasella[72a,72b] M. Naseri[35]
S. Nasri[119b] C. Nass[25] G. Navarro[23a] J. Navarro-Gonzalez[166] R. Nayak[154] A. Nayaz[19] P. Y. Nechaeva[38]
S. Nechaeva[24b,24a] F. Nechansky[49] L. Nedic[129] T. J. Neep[21] A. Negri[74a,74b] M. Negrini[24b] C. Nellist[117]
C. Nelson[106] K. Nelson[108] S. Nemecek[134] M. Nessi,[37,cc] M. S. Neubauer[165] F. Neuhaus[102] J. Neundorf[49]
P. R. Newman[21] C. W. Ng[132] Y. W. Y. Ng[49] B. Ngair[119a] H. D. N. Nguyen[110] R. B. Nickerson[129]
R. Nicolaidou[138] J. Nielsen[139] M. Niemeyer[56] J. Niermann[56] N. Nikiforou[37] V. Nikolaenko,[38,j]
I. Nikolic-Audit[130] K. Nikolopoulos[21] P. Nilsson[30] I. Ninca[49] G. Ninio[154] A. Nisati[76a] N. Nishu[2]
R. Nisius[112] J-E. Nitschke[51] E. K. Nkadimeng[34g] T. Nobe[156] T. Nommensen[150] M. B. Norfolk[142]
B. J. Norman[35] M. Noury[36a] J. Novak[95] T. Novak[95] L. Novotny[135] R. Novotny[115] L. Nozka[125]
K. Ntekas[162] N. M. J. Nunes De Moura Junior[84d] J. Ocariz[130] A. Ochi[86] I. Ochoa[133a] S. Oerdek,[49,dd]
J. T. Offermann[40] A. Ogrodnik[136] A. Oh[103] C. C. Ohm[147] H. Oide[85] R. Oishi[156] M. L. Ojeda[49]
Y. Okumura[156] L. F. Oleiro Seabra[133a] I. Oleksiyuk[57] S. A. Olivares Pino[140d] G. Oliveira Correa[13]
D. Oliveira Damazio[30] J. L. Oliver[162] Ö. O. Öncel[55] A. P. O'Neill[20] A. Onofre,[133a,133e] P. U. E. Onyisi[11]
M. J. Oreglia[40] G. E. Orellana[92] D. Orestano[78a,78b] N. Orlando[13] R. S. Orr[158] L. M. Osojnak[131]
R. Ospanov,[63a] G. Otero y Garzon[31] H. Otono[90] P. S. Ott[64a] G. J. Ottino[18a] M. Ouchrif[36d] F. Ould-Saada[128]
T. Ovsiannikova[141] M. Owen[60] R. E. Owen[137] V. E. Ozcan[22a] F. Ozturk[88] N. Ozturk[8] S. Ozturk[83]
H. A. Pacey[129] A. Pacheco Pages[13] C. Padilla Aranda[13] G. Padovano[76a,76b] S. Pagan Griso[18a] G. Palacino[69]
A. Palazzo[71a,71b] J. Pampel[25] J. Pan[175] T. Pan[65a] D. K. Panchal[11] C. E. Pandini[117] J. G. Panduro Vazquez[137]
H. D. Pandya[1] H. Pang[15] P. Pani[49] G. Panizzo[70a,70c] L. Panwar[130] L. Paolozzi[57] S. Parajuli[165]
A. Paramonov[6] C. Paraskevopoulos[54] D. Paredes Hernandez[65b] A. Pareti[74a,74b] K. R. Park[42] T. H. Park[158]
M. A. Parker[33] F. Parodi,[58b,58a] E. W. Parrish[118] V. A. Parrish[53] J. A. Parsons[42] U. Parzefall[55]
B. Pascual Dias[110] L. Pascual Dominguez[101] E. Pasqualucci[76a] S. Passaggio[58b] F. Pastore[97] P. Patel[88]
U. M. Patel[52] J. R. Pater[103] T. Pauly[37] C. I. Pazos[161] J. Pearkes[146] M. Pedersen[128] R. Pedro[133a]
S. V. Peleganchuk[38] O. Penc[37] E. A. Pender[53] G. D. Penn[175] K. E. Penski[111] M. Penzin[38] B. S. Peralva[84d]
A. P. Pereira Peixoto[141] L. Pereira Sanchez[146] D. V. Perepelitsa,[30,n] G. Perera[105] E. Perez Codina[159a]
M. Perganti[10] H. Pernegger[37] S. Perrella[76a,76b] O. Perrin[41] K. Peters[49] R. F. Y. Peters[103] B. A. Petersen[37]
T. C. Petersen[43] E. Petit[104] V. Petousis[135] C. Petridou,[155,y] T. Petru[136] A. Petrukhin[144] M. Pettee[18a]
A. Petukhov[38] K. Petukhova[37] R. Pezoa[140f] L. Pezzotti[37] G. Pezzullo[175] T. M. Pham[173] T. Pham[107]
P. W. Phillips[137] G. Piacquadio[148] E. Pianori[18a] F. Piazza[126] R. Piegaia[31] D. Pietreanu[28b] A. D. Pilkington[103]
M. Pinamonti[70a,70c] J. L. Pinfold[2] B. C. Pinheiro Pereira[133a] J. Pinol Bel[13] A. E. Pinto Pinoargote[138,138]
L. Pintucci[70a,70c] K. M. Piper[149] A. Pirttikoski[57] D. A. Pizzi[35] L. Pizzimento[65b] A. Pizzini[117] M.-A. Pleier[30]
V. Pleskot[136] E. Plotnikova,[39] G. Poddar[96] R. Poettgen[100] L. Poggioli[130] I. Pokharel[56] S. Polacek[136]
G. Polesello[74a] A. Poley,[145,159a] A. Polini[24b] C. S. Pollard[170] Z. B. Pollock[122] E. Pompa Pacchi[76a,76b]
N. I. Pond[98] D. Ponomarenko[69] L. Pontecorvo[37] S. Popa[28a] G. A. Popeneciu[28d] A. Poreba[37]

D. M. Portillo Quintero[159a] S. Pospisil[135] M. A. Postill[142] P. Postolache[28c] K. Potamianos[170] P. A. Potepa[87a] I. N. Potrap[39] C. J. Potter[33] H. Potti[150] J. Poveda[166] M. E. Pozo Astigarraga[37] A. Prades Ibanez[77a,77b] J. Pretel[168] D. Price[103] M. Primavera[71a] L. Primomo[70a,70c] M. A. Principe Martin[101] R. Privara[125] T. Procter[60] M. L. Proffitt[141] N. Proklova[131] K. Prokofiev[65c] G. Proto[112] J. Proudfoot[6] M. Przybycien[87a] W. W. Przygoda[87b] A. Psallidas[47] J. E. Puddefoot[142] D. Pudzha[55] D. Pyatiizbyantseva[38] J. Qian[108] D. Qichen[103] Y. Qin[13] T. Qiu[53] A. Quadt[56] M. Queitsch-Maitland[103] G. Quetant[57] R. P. Quinn[167] G. Rabanal Bolanos[62] D. Rafanoharana[55] F. Raffaeli[77a,77b] F. Ragusa[72a,72b] J. L. Rainbolt[40] J. A. Raine[57] S. Rajagopalan[30] E. Ramakoti[38] L. Rambelli[58b,58a] I. A. Ramirez-Berend[35] K. Ran[49,114c] D. S. Rankin[131] N. P. Rapheeha[34g] H. Rasheed[28b] V. Raskina[130] D. F. Rassloff[64a] A. Rastogi[18a] S. Rave[102] S. Ravera[58b,58a] B. Ravina[56] I. Ravinovich[172] M. Raymond[37] A. L. Read[128] N. P. Readioff[142] D. M. Rebuzzi[74a,74b] G. Redlinger[30] A. S. Reed[112] K. Reeves[27] J. A. Reidelsturz[174] D. Reikher[126] A. Rej[50] C. Rembser[37] M. Renda[28b] F. Renner[49] A. G. Rennie[162] A. L. Rescia[49] S. Resconi[72a] M. Ressegotti[58b,58a] S. Rettie[37] J. G. Reyes Rivera[109] E. Reynolds[18a] O. L. Rezanova[38] P. Reznicek[136] H. Riani[36d] N. Ribaric[93] E. Ricci[79a,79b] R. Richter[112] S. Richter[48a,48b] E. Richter-Was[87b] M. Ridel[130] S. Ridouani[36d] P. Rieck[120] P. Riedler[37] E. M. Riefel[48a,48b] J. O. Rieger[117] M. Rijssenbeek[148] M. Rimoldi[37] L. Rinaldi[24b,24a] P. Rincke[56,164] T. T. Rinn[30] M. P. Rinnagel[111] G. Ripellino[164] I. Riu[13] J. C. Rivera Vergara[168] F. Rizatdinova[124] E. Rizvi[96] B. R. Roberts[18a] S. S. Roberts[139] S. H. Robertson[106,m] D. Robinson[33] M. Robles Manzano[102] A. Robson[60] A. Rocchi[77a,77b] C. Roda[75a,75b] S. Rodriguez Bosca[37] Y. Rodriguez Garcia[23a] A. Rodriguez Rodriguez[55] A. M. Rodríguez Vera[118] S. Roe[37] J. T. Roemer[37] A. R. Roepe-Gier[139] O. Røhne[128] R. A. Rojas[105] C. P. A. Roland[130] J. Roloff[30] A. Romaniouk[38] E. Romano[74a,74b] M. Romano[24b] A. C. Romero Hernandez[165] N. Rompotis[94] L. Roos[130] S. Rosati[76a] B. J. Rosser[40] E. Rossi[129] E. Rossi[73a,73b] L. P. Rossi[62] L. Rossini[55] R. Rosten[122] M. Rotaru[28b] B. Rottler[55] C. Rougier[91] D. Rousseau[67] D. Rousso[49] A. Roy[165] S. Roy-Garand[158] A. Rozanov[104] Z. M. A. Rozario[60] Y. Rozen[153] A. Rubio Jimenez[166] A. J. Ruby[94] V. H. Ruelas Rivera[19] T. A. Ruggeri[1] A. Ruggiero[129] A. Ruiz-Martinez[166] A. Rummler[37] Z. Rurikova[55] N. A. Rusakovich[39] H. L. Russell[168] G. Russo[76a,76b] J. P. Rutherfoord[7] S. Rutherford Colmenares[33] M. Rybar[136] E. B. Rye[128] A. Ryzhov[45] J. A. Sabater Iglesias[57] H. F-W. Sadrozinski[139] F. Safai Tehrani[76a] B. Safarzadeh Samani[137] S. Saha[1] M. Sahinsoy[83] A. Saibel[166] M. Saimpert[138] M. Saito[156] T. Saito[156] A. Sala[72a,72b] D. Salamani[37] A. Salnikov[146] J. Salt[166] A. Salvador Salas[154] D. Salvatore[44b,44a] F. Salvatore[149] A. Salzburger[37] D. Sammel[55] E. Sampson[93] D. Sampsonidis[155,y] D. Sampsonidou[126] J. Sánchez[166] V. Sanchez Sebastian[166] H. Sandaker[128] C. O. Sander[49] J. A. Sandesara[105] M. Sandhoff[174] C. Sandoval[23b] L. Sanfilippo[64a] D. P. C. Sankey[137] T. Sano[89] A. Sansoni[54] L. Santi[37,76b] C. Santoni[41] H. Santos[133a,133b] A. Santra[172] E. Sanzani[24b,24a] K. A. Saoucha[163] J. G. Saraiva[133a,133d] J. Sardain[7] O. Sasaki[85] K. Sato[160] C. Sauer[64b] E. Sauvan[4] P. Savard[158,d] R. Sawada[156] C. Sawyer[137] L. Sawyer[99] C. Sbarra[24b] A. Sbrizzi[24b,24a] T. Scanlon[98] J. Schaarschmidt[141] U. Schäfer[102] A. C. Schaffer[67,45] D. Schaile[111] R. D. Schamberger[148] C. Scharf[19] M. M. Schefer[20] V. A. Schegelsky[38] D. Scheirich[136] M. Schernau[162] C. Scheulen[56] C. Schiavi[58b,58a] M. Schioppa[44b,44a] B. Schlag[146,ee] K. E. Schleicher[55] S. Schlenker[37] J. Schmeing[174] M. A. Schmidt[174] K. Schmieden[102] C. Schmitt[102] N. Schmitt[102] S. Schmitt[49] L. Schoeffel[138] A. Schoening[64b] P. G. Scholer[35] E. Schopf[129] M. Schott[25] J. Schovancova[37] S. Schramm[57] T. Schroer[57] H-C. Schultz-Coulon[64a] M. Schumacher[55] B. A. Schumm[139] Ph. Schune[138] A. J. Schuy[141] H. R. Schwartz[139] A. Schwartzman[146] T. A. Schwarz[108] Ph. Schwemling[138] R. Schwienhorst[109] F. G. Sciacca[20] A. Sciandra[30] G. Sciolla[27] F. Scuri[75a] C. D. Sebastiani[94] K. Sedlaczek[118] S. C. Seidel[115] A. Seiden[139] B. D. Seidlitz[42] C. Seitz[49] J. M. Seixas[84b] G. Sekhniaidze[73a] L. Selem[61] N. Semprini-Cesari[24b,24a] D. Sengupta[57] V. Senthilkumar[166] L. Serin[67] M. Sessa[77a,77b] H. Severini[123] F. Sforza[58b,58a] A. Sfyrla[57] Q. Sha[14] E. Shabalina[56] A. H. Shah[33] R. Shaheen[147] J. D. Shahinian[131] D. Shaked Renous[172] L. Y. Shan[14] M. Shapiro[18a] A. Sharma[37] A. S. Sharma[167] P. Sharma[81] P. B. Shatalov[38] K. Shaw[149] S. M. Shaw[103] Q. Shen[63c] D. J. Sheppard[145] P. Sherwood[98] L. Shi[98] X. Shi[14] S. Shimizu[85] C. O. Shimmin[175] J. D. Shinner[97] I. P. J. Shipsey[129] S. Shirabe[90] M. Shiyakova[39,ff] M. J. Shochet[40] D. R. Shope[128] B. Shrestha[123] S. Shrestha[122,gg] M. J. Shroff[168] P. Sicho[134] A. M. Sickles[165] E. Sideras Haddad[34g] A. C. Sidley[117] A. Sidoti[24b] F. Siegert[51] Dj. Sijacki[16] F. Sili[92] J. M. Silva[53]

I. Silva Ferreira,[84b] M. V. Silva Oliveira,[30] S. B. Silverstein,[48a] S. Simion,[67] R. Simoniello,[37] E. L. Simpson,[103] H. Simpson,[149] L. R. Simpson,[108] N. D. Simpson,[100] S. Simsek,[83] S. Sindhu,[56] P. Sinervo,[158] S. Singh,[158] S. Sinha,[49] S. Sinha,[103] M. Sioli,[24b,24a] I. Siral,[37] E. Sitnikova,[49] J. Sjölin,[48a,48b] A. Skaf,[56] E. Skorda,[21] P. Skubic,[123] M. Slawinska,[88] V. Smakhtin,[172] B. H. Smart,[137] S. Yu. Smirnov,[38] Y. Smirnov,[38] L. N. Smirnova,[38,j] O. Smirnova,[100] A. C. Smith,[42] D. R. Smith,[162] E. A. Smith,[40] J. L. Smith,[103] R. Smith,[146] R. Smizanska,[93] K. Smolek,[135] A. A. Snesarev,[38] S. R. Snider,[158] H. L. Snoek,[117] S. Snyder,[30] R. Sobie,[168,m] A. Soffer,[154] C. A. Solans Sanchez,[37] E. Yu. Soldatov,[38] U. Soldevila,[166] A. A. Solodkov,[38] S. Solomon,[27] A. Soloshenko,[39] K. Solovieva,[55] O. V. Solovyanov,[41] P. Sommer,[51] A. Sonay,[13] W. Y. Song,[159b] A. Sopczak,[135] A. L. Sopio,[98] F. Sopkova,[29b] J. D. Sorenson,[115] I. R. Sotarriva Alvarez,[157] V. Sothilingam,[64a] O. J. Soto Sandoval,[140c,140b] S. Sottocornola,[69] R. Soualah,[163] Z. Soumaimi,[36e] D. South,[49] N. Soybelman,[172] S. Spagnolo,[71a,71b] M. Spalla,[112] D. Sperlich,[55] G. Spigo,[37] B. Spisso,[73a,73b] D. P. Spiteri,[60] M. Spousta,[136] E. J. Staats,[35] R. Stamen,[64a] A. Stampekis,[21] M. Standke,[25] E. Stanecka,[88] W. Stanek-Maslouska,[49] M. V. Stange,[51] B. Stanislaus,[18a] M. M. Stanitzki,[49] B. Stapf,[49] E. A. Starchenko,[38] G. H. Stark,[139] J. Stark,[91] P. Staroba,[134] P. Starovoitov,[64a] S. Stärz,[106] R. Staszewski,[88] G. Stavropoulos,[47] P. Steinberg,[30] B. Stelzer,[145,159a] H. J. Stelzer,[132] O. Stelzer-Chilton,[159a] H. Stenzel,[59] T. J. Stevenson,[149] G. A. Stewart,[37] J. R. Stewart,[124] M. C. Stockton,[37] G. Stoicea,[28b] M. Stolarski,[133a] S. Stonjek,[112] A. Straessner,[51] J. Strandberg,[147] S. Strandberg,[48a,48b] M. Stratmann,[174] M. Strauss,[123] T. Strebler,[104] P. Strizenec,[29b] R. Ströhmer,[169] D. M. Strom,[126] R. Stroynowski,[45] A. Strubig,[48a,48b] S. A. Stucci,[30] B. Stugu,[17] J. Stupak,[123] N. A. Styles,[49] D. Su,[146] S. Su,[63a] W. Su,[63d] X. Su,[63a] D. Suchy,[29a] K. Sugizaki,[156] V. V. Sulin,[38] M. J. Sullivan,[94] D. M. S. Sultan,[129] L. Sultanaliyeva,[38] S. Sultansoy,[3b] T. Sumida,[89] S. Sun,[173] O. Sunneborn Gudnadottir,[164] N. Sur,[104] M. R. Sutton,[149] H. Suzuki,[160] M. Svatos,[134] M. Swiatlowski,[159a] T. Swirski,[169] I. Sykora,[29a] M. Sykora,[136] T. Sykora,[136] D. Ta,[102] K. Tackmann,[49,dd] A. Taffard,[162] R. Tafirout,[159a] J. S. Tafoya Vargas,[67] Y. Takubo,[85] M. Talby,[104] A. A. Talyshev,[38] K. C. Tam,[65b] N. M. Tamir,[154] A. Tanaka,[156] J. Tanaka,[156] R. Tanaka,[67] M. Tanasini,[148] Z. Tao,[167] S. Tapia Araya,[140f] S. Tapprogge,[102] A. Tarek Abouelfadl Mohamed,[109] S. Tarem,[153] K. Tariq,[14] G. Tarna,[28b] G. F. Tartarelli,[72a] M. J. Tartarin,[91] P. Tas,[136] M. Tasevsky,[134] E. Tassi,[44b,44a] A. C. Tate,[165] G. Tateno,[156] Y. Tayalati,[36e,hh] G. N. Taylor,[107] W. Taylor,[159b] R. Teixeira De Lima,[146] P. Teixeira-Dias,[97] J. J. Teoh,[158] K. Terashi,[156] J. Terron,[101] S. Terzo,[13] M. Testa,[54] R. J. Teuscher,[158,m] A. Thaler,[80] O. Theiner,[57] N. Themistokleous,[53] T. Theveneaux-Pelzer,[104] O. Thielmann,[174] D. W. Thomas,[97] J. P. Thomas,[21] E. A. Thompson,[18a] P. D. Thompson,[21] E. Thomson,[131] R. E. Thornberry,[45] C. Tian,[63a] Y. Tian,[56] V. Tikhomirov,[38,j] Yu. A. Tikhonov,[38] S. Timoshenko,[38] D. Timoshyn,[136] E. X. L. Ting,[1] P. Tipton,[175] A. Tishelman-Charny,[30] S. H. Tlou,[34g] K. Todome,[157] S. Todorova-Nova,[136] S. Todt,[51] L. Toffolin,[70a,70c] M. Togawa,[85] J. Tojo,[90] S. Tokár,[29a] K. Tokushuku,[85] O. Toldaiev,[69] M. Tomoto,[85,113] L. Tompkins,[146,ee] K. W. Topolnicki,[87b] E. Torrence,[126] H. Torres,[91] E. Torró Pastor,[166] M. Toscani,[31] C. Tosciri,[40] M. Tost,[11] D. R. Tovey,[142] I. S. Trandafir,[28b] T. Trefzger,[169] A. Tricoli,[30] I. M. Trigger,[159a] S. Trincaz-Duvoid,[130] D. A. Trischuk,[27] B. Trocmé,[61] A. Tropina,[39] L. Truong,[34c] M. Trzebinski,[88] A. Trzupek,[88] F. Tsai,[148] M. Tsai,[108] A. Tsiamis,[155] P. V. Tsiareshka,[38] S. Tsigaridas,[159a] A. Tsirigotis,[155,z] V. Tsiskaridze,[158] E. G. Tskhadadze,[152a] M. Tsopoulou,[155] Y. Tsujikawa,[89] I. I. Tsukerman,[38] V. Tsulaia,[18a] S. Tsuno,[85] K. Tsuri,[121] D. Tsybychev,[148] Y. Tu,[65b] A. Tudorache,[28b] V. Tudorache,[28b] A. N. Tuna,[62] S. Turchikhin,[58b,58a] I. Turk Cakir,[3a] R. Turra,[72a] T. Turtuvshin,[39] P. M. Tuts,[42] S. Tzamarias,[155,y] E. Tzovara,[102] F. Ukegawa,[160] P. A. Ulloa Poblete,[140c,140b] E. N. Umaka,[30] G. Unal,[37] A. Undrus,[30] G. Unel,[162] J. Urban,[29b] P. Urrejola,[140a] G. Usai,[8] R. Ushioda,[157] M. Usman,[110] F. Ustuner,[53] Z. Uysal,[83] V. Vacek,[135] B. Vachon,[106] T. Vafeiadis,[37] A. Vaitkus,[98] C. Valderanis,[111] E. Valdes Santurio,[48a,48b] M. Valente,[159a] S. Valentinetti,[24b,24a] A. Valero,[166] E. Valiente Moreno,[166] A. Vallier,[91] J. A. Valls Ferrer,[166] D. R. Van Arneman,[117] T. R. Van Daalen,[141] A. Van Der Graaf,[50] P. Van Gemmeren,[6] M. Van Rijnbach,[37] S. Van Stroud,[98] I. Van Vulpen,[117] P. Vana,[136] M. Vanadia,[77a,77b] W. Vandelli,[37] E. R. Vandewall,[124] D. Vannicola,[154] L. Vannoli,[54] R. Vari,[76a] E. W. Varnes,[7] C. Varni,[18b] T. Varol,[151] D. Varouchas,[67] L. Varriale,[166] K. E. Varvell,[150] M. E. Vasile,[28b] L. Vaslin,[85] G. A. Vasquez,[168] A. Vasyukov,[39] L. M. Vaughan,[124] R. Vavricka,[102] T. Vazquez Schroeder,[37] J. Veatch,[32] V. Vecchio,[103] M. J. Veen,[105] I. Veliscek,[30] L. M. Veloce,[158] F. Veloso,[133a,133c] S. Veneziano,[76a] A. Ventura,[71a,71b] S. Ventura Gonzalez,[138] A. Verbytskyi,[112] M. Verducci,[75a,75b] C. Vergis,[96] M. Verissimo De Araujo,[84b]

W. Verkerke[117], J. C. Vermeulen[117], C. Vernieri[146], M. Vessella[105], M. C. Vetterli[145,d], A. Vgenopoulos[102], N. Viaux Maira[140f], T. Vickey[142], O. E. Vickey Boeriu[142], G. H. A. Viehhauser[129], L. Vigani[64b], M. Vigl[112], M. Villa[24b,24a], M. Villaplana Perez[166], E. M. Villhauer[53], E. Vilucchi[54], M. G. Vincter[35], A. Visibile[117], C. Vittori[37], I. Vivarelli[24b,24a], E. Voevodina[112], F. Vogel[111], J. C. Voigt[51], P. Vokac[135], Yu. Volkotrub[87b], J. Von Ahnen[49], E. Von Toerne[25], B. Vormwald[37], V. Vorobel[136], K. Vorobev[38], M. Vos[166], K. Voss[144], M. Vozak[117], L. Vozdecky[123], N. Vranjes[16], M. Vranjes Milosavljevic[16], M. Vreeswijk[117], N. K. Vu[63d,63c], R. Vuillermet[37], O. Vujinovic[102], I. Vukotic[40], S. Wada[160], C. Wagner[105], J. M. Wagner[18a], W. Wagner[174], S. Wahdan[174], H. Wahlberg[92], J. Walder[137], R. Walker[111], W. Walkowiak[144], A. Wall[131], E. J. Wallin[100], T. Wamorkar[6], A. Z. Wang[139], C. Wang[102], C. Wang[11], H. Wang[18a], J. Wang[65c], P. Wang[98], R. Wang[62], R. Wang[6], S. M. Wang[151], S. Wang[63b], S. Wang[14], T. Wang[63a], W. T. Wang[81], W. Wang[14], X. Wang[114a], X. Wang[165], X. Wang[63c], Y. Wang[63d], Y. Wang[114a], Y. Wang[63a], Z. Wang[108], Z. Wang[63d,52,63c], Z. Wang[108], A. Warburton[106], R. J. Ward[21], N. Warrack[60], S. Waterhouse[97], A. T. Watson[21], H. Watson[60], M. F. Watson[21], E. Watton[60,137], G. Watts[141], B. M. Waugh[98], J. M. Webb[55], C. Weber[30], H. A. Weber[19], M. S. Weber[20], S. M. Weber[64a], C. Wei[63a], Y. Wei[55], A. R. Weidberg[129], E. J. Weik[120], J. Weingarten[50], C. Weiser[55], C. J. Wells[49], T. Wenaus[30], B. Wendland[50], T. Wengler[37], N. S. Wenke[112], N. Wermes[25], M. Wessels[64a], A. M. Wharton[93], A. S. White[62], A. White[8], M. J. White[1], D. Whiteson[162], L. Wickremasinghe[127], W. Wiedenmann[173], M. Wielers[137], C. Wiglesworth[43], D. J. Wilbern[123], H. G. Wilkens[37], J. J. H. Wilkinson[33], D. M. Williams[42], H. H. Williams[131], S. Williams[33], S. Willocq[105], B. J. Wilson[103], P. J. Windischhofer[40], F. I. Winkel[31], F. Winklmeier[126], B. T. Winter[55], J. K. Winter[103], M. Wittgen[146], M. Wobisch[99], T. Wojtkowski[61], Z. Wolffs[117], J. Wollrath[162], M. W. Wolter[88], H. Wolters[133a,133c], M. C. Wong[139], E. L. Woodward[42], S. D. Worm[49], B. K. Wosiek[88], K. W. Woźniak[88], S. Wozniewski[56], K. Wraight[60], C. Wu[21], M. Wu[114b], M. Wu[116], S. L. Wu[173], X. Wu[57], Y. Wu[63a], Z. Wu[4], J. Wuerzinger[112,t], T. R. Wyatt[103], B. M. Wynne[53], S. Xella[43], L. Xia[114a], M. Xia[15], M. Xie[63a], S. Xin[14,114c], A. Xiong[126], J. Xiong[18a], D. Xu[14], H. Xu[63a], L. Xu[63a], R. Xu[131], T. Xu[108], Y. Xu[15], Z. Xu[53], Z. Xu[114a], B. Yabsley[150], S. Yacoob[34a], Y. Yamaguchi[85], E. Yamashita[156], H. Yamauchi[160], T. Yamazaki[18a], Y. Yamazaki[86], J. Yan[63c], S. Yan[60], Z. Yan[105], H. J. Yang[63c,63d], H. T. Yang[63a], S. Yang[63a], T. Yang[65c], X. Yang[37], X. Yang[14], Y. Yang[45], Y. Yang[63a], Z. Yang[63a], W-M. Yao[18a], H. Ye[114a], H. Ye[56], J. Ye[14], S. Ye[30], X. Ye[63a], Y. Yeh[98], I. Yeletskikh[39], B. K. Yeo[18b], M. R. Yexley[98], T. P. Yildirim[129], P. Yin[42], K. Yorita[171], S. Younas[28b], C. J. S. Young[37], C. Young[146], C. Yu[14,114c], Y. Yu[63a], J. Yuan[14,114c], M. Yuan[108], R. Yuan[63d,63c], L. Yue[98], M. Zaazoua[63a], B. Zabinski[88], E. Zaid[53], Z. K. Zak[88], T. Zakareishvili[166], S. Zambito[57], J. A. Zamora Saa[140d,140b], J. Zang[156], D. Zanzi[55], O. Zaplatilek[135], C. Zeitnitz[174], H. Zeng[14], J. C. Zeng[165], D. T. Zenger Jr.[27], O. Zenin[38], T. Ženiš[29a], S. Zenz[96], S. Zerradi[36a], D. Zerwas[67], M. Zhai[14,114c], D. F. Zhang[142], J. Zhang[63b], J. Zhang[6], K. Zhang[14,114c], L. Zhang[63a], L. Zhang[114a], P. Zhang[14,114c], R. Zhang[173], S. Zhang[108], S. Zhang[91], T. Zhang[156], X. Zhang[63c], X. Zhang[63b], Y. Zhang[63c], Y. Zhang[98], Y. Zhang[114a], Z. Zhang[18a], Z. Zhang[63b], Z. Zhang[67], H. Zhao[141], T. Zhao[63b], Y. Zhao[139], Z. Zhao[63a], Z. Zhao[63a], A. Zhemchugov[39], J. Zheng[114a], K. Zheng[165], X. Zheng[63a], Z. Zheng[146], D. Zhong[165], B. Zhou[108], H. Zhou[7], N. Zhou[63c], Y. Zhou[15], Y. Zhou[114a], Y. Zhou[7], C. G. Zhu[63b], J. Zhu[108], X. Zhu[63d], Y. Zhu[63c], Y. Zhu[63a], X. Zhuang[14], K. Zhukov[69], N. I. Zimine[39], J. Zinsser[64b], M. Ziolkowski[144], L. Živković[16], A. Zoccoli[24b,24a], K. Zoch[62], T. G. Zorbas[142], O. Zormpa[47], W. Zou[42], and L. Zwalinski[37]

(ATLAS Collaboration)

[1]*Department of Physics, University of Adelaide, Adelaide, Australia*
[2]*Department of Physics, University of Alberta, Edmonton, Alberta, Canada*
[3a]*Department of Physics, Ankara University, Ankara, Türkiye*
[3b]*Division of Physics, TOBB University of Economics and Technology, Ankara, Türkiye*
[4]*LAPP, Université Savoie Mont Blanc, CNRS/IN2P3, Annecy, France*
[5]*APC, Université Paris Cité, CNRS/IN2P3, Paris, France*
[6]*High Energy Physics Division, Argonne National Laboratory, Argonne, Illinois, USA*
[7]*Department of Physics, University of Arizona, Tucson, Arizona, USA*
[8]*Department of Physics, University of Texas at Arlington, Arlington, Texas, USA*
[9]*Physics Department, National and Kapodistrian University of Athens, Athens, Greece*

[10]*Physics Department, National Technical University of Athens, Zografou, Greece*

[11]*Department of Physics, University of Texas at Austin, Austin, Texas, USA*

[12]*Institute of Physics, Azerbaijan Academy of Sciences, Baku, Azerbaijan*

[13]*Institut de Física d'Altes Energies (IFAE), Barcelona Institute of Science and Technology, Barcelona, Spain*

[14]*Institute of High Energy Physics, Chinese Academy of Sciences, Beijing, China*

[15]*Physics Department, Tsinghua University, Beijing, China*

[16]*Institute of Physics, University of Belgrade, Belgrade, Serbia*

[17]*Department for Physics and Technology, University of Bergen, Bergen, Norway*

[18a]*Physics Division, Lawrence Berkeley National Laboratory, Berkeley, California, USA*

[18b]*University of California, Berkeley, California, USA*

[19]*Institut für Physik, Humboldt Universität zu Berlin, Berlin, Germany*

[20]*Albert Einstein Center for Fundamental Physics and Laboratory for High Energy Physics, University of Bern, Bern, Switzerland*

[21]*School of Physics and Astronomy, University of Birmingham, Birmingham, United Kingdom*

[22a]*Department of Physics, Bogazici University, Istanbul, Türkiye*

[22b]*Department of Physics Engineering, Gaziantep University, Gaziantep, Türkiye*

[22c]*Department of Physics, Istanbul University, Istanbul, Türkiye*

[23a]*Facultad de Ciencias y Centro de Investigaciónes, Universidad Antonio Nariño, Bogotá, Colombia*

[23b]*Departamento de Física, Universidad Nacional de Colombia, Bogotá, Colombia*

[24a]*Dipartimento di Fisica e Astronomia A. Righi, Università di Bologna, Bologna, Italy*

[24b]*INFN Sezione di Bologna, Italy*

[25]*Physikalisches Institut, Universität Bonn, Bonn, Germany*

[26]*Department of Physics, Boston University, Boston, Massachusetts, USA*

[27]*Department of Physics, Brandeis University, Waltham, Massachusetts, USA*

[28a]*Transilvania University of Brasov, Brasov, Romania*

[28b]*Horia Hulubei National Institute of Physics and Nuclear Engineering, Bucharest, Romania*

[28c]*Department of Physics, Alexandru Ioan Cuza University of Iasi, Iasi, Romania*

[28d]*National Institute for Research and Development of Isotopic and Molecular Technologies, Physics Department, Cluj-Napoca, Romania*

[28e]*National University of Science and Technology Politechnica, Bucharest, Romania*

[28f]*West University in Timisoara, Timisoara, Romania*

[28g]*Faculty of Physics, University of Bucharest, Bucharest, Romania*

[29a]*Faculty of Mathematics, Physics and Informatics, Comenius University, Bratislava, Slovak Republic*

[29b]*Department of Subnuclear Physics, Institute of Experimental Physics of the Slovak Academy of Sciences, Kosice, Slovak Republic*

[30]*Physics Department, Brookhaven National Laboratory, Upton, New York, USA*

[31]*Universidad de Buenos Aires, Facultad de Ciencias Exactas y Naturales, Departamento de Física, y CONICET, Instituto de Física de Buenos Aires (IFIBA), Buenos Aires, Argentina*

[32]*California State University, East Bay, Hayward, California, USA*

[33]*Cavendish Laboratory, University of Cambridge, Cambridge, United Kingdom*

[34a]*Department of Physics, University of Cape Town, Cape Town, South Africa*

[34b]*iThemba Labs, Western Cape, South Africa*

[34c]*Department of Mechanical Engineering Science, University of Johannesburg, Johannesburg, South Africa*

[34d]*National Institute of Physics, University of the Philippines Diliman (Philippines), Philippines*

[34e]*University of South Africa, Department of Physics, Pretoria, South Africa*

[34f]*University of Zululand, KwaDlangezwa, South Africa*

[34g]*School of Physics, University of the Witwatersrand, Johannesburg, South Africa*

[35]*Department of Physics, Carleton University, Ottawa, Ontario, Canada*

[36a]*Faculté des Sciences Ain Chock, Réseau Universitaire de Physique des Hautes Energies - Université Hassan II, Casablanca, Morocco*

[36b]*Faculté des Sciences, Université Ibn-Tofail, Kénitra, Morocco*

[36c]*Faculté des Sciences Semlalia, Université Cadi Ayyad, LPHEA-Marrakech, Morocco*

[36d]*LPMR, Faculté des Sciences, Université Mohamed Premier, Oujda, Morocco*

[36e]*Faculté des sciences, Université Mohammed V, Rabat, Morocco*

[36f]*Institute of Applied Physics, Mohammed VI Polytechnic University, Ben Guerir, Morocco*

[37]*CERN, Geneva, Switzerland*

[38]*Affiliated with an institute covered by a cooperation agreement with CERN*

[39]*Affiliated with an international laboratory covered by a cooperation agreement with CERN*

[40]Enrico Fermi Institute, University of Chicago, Chicago, Illinois, USA

[41]LPC, Université Clermont Auvergne, CNRS/IN2P3, Clermont-Ferrand, France

[42]Nevis Laboratory, Columbia University, Irvington, New York, USA

[43]Niels Bohr Institute, University of Copenhagen, Copenhagen, Denmark

[44a]Dipartimento di Fisica, Università della Calabria, Rende, Italy

[44b]INFN Gruppo Collegato di Cosenza, Laboratori Nazionali di Frascati, Italy

[45]Physics Department, Southern Methodist University, Dallas, Texas, USA

[46]Physics Department, University of Texas at Dallas, Richardson, Texas, USA

[47]National Centre for Scientific Research "Demokritos", Agia Paraskevi, Greece

[48a]Department of Physics, Stockholm University, Sweden

[48b]Oskar Klein Centre, Stockholm, Sweden

[49]Deutsches Elektronen-Synchrotron DESY, Hamburg and Zeuthen, Germany

[50]Fakultät Physik, Technische Universität Dortmund, Dortmund, Germany

[51]Institut für Kern- und Teilchenphysik, Technische Universität Dresden, Dresden, Germany

[52]Department of Physics, Duke University, Durham, North Carolina, USA

[53]SUPA - School of Physics and Astronomy, University of Edinburgh, Edinburgh, United Kingdom

[54]INFN e Laboratori Nazionali di Frascati, Frascati, Italy

[55]Physikalisches Institut, Albert-Ludwigs-Universität Freiburg, Freiburg, Germany

[56]II. Physikalisches Institut, Georg-August-Universität Göttingen, Göttingen, Germany

[57]Département de Physique Nucléaire et Corpusculaire, Université de Genève, Genève, Switzerland

[58a]Dipartimento di Fisica, Università di Genova, Genova, Italy

[58b]INFN Sezione di Genova, Italy

[59]II. Physikalisches Institut, Justus-Liebig-Universität Giessen, Giessen, Germany

[60]SUPA - School of Physics and Astronomy, University of Glasgow, Glasgow, United Kingdom

[61]LPSC, Université Grenoble Alpes, CNRS/IN2P3, Grenoble INP, Grenoble, France

[62]Laboratory for Particle Physics and Cosmology, Harvard University, Cambridge, Massachusetts, USA

[63a]Department of Modern Physics and State Key Laboratory of Particle Detection and Electronics, University of Science and Technology of China, Hefei, China

[63b]Institute of Frontier and Interdisciplinary Science and Key Laboratory of Particle Physics and Particle Irradiation (MOE), Shandong University, Qingdao, China

[63c]School of Physics and Astronomy, Shanghai Jiao Tong University, Key Laboratory for Particle Astrophysics and Cosmology (MOE), SKLPPC, Shanghai, China

[63d]Tsung-Dao Lee Institute, Shanghai, China

[63e]School of Physics and Microelectronics, Zhengzhou University, China

[64a]Kirchhoff-Institut für Physik, Ruprecht-Karls-Universität Heidelberg, Heidelberg, Germany

[64b]Physikalisches Institut, Ruprecht-Karls-Universität Heidelberg, Heidelberg, Germany

[65a]Department of Physics, Chinese University of Hong Kong, Shatin, N.T., Hong Kong, China

[65b]Department of Physics, University of Hong Kong, Hong Kong, China

[65c]Department of Physics and Institute for Advanced Study, Hong Kong University of Science and Technology, Clear Water Bay, Kowloon, Hong Kong, China

[66]Department of Physics, National Tsing Hua University, Hsinchu, Taiwan

[67]IJCLab, Université Paris-Saclay, CNRS/IN2P3, 91405, Orsay, France

[68]Centro Nacional de Microelectrónica (IMB-CNM-CSIC), Barcelona, Spain

[69]Department of Physics, Indiana University, Bloomington, Indiana, USA

[70a]INFN Gruppo Collegato di Udine, Sezione di Trieste, Udine, Italy

[70b]ICTP, Trieste, Italy

[70c]Dipartimento Politecnico di Ingegneria e Architettura, Università di Udine, Udine, Italy

[71a]INFN Sezione di Lecce, Italy

[71b]Dipartimento di Matematica e Fisica, Università del Salento, Lecce, Italy

[72a]INFN Sezione di Milano, Italy

[72b]Dipartimento di Fisica, Università di Milano, Milano, Italy

[73a]INFN Sezione di Napoli, Italy

[73b]Dipartimento di Fisica, Università di Napoli, Napoli, Italy

[74a]INFN Sezione di Pavia, Italy

[74b]Dipartimento di Fisica, Università di Pavia, Pavia, Italy

[75a]INFN Sezione di Pisa, Italy

[75b]Dipartimento di Fisica E. Fermi, Università di Pisa, Pisa, Italy

[76a]INFN Sezione di Roma, Italy

[76b]Dipartimento di Fisica, Sapienza Università di Roma, Roma, Italy

[77a]INFN Sezione di Roma Tor Vergata, Italy

[77b]*Dipartimento di Fisica, Università di Roma Tor Vergata, Roma, Italy*
[78a]*INFN Sezione di Roma Tre, Italy*
[78b]*Dipartimento di Matematica e Fisica, Università Roma Tre, Roma, Italy*
[79a]*INFN-TIFPA, Italy*
[79b]*Università degli Studi di Trento, Trento, Italy*
[80]*Universität Innsbruck, Department of Astro and Particle Physics, Innsbruck, Austria*
[81]*University of Iowa, Iowa City, Iowa, USA*
[82]*Department of Physics and Astronomy, Iowa State University, Ames, Iowa, USA*
[83]*Istinye University, Sariyer, Istanbul, Türkiye*
[84a]*Departamento de Engenharia Elétrica, Universidade Federal de Juiz de Fora (UFJF),
Juiz de Fora, Brazil*
[84b]*Universidade Federal do Rio De Janeiro COPPE/EE/IF, Rio de Janeiro, Brazil*
[84c]*Instituto de Física, Universidade de São Paulo, São Paulo, Brazil*
[84d]*Rio de Janeiro State University, Rio de Janeiro, Brazil*
[84e]*Federal University of Bahia, Bahia, Brazil*
[85]*KEK, High Energy Accelerator Research Organization, Tsukuba, Japan*
[86]*Graduate School of Science, Kobe University, Kobe, Japan*
[87a]*AGH University of Krakow, Faculty of Physics and Applied Computer Science, Krakow, Poland*
[87b]*Marian Smoluchowski Institute of Physics, Jagiellonian University, Krakow, Poland*
[88]*Institute of Nuclear Physics Polish Academy of Sciences, Krakow, Poland*
[89]*Faculty of Science, Kyoto University, Kyoto, Japan*
[90]*Research Center for Advanced Particle Physics and Department of Physics, Kyushu University,
Fukuoka, Japan*
[91]*L2IT, Université de Toulouse, CNRS/IN2P3, UPS, Toulouse, France*
[92]*Instituto de Física La Plata, Universidad Nacional de La Plata and CONICET, La Plata, Argentina*
[93]*Physics Department, Lancaster University, Lancaster, United Kingdom*
[94]*Oliver Lodge Laboratory, University of Liverpool, Liverpool, United Kingdom*
[95]*Department of Experimental Particle Physics, Jožef Stefan Institute and Department of Physics,
University of Ljubljana, Ljubljana, Slovenia*
[96]*School of Physics and Astronomy, Queen Mary University of London, London, United Kingdom*
[97]*Department of Physics, Royal Holloway University of London, Egham, United Kingdom*
[98]*Department of Physics and Astronomy, University College London, London, United Kingdom*
[99]*Louisiana Tech University, Ruston, Louisiana, USA*
[100]*Fysiska institutionen, Lunds universitet, Lund, Sweden*
[101]*Departamento de Física Teorica C-15 and CIAFF, Universidad Autónoma de Madrid, Madrid, Spain*
[102]*Institut für Physik, Universität Mainz, Mainz, Germany*
[103]*School of Physics and Astronomy, University of Manchester, Manchester, United Kingdom*
[104]*CPPM, Aix-Marseille Université, CNRS/IN2P3, Marseille, France*
[105]*Department of Physics, University of Massachusetts, Amherst, Massachusetts, USA*
[106]*Department of Physics, McGill University, Montreal, Quebec City, Canada*
[107]*School of Physics, University of Melbourne, Victoria, Australia*
[108]*Department of Physics, University of Michigan, Ann Arbor, Michigan, USA*
[109]*Department of Physics and Astronomy, Michigan State University, East Lansing, Michigan, USA*
[110]*Group of Particle Physics, University of Montreal, Montreal, Quebec City, Canada*
[111]*Fakultät für Physik, Ludwig-Maximilians-Universität München, München, Germany*
[112]*Max-Planck-Institut für Physik (Werner-Heisenberg-Institut), München, Germany*
[113]*Graduate School of Science and Kobayashi-Maskawa Institute, Nagoya University, Nagoya, Japan*
[114a]*Department of Physics, Nanjing University, Nanjing, China*
[114b]*School of Science, Shenzhen Campus of Sun Yat-sen University, China*
[114c]*University of Chinese Academy of Science (UCAS), Beijing, China*
[115]*Department of Physics and Astronomy, University of New Mexico, Albuquerque, New Mexico, USA*
[116]*Institute for Mathematics, Astrophysics and Particle Physics, Radboud University/Nikhef,
Nijmegen, Netherlands*
[117]*Nikhef National Institute for Subatomic Physics and University of Amsterdam, Amsterdam, Netherlands*
[118]*Department of Physics, Northern Illinois University, DeKalb, Illinois, USA*
[119a]*New York University Abu Dhabi, Abu Dhabi, United Arab Emirates*
[119b]*United Arab Emirates University, Al Ain, United Arab Emirates*
[120]*Department of Physics, New York University, New York, New York, USA*
[121]*Ochanomizu University, Otsuka, Bunkyo-ku, Tokyo, Japan*
[122]*The Ohio State University, Columbus, Ohio, USA*

[123]Homer L. Dodge Department of Physics and Astronomy, University of Oklahoma, Norman, Oklahoma, USA

[124]Department of Physics, Oklahoma State University, Stillwater, Oklahoma, USA

[125]Palacký University, Joint Laboratory of Optics, Olomouc, Czech Republic

[126]Institute for Fundamental Science, University of Oregon, Eugene, Oregon, USA

[127]Graduate School of Science, Osaka University, Osaka, Japan

[128]Department of Physics, University of Oslo, Oslo, Norway

[129]Department of Physics, Oxford University, Oxford, United Kingdom

[130]LPNHE, Sorbonne Université, Université Paris Cité, CNRS/IN2P3, Paris, France

[131]Department of Physics, University of Pennsylvania, Philadelphia, Pennsylvania, USA

[132]Department of Physics and Astronomy, University of Pittsburgh, Pittsburgh, Pennsylvania, USA

[133a]Laboratório de Instrumentação e Física Experimental de Partículas - LIP, Lisboa, Portugal

[133b]Departamento de Física, Faculdade de Ciências, Universidade de Lisboa, Lisboa, Portugal

[133c]Departamento de Física, Universidade de Coimbra, Coimbra, Portugal

[133d]Centro de Física Nuclear da Universidade de Lisboa, Lisboa, Portugal

[133e]Departamento de Física, Universidade do Minho, Braga, Portugal

[133f]Departamento de Física Teórica y del Cosmos, Universidad de Granada, Granada (Spain), Spain

[133g]Departamento de Física, Instituto Superior Técnico, Universidade de Lisboa, Lisboa, Portugal

[134]Institute of Physics of the Czech Academy of Sciences, Prague, Czech Republic

[135]Czech Technical University in Prague, Prague, Czech Republic

[136]Charles University, Faculty of Mathematics and Physics, Prague, Czech Republic

[137]Particle Physics Department, Rutherford Appleton Laboratory, Didcot, United Kingdom

[138]IRFU, CEA, Université Paris-Saclay, Gif-sur-Yvette, France

[139]Santa Cruz Institute for Particle Physics, University of California Santa Cruz, Santa Cruz, California, USA

[140a]Departamento de Física, Pontificia Universidad Católica de Chile, Santiago, Chile

[140b]Millennium Institute for Subatomic physics at high energy frontier (SAPHIR), Santiago, Chile

[140c]Instituto de Investigación Multidisciplinario en Ciencia y Tecnología, y Departamento de Física, Universidad de La Serena, Chile

[140d]Universidad Andres Bello, Department of Physics, Santiago, Chile

[140e]Instituto de Alta Investigación, Universidad de Tarapacá, Arica, Chile

[140f]Departamento de Física, Universidad Técnica Federico Santa María, Valparaíso, Chile

[141]Department of Physics, University of Washington, Seattle, Washington, USA

[142]Department of Physics and Astronomy, University of Sheffield, Sheffield, United Kingdom

[143]Department of Physics, Shinshu University, Nagano, Japan

[144]Department Physik, Universität Siegen, Siegen, Germany

[145]Department of Physics, Simon Fraser University, Burnaby, Bristish Columbia, Canada

[146]SLAC National Accelerator Laboratory, Stanford, California, USA

[147]Department of Physics, Royal Institute of Technology, Stockholm, Sweden

[148]Departments of Physics and Astronomy, Stony Brook University, Stony Brook, New York, USA

[149]Department of Physics and Astronomy, University of Sussex, Brighton, United Kingdom

[150]School of Physics, University of Sydney, Sydney, Australia

[151]Institute of Physics, Academia Sinica, Taipei, Taiwan

[152a]E. Andronikashvili Institute of Physics, Iv. Javakhishvili Tbilisi State University, Tbilisi, Georgia

[152b]High Energy Physics Institute, Tbilisi State University, Tbilisi, Georgia

[152c]University of Georgia, Tbilisi, Georgia

[153]Department of Physics, Technion, Israel Institute of Technology, Haifa, Israel

[154]Raymond and Beverly Sackler School of Physics and Astronomy, Tel Aviv University, Tel Aviv, Israel

[155]Department of Physics, Aristotle University of Thessaloniki, Thessaloniki, Greece

[156]International Center for Elementary Particle Physics and Department of Physics, University of Tokyo, Tokyo, Japan

[157]Department of Physics, Tokyo Institute of Technology, Tokyo, Japan

[158]Department of Physics, University of Toronto, Toronto, Ontario, Canada

[159a]TRIUMF, Vancouver BC, Canada

[159b]Department of Physics and Astronomy, York University, Toronto, Ontario, Canada

[160]Division of Physics and Tomonaga Center for the History of the Universe, Faculty of Pure and Applied Sciences, University of Tsukuba, Tsukuba, Japan

[161]Department of Physics and Astronomy, Tufts University, Medford, Massachusetts, USA

[162]Department of Physics and Astronomy, University of California Irvine, Irvine, California, USA

[163]University of Sharjah, Sharjah, United Arab Emirates

[164]*Department of Physics and Astronomy, University of Uppsala, Uppsala, Sweden*
[165]*Department of Physics, University of Illinois, Urbana, Illinois, USA*
[166]*Instituto de Física Corpuscular (IFIC), Centro Mixto Universidad de Valencia - CSIC, Valencia, Spain*
[167]*Department of Physics, University of British Columbia, Vancouver, British Columbia, Canada*
[168]*Department of Physics and Astronomy, University of Victoria, Victoria, British Columbia, Canada*
[169]*Fakultät für Physik und Astronomie, Julius-Maximilians-Universität Würzburg, Würzburg, Germany*
[170]*Department of Physics, University of Warwick, Coventry, United Kingdom*
[171]*Waseda University, Tokyo, Japan*
[172]*Department of Particle Physics and Astrophysics, Weizmann Institute of Science, Rehovot, Israel*
[173]*Department of Physics, University of Wisconsin, Madison, Wisconsin, USA*
[174]*Fakultät für Mathematik und Naturwissenschaften, Fachgruppe Physik,*
Bergische Universität Wuppertal, Wuppertal, Germany
[175]*Department of Physics, Yale University, New Haven, Connecticut, USA*

[a]Deceased.
[b]Also at Department of Physics, King's College London, London, United Kingdom.
[c]Also at Institute of Physics, Azerbaijan Academy of Sciences, Baku, Azerbaijan.
[d]Also at TRIUMF, Vancouver, British Columbia, Canada.
[e]Also at Department of Physics, University of Thessaly, Greece.
[f]Also at An-Najah National University, Nablus, Palestine.
[g]Also at Department of Physics, University of Fribourg, Fribourg, Switzerland.
[h]Also at Department of Physics, Westmont College, Santa Barbara, USA.
[i]Also at Departament de Fisica de la Universitat Autonoma de Barcelona, Barcelona, Spain.
[j]Also at Affiliated with an institute covered by a cooperation agreement with CERN.
[k]Also at The Collaborative Innovation Center of Quantum Matter (CICQM), Beijing, China.
[l]Also at Università di Napoli Parthenope, Napoli, Italy.
[m]Also at Institute of Particle Physics (IPP), Canada.
[n]Also at University of Colorado Boulder, Department of Physics, Colorado, USA.
[o]Also at Borough of Manhattan Community College, City University of New York, New York, New York, USA.
[p]Also at National Institute of Physics, University of the Philippines Diliman (Philippines), Philippines.
[q]Also at Department of Financial and Management Engineering, University of the Aegean, Chios, Greece.
[r]Also at Centro Studi e Ricerche Enrico Fermi, Italy.
[s]Also at Institucio Catalana de Recerca i Estudis Avancats, ICREA, Barcelona, Spain.
[t]Also at Technical University of Munich, Munich, Germany.
[u]Also at CMD-AC UNEC Research Center, Azerbaijan State University of Economics (UNEC), Azerbaijan.
[v]Also at Yeditepe University, Physics Department, Istanbul, Türkiye.
[w]Also at Institute of Theoretical Physics, Ilia State University, Tbilisi, Georgia.
[x]Also at CERN, Geneva, Switzerland.
[y]Also at Center for Interdisciplinary Research and Innovation (CIRI-AUTH), Thessaloniki, Greece.
[z]Also at Hellenic Open University, Patras, Greece.
[aa]Also at Department of Physics, Stellenbosch University, South Africa.
[bb]Also at Department of Physics, California State University, Sacramento, USA.
[cc]Also at Département de Physique Nucléaire et Corpusculaire, Université de Genève, Genève, Switzerland.
[dd]Also at Institut für Experimentalphysik, Universität Hamburg, Hamburg, Germany.
[ee]Also at Department of Physics, Stanford University, Stanford, California, USA.
[ff]Also at Institute for Nuclear Research and Nuclear Energy (INRNE) of the Bulgarian Academy of Sciences, Sofia, Bulgaria.
[gg]Also at Washington College, Chestertown, Maryland, USA.
[hh]Also at Institute of Applied Physics, Mohammed VI Polytechnic University, Ben Guerir, Morocco.